



Instituto de Geociências – IGD/UnB

Programa de Pós-Graduação

DISSERTAÇÃO DE MESTRADO Nº 415

Estudo geoquímico e isotópico de anfibolitos e rochas metassedimentares da Sequência

Metavulcanossedimentar Veríssimo e Grupo Araxá, Pires do Rio – GO.

ÁREA DE CONCENTRAÇÃO: GEOLOGIA REGIONAL

Aluno: Pedro Ferreira Piauilino

Prof. Orientador: Dra. Natalia Hauser

Prof. Co-Orientador: Dr. Elton Luiz Dantas

Brasília, Maio de 2018

À minha família, pelo incentivo, suporte e paciência;
Aos meus amigos, pelo companheirismo e apoio;
Ao meu amor, por todo amor.

AGRADECIMENTOS

Agradeço ao Programa de Pós-Graduação do Instituto de Geociências da Universidade de Brasília e ao CNPq a oportunidade de realização desta dissertação de mestrado, e à todos os funcionários envolvidos por toda a assistência e atenção dispensadas;

Ao Laboratório de Geocronologia da Universidade de Brasília, seus funcionários e colegas, pelo suporte durante a análise dos dados, ajuda nas discussões, interpretações e momentos de pausas e descontração, sempre com prontidão e simpatia;

À Profa. Orientadora Natalia Hauser por toda atenção e ajuda em todos os processos envolvidos para o desenvolvimento da dissertação, sempre com toda preocupação, proatividade e empatia;

Ao Prof. Co-orientador Elton Luiz Dantas pelos incentivos, conhecimentos e momentos de iluminação nas discussões geológicas;

Agradeço também aos professores Massimo Matteini, Lucieth C. Vieira e José Eloi G. Campos, pelas discussões e apoio; e em especial aos professores Márcio M. Pimentel e Reinhardt A. Fuck, pelos trabalhos anteriores na área de estudo e pelo humilde encorajamento a levantar questões pertinentes;

E aos meus colegas de Geologia, principalmente os participantes do Projeto Pires do Rio, pelos dados oferecidos, por todos os momentos que vivemos juntos, pelas discussões acalouradas a respeito da evolução geológica da área e, principalmente, pela amizade.

“A tarefa não é tanto ver aquilo que ninguém viu, mas pensar o que ninguém ainda pensou sobre aquilo que todo mundo vê”.

- Arthur Schopenhauer

RESUMO

A porção Sudeste da Faixa Brasília, no Brasil Central, apresenta rochas maficas de idade Neoproterozóica em fácies metamórfica anfibolito. Elas estão intrudidas em sequências metassedimentares relacionadas à colisão dos crátons Amazônico, São Francisco e Paranapanema. Na área de Pires do Rio-Catalão, rochas maficas puderam ser relacionadas a três eventos principais: o primeiro, com idade U-Pb em zircão de 979.4 ± 17 Ma relacionado a basaltos toleíticos de baixo K na Sequência Metavulcanossedimentar Veríssimo. Tais basaltos possuem anomalias negativas de Rb, K, P, e Ti em diagramas normalizados para o manto primitivo e são enriquecidos em ETRL, similar ao padrão de fonte de basaltos de cadeia oceânica enriquecidos (E-MORB). Basaltos transicionais também interpretados a esse evento são caracterizados por altas razões La/Lu e possuem anomalias negativas em Rb, K, Pb e Sr quando normalizados ao manto primitivo, e apresentam afinidade geoquímica com fontes tipo basaltos de ilha oceânica (OIB). Tal evento é associado à sequência vulcano-sedimentar de aproximadamente 1 Ga, com dominante proveniência cratônica. Dados isotópicos de Sm-Nd apresentam uma idade-modelo T_{DM} entre 1,26 e 1,4 Ga e valores $\epsilon_{Nd(t)}$ de +2,69 a +4,57 para amostras tipo MORB menos contaminadas, e valores a cerca de +2,5 para basaltos tipo OIB. A configuração tectônica para esse evento provavelmente envolve afinamento crustal e ascenção mantélica em um regime de extensão continental, durante o desenvolvimento de uma margem passiva. O segundo evento magmático mafico do tipo MORB, foi representado por basaltos intrudidos ao longo da sedimentação do Grupo Araxá, pode ser relacionado a uma extensão incipiente de *forearc/back-arc* em 870.7 ± 4.1 Ma para o magmatismo tipo E-MORB e 819.7 ± 6.3 Ma para magmatismo tipo OIB. Essas rochas apresentam uma distinta anomalia negativa de Nb-Ta, juntamente com valores levemente positivos de $\epsilon_{Nd(t)}$ entre +0,78 a +2,71 e idades mais velhas de T_{DM} entre 1,32 a 1,8 Ga sugerem um ambiente relacionado a processos de subducção. O terceiro evento é representado por magmatismo basáltico/gabróico do tipo OIB sin- a tardi-tectônico em 651.7 ± 6.5 Ma, com idades T_{DM} de 1.0 Ga e valores positivos de $\epsilon_{Nd(t)}$ de +1,82 a +2,57 que podem ser atribuídos à colisão continental regional e o fechamento do oceano Neoproterozoico. Tais resultados sugerem que bacias tectonicamente superpostas no Brasil Central podem ser associadas com a ocorrência de magmatismo mafico através de um intervalo de tempo tão extenso quanto a longa duração da evolução da Faixa Brasília (1.0-0.6 Ma). Ademais, tais configurações podem ser aplicáveis em outros cenários tectônicos modernos e pretéritos ao redor do mundo.

Palavras-chave: E-MORB; OIB; Neoproterozoico; Faixa Brasília; U-Pb em zircão; Sm-Nd em rocha total.

ABSTRACT

The Southeastern Brasília Belt of Central Brazil exhibits Neoproterozoic mafic rocks of amphibolite metamorphic grade that were emplaced in metasedimentary sequences related to the collision of the Amazonian and São Francisco cratons at the end of the Neoproterozoic. In the Pires do Rio-Catalão area, mafic rocks can be classified to be related to three main events: The first one, at 979.4 ± 17 Ma as recorded in U-Pb data for zircon, is related to low-K tholeiitic basalts and related alkali basalts. The low-K tholeiitic basalts have negative Rb, K, P and Ti anomalies in a primitive mantle-normalized trace element spider diagram and are LREE-enriched, similar to E-MORB source patterns. The related alkali basalts are characterized by higher La/Lu ratios, have negative Rb, K, Pb and Sr anomalies when normalized to primitive mantle, and have a chemical affinity to OIB. This event can be associated with a 1 Ga volcano- sedimentary sequence that is dominated by cratonic provenance. Sm-Nd isotopic data that give T_{DM} model ages between 1.26 and 1.4 Ga and $\epsilon_{Nd(t)}$ values of +2.69 to +4.57 for uncontaminated MORB-like, and ca. +2.5 values for OIB-like basalts. The tectonic setting for this event would be into a continental extension of crustal thinning and mantle upwelling during passive margin development. The second mafic magmatic event, represented by Araxá Group syn- sedimentary basalts, can be related with an incipient forearc/back-arc extension at 870.7 ± 4.1 Ma for E-MORB basalts and 819.7 ± 6.3 Ma for OIB-like basalts. These rocks show a distinct Nb-Ta negative anomaly, slightly lower $\epsilon_{Nd(t)}$ values of +0.78 to +2.71 and older T_{DM} ages from 1.32 to 1.8 Ga suggesting a syn-subduction tectonic environment. The third event is represented by syn- to late-tectonic OIB-like basaltic/gabbroic magmatism at ca. 650 Ma, with younger T_{DM} ages at ca. 1.0 Ga and positive $\epsilon_{Nd(t)}$ values of +1.82 to +2.57 that can be associated to regional continental collision and final closure of the Neoproterozoic ocean. These findings suggest that some tectonically superposed basins in Central Brazil might have individual association to occurrence of mafic magmatism along a timespan as wide as the long-lived evolution of the Brasília Belt (1.0-0.6 Ma). Furthermore, this scenario may be applicable to other ancient and modern scenarios worldwide.

Keywords: E-MORB; OIB; Neoproterozoic; Whole-rock Geochemistry; U-Pb in zircon; Whole-rock Sm-Nd; Brasilia Belt.

Sumário

1 CAPÍTULO 1 – INTRODUÇÃO	8
1.1 Objetivos	8
1.2 Localização da área e Vias de Acesso	8
1.3 Estruturação da Tese	9
1.4 Justificativas.....	10
2 CAPÍTULO 2 - MATERIAIS E MÉTODOS	10
2.1 Procedimentos Analíticos	10
2.1.1 Geoquímica de Rocha total	10
2.1.2 U-Pb.....	10
2.1.3 Sm-Nd.....	11
3 CAPÍTULO 3 - GEOLOGIA REGIONAL	11
3.1 Associação Ortognáissica Migmatítica	13
3.2 O Complexo Anápolis-Itauçu	13
3.3 Sequências Supracrustais.....	13
3.3.1 Grupo Canastra.....	13
3.3.2 Grupo Araxá.....	14
3.3.3 Sequência Vulcanossedimentar de Maratá	15
3.3.4 Sequência vulcanossedimentar Veríssimo	15
3.4 Granitos tipo-Ipameri.....	15
3.4.1 Grupo Ibiá	15
4 CAPÍTULO 4 - ARTIGO	17
4.1 Introduction	17
4.2 Regional Geologic Setting	19
4.3 Local Geology and Petrography	24
4.3.1 Amphibolites.....	26
4.3.2 Supracrustal rocks from Veríssimo Sequence and Araxá Group	27
4.4 Analytical Procedures.....	28
4.4.1 Major, Trace and Rare-Earth Element geochemistry	28
4.4.2 U-Pb.....	28
4.4.3 Sm-Nd.....	29
4.5 Results	29
4.5.1 Geochemistry	29
4.5.2 U-Pb age data	34
4.5.3 U-Pb provenance data.....	39
4.5.4 Sm-Nd results.....	42

4.6	Discussions	44
4.6.1	Tectonic setting of mafic magmatism.....	44
4.6.2	Araxá and Veríssimo supracrustal rocks.....	48
4.7	Conclusions.....	50
4.8	References.....	50
4.9	Appendix	55
5	CAPÍTULO 5 - DISCUSSÕES	66
5.1	Ambiente tectônico do magmatismo máfico.....	66
5.1.1	Anfibolitos tipo E-MORB na Sequência Veríssimo e Grupo Araxá	66
5.1.2	Anfibolitos tipo OIB da Sequência Veríssimo e do Grupo Araxá	67
5.2	Rochas supracrustais do Grupo Araxá e Sequência Veríssimo	68
6	CAPÍTULO 6 - CONCLUSÕES.....	70
7	REFERÊNCIAS BIBLIOGRÁFICAS	70

LISTA DE FIGURAS

Figura 1.1 – Mapa de localização da região de Pires do Rio – GO e principais vias de acesso. Retângulo vermelho delimita a área de estudo	9
Figura 3.1 - Mapa geológico simplificado da porção sudeste de Goiás (adaptado de SIEG)	12
Figura 3.2 - Coluna estratigráfica dos Grupos Canastra, Ibiá e Araxá (modificado de Seer, 1999).....	16
Figure 4.1 - Schematic tectonostratigraphic map of Southeast Brasília Belt. Rectangle shows the studied area (Adapted from Fuck et al., 1994).....	20
Figure 4.2 - Provenance patterns of most expressive sedimentary sequences in South Brasília Belt (from Pimentel et al., 2016).	21
Figure 4.3 - Geological map of Pires do Rio – Catalão área	25
Figure 4.4 - Major macroscopic and microscopic amphibolite lithologies found in Pires do Rio – Catalão area. Images a and b show basaltic protoliths, whereas images c and d are representative for gabbroic protoliths	26
Figure 4.5 - (a) syn-tectonic garnet with oriented quartz inclusions (diagonal), and quartz stress shadows in oriented amphibole matrix (horizontal); (b) Plagioclase with lamellar twinning.....	27
Figure 4.6 - (a) Folded chlorite schist; (b) calc-feldspar-chlorite schist; and (c) syn-tectonic garnet with reabsorption textures, recrystallized rim and quartz stress shadows.....	28
Figure 4.7 - (a)- AFM diagram (Irvine & Barangar, 1979) showing the tholeitic affinity. (b)- Zr/TiO ₂ -Nb/Y diagram and (c) - Ti/Y-Nb/Y diagram (Pearce, 1982) plots evidence MORB and OIB-like samples	30
Figure 4.8 - Amphibolite samples chondrite-normalized (Sun & McDonough, 1989) (a), N-MORB normalized (Sun & McDonough, 1989) and(b) primitive mantle-normalized (Sun & McDonough, 1989) (c, d)	31
Figure 4.9 - V-Ni-Th diagram (left) and Th/Sc-Zr/Sc diagram (right) plotting metasedimentary samples with possible mixing between felsic and mafic sources.....	32
Figure 4.10 - From top to bottom: REE pattern for chondrite-normalized and upper continental crust-normalized. Bottom most diagram show minor and trace-elements normalized to upper continental crust. Symbols as in Fig. 4.9.	33
Figure 4.11 - Metavolcanic rock samples normalized to primitive mantle. Symbols as in Fig. 4.9	34
Figure 4.12 - Zircon backscattered images of sample PR-09 and associated U-Pb age exemplifying complex internal structures represented by lighter and darker domains.....	34
Figure 4.13 - Concordia age of sample PR-10 Grupo Araxá OIB-like.	37
Figure 4.14 - Zircon grains from OIB sample PR-01a and its respective analized U-Pb ages	38
Figure 4.15 - Concordia age for PR-01a OIB-like amphibolite.....	38
Figure 4.16 - Cathodoluminescence imaging from low Th/U ratios zircon crystals of OIB-like amphibolite. Magmatic zonation and overgrowth are remarkable and allow an igneous provenance for these crystals.....	39
Figure 4.17- Representative zircon grains from main populations of sample PR-04 and its analyzed ages (circles, in Ma)	40
Figure 4.18 - Representative zircon grains from main populations of sample PR-11b and its analyzed ages (circles, in Ma)	40
Figure 4.19 - Representative zircon grains from main populations of sample PR-12b and its analyzed ages (circles, in Ma)	41
Figure 4.20 - Probability density plots for analyzed metasedimentary samples	41
Figure 4.21 - Sm-Nd isochron ages for MORB-like amphibolites from Veríssimo Sequence (A) and Araxá Group (B).43	43
Figure 4.22 - Nd evolution diagram. Light green - Veríssimo Sequence; dark green - Araxá Group; light blue - supracrustal rocks	44
Figure 4.23 - Th/Yb-Nb/Yb diagram and V-Ti diagram for amphibolite samples. Symbols as in Fig. 4.7.....	45
Figure 4.24 - Bowen diagrams (after Dilek & Furnes, 2011), showing the possible subduction-unrelated correlation for Veríssimo Sequence MORB-like basalts	46
Figure 4.25 - TiO ₂ /Yb-Nb/Yb diagram showing a possible diagonal trend between MORB and OIB for amphibolite in Pires do Rio – Catalão area. Symbols as in Fig. 4.7.....	46
Figure 4.26 - Zr-Th-Nb diagram (Wood et al., 1980) for MORB-like samples. Araxá Group samples plot preferentially in arc-basalts field, whereas Veríssimo Sequence samples plot in E-MORB field. Symbols as in Fig. 4.7.....	47

LISTA DE TABELAS

Table 4.1 - Summary chart of isotopic data and tectonic setting interpretations for geological units whithin Pires do Rio – Catalão region.....	23
Table 4.2 - Sm-Nd data for rocks in Pires do Rio – Catalão area.....	42
Table 4.3 - Coordinates (UTM) from rock samples.....	55
Table 4.4 - Geochemical data from amphibolite samples.....	56
Table 4.5 - Geochemical data from supracrustal rock samples.....	57
Table 4.6 - U-Pb isotopic data results from sample PR-09.....	58
Table 4.7 - U-Pb isotopic data results from sample IPC 184.....	59
Table 4.8 - U-Pb isotopic data results from sample PR-01a.....	60
Table 4.9: U-Pb isotopic data results from sample PR-10.....	61
Tabela 4.10: U-Pb isotopic data results from supracrustal rock samples.....	62
Table 4.11 - U-Pb isotopic data results from supracrustal rock samples (continuation).....	63
Table 4.12 - U-Pb isotopic data results from supracrustal rock samples (continuation).....	64
Table 4.13 - U-Pb isotopic data results from supracrustal rock samples (continuation).....	65

1 CAPÍTULO 1 – INTRODUÇÃO

1.1 Objetivos

O objetivo central deste projeto é a contribuição de conhecimento geológico regional da porção sudeste da Faixa Brasília Sul, à margem oeste do Cráton São Francisco, pelo levantamento de dados inéditos da Sequência Metavulcanosedimentar Veríssimo e do Grupo Araxá, com ênfase no magmatismo mafico e proveniência detritica dos sedimentos associados na região de Pires do Rio-Catalão, sudeste do estado de Goiás (GO).

Os objetivos específicos desenvolvidos foram:

- Caracterização geoquímica e isotópica das rochas básicas, mapeadas como anfíbolitos na região de Pires do Rio-Catalão;
- Datação isotópica dos corpos ígneos maficos reconhecidos (análises U-Pb em zircão por LA-MC-ICP-MS) para estabelecer uma cronologia das intrusões;
- Estudo de proveniência da Sequência Metavulcanosedimentar Veríssimo e do Grupo Araxá na região de Pires do Rio-Catalão, utilizando os métodos U-Pb em zircão e Sm-Nd em rocha total, com o intuito de obter as idades máximas de sedimentação, as áreas-fonte dos sedimentos e evolução crustal da área;
- Contribuição para a reconstrução da história evolutiva desta Sequência dentro da porção sul da Faixa Brasília, para a elaboração de um modelo evolutivo regional e seu papel desenvolvido durante o período Neoproterozoico;

Com a obtenção e integração de novos dados buscou-se identificar os processos de geração de magmas, ambiente tectônico e retrabalhamento crustal, e assim, o melhor entendimento dos corpos anfibolíticos e suas relações com as rochas encaixantes. Consequentemente, a caracterização hipotética do ambiente tectônico de formação e a evolução geológica regional foram discutidas, levando em conta discussões presentes em trabalhos anteriores a respeito de rochas e unidades geológicas semelhantes na área de estudo e adjacências. O uso de análises geoquímicas e isotópicas (Sm-Nd e U-Pb) possibilitam certa consistência dos dados e uma melhor clareza dos processos envolvidos, levando a um melhor posicionamento do ambiente geológico em âmbitos tanto local quanto regional.

1.2 Localização da área e Vias de Acesso

A área de estudo Pires do Rio - Catalão está localizada na porção sudeste do Estado de Goiás, e está situada nas proximidades das cidades de Pires do Rio, Ipameri, Orizona e Catalão (Figura 1.1). A área está inserida na porção sudeste da Faixa Brasília, próxima à margem oeste do Cráton São Francisco. Para acessar Pires do Rio partindo de Brasília - DF segue-se pelas rodovias DF-003 e BR-040 sentido Luziânia – GO; e pelas rodovias estaduais GO-010 e GO-330, respectivamente sentido Vianópolis – GO e Pires do Rio - GO, totalizando 230 km de distância. A GO-330 também dá acesso de Pires do Rio para as cidades goianas de Ipameri e Catalão. A partir de Goiânia – GO, percorre-se 149 km pela BR-352 até o município de Pires do Rio - GO.

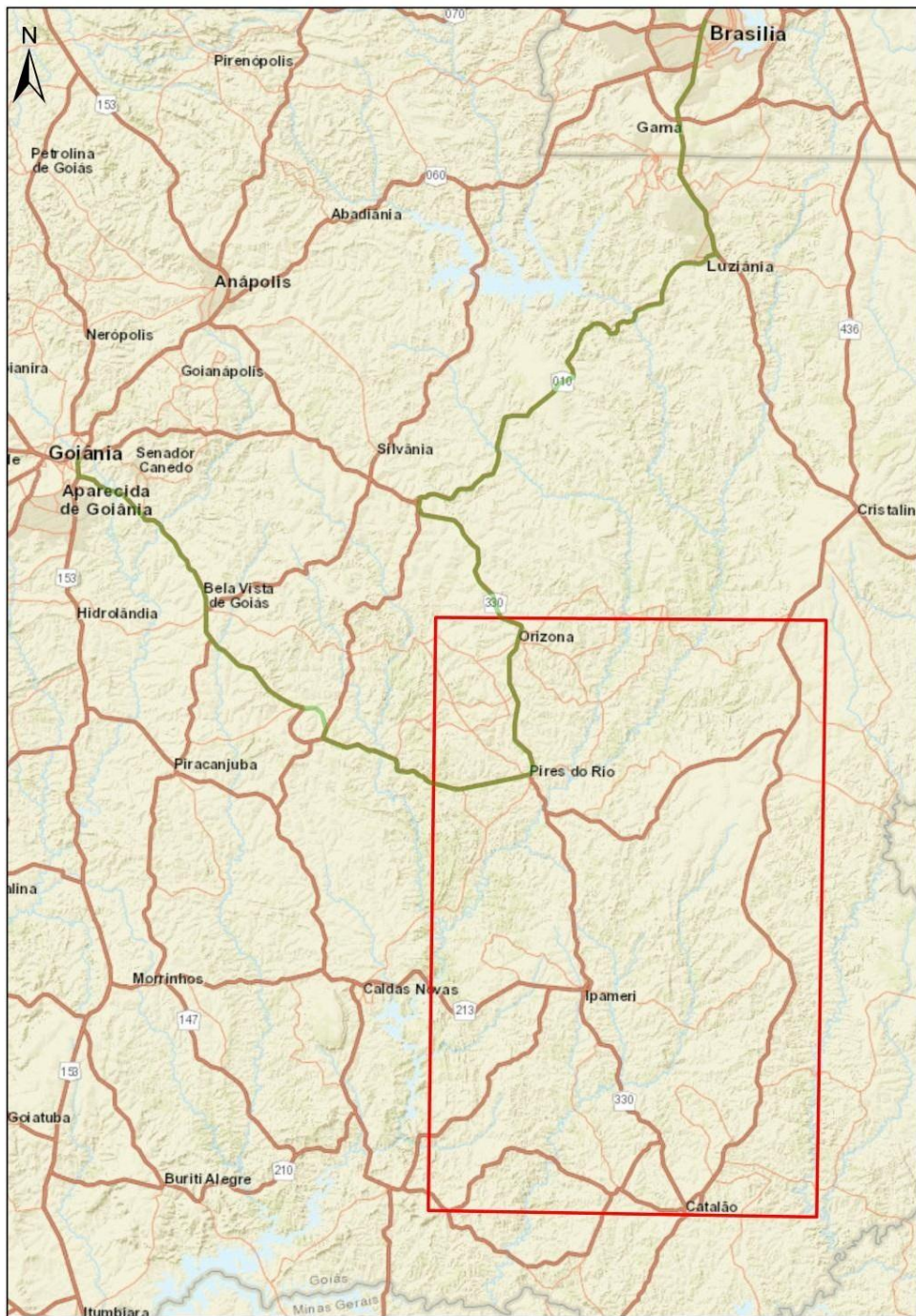


Figura 1.1 – Mapa de localização da região de Pires do Rio – GO e principais vias de acesso. Retângulo vermelho delimita a área de estudo.

1.3 Estruturação da Tese

A tese está estruturada em 7 capítulos, a saber: 1. Introdução, que compreende os subcapítulos de Apresentação, Objetivos, Organização da tese e Justificativas; 2. Materiais e Métodos; 3. Geologia Regional; 4. Artigo “From passive margin to continental collision: geochemical and isotopic constrains for E-MORB and OIB-like magmatism during the Neoproterozoic evolution of the southeast Brasília Belt”, submetido à Precambrian Research; 5. Discussões; 6. Conclusões; e 7. Referências Bibliográficas.

1.4 Justificativas

A área do projeto foi selecionada pela sua importância regional, já que situa-se na transição de ambientes geotectônicos conhecidamente distintos, além de apresentar rochas características e possivelmente diagnósticas para a melhor interpretação da evolução geológica regional.

2 CAPÍTULO 2 - MATERIAIS E MÉTODOS

Na execução deste estudo, foram compiladas informações das bases cartográficas e mapas geológicos desenvolvidos pela CPRM (Serviço Geológico do Brasil) em escala de 1:100.000 nas folhas Pires do Rio, Ipameri, Goiandira, Cavaleiros, Campo Alegre de Goiás e Catalão, além do mapeamento 1:50.000 realizado pelo Trabalho Final de Graduação da Universidade de Brasília do ano de 2013, intitulado projeto Pires do Rio. Foi também consultada a tese de doutorado de Klein (2008).

A sistemática adotada para o desenvolvimento desta tese foi definida pelos seguintes procedimentos técnicos: (i) revisão bibliográfica e levantamento das informações geológicas disponíveis, levando em conta as descrições das unidades presentes e suas relações temporais/espaciais, interpretação de dados geofísicos, compilação de dados geocronológicos e elaboração de mapa geológico integrado; (ii) execução de duas excursões a campo para a coleta de dados e amostras, a fim da análise petrográfica, geoquímica e isotópica das rochas anfibolíticas e suas respectivas rochas encaixantes levando em conta as características estruturais da área; (iii) A aquisição, processamento e análise dos dados referentes à petrografia, análises químicas de rocha total (elementos maiores, menores, traço e terras raras), e características isotópicas e geocronológicas (Sm-Nd e U-Pb); (iv) integração dos dados obtidos e interpretação dos resultados analíticos, elaboração da tese e submissão de artigo científico.

2.1 Procedimentos Analíticos

Os procedimentos analíticos em laboratório compreendem a confecção de lâminas delgadas e análise petrográfica das amostras selecionadas, análise geoquímica de elementos maiores, menores, traço e terras raras, e análises isotópicas de U-Pb e Sm-Nd.

2.1.1 Geoquímica de Rocha total

As amostras de rocha total foram encaminhadas para o laboratório Acme Analytical Laboratories Ltda, onde foram fundidas com LiBO₂, e então digeridas e diluídas em HNO₃. Os elementos maiores e menores foram obtidos através de um espectrômetro de emissão atômica por plasma acoplado (ICP-AES), com erro analítico de $\pm 2\%$ e os elementos-traço e terras raras foram determinados através de um espectrômetro de massa por plasma indutivamente acoplado (ICP-MS), com erro analíticos de $\pm 5\%$, ambos para concentrações 50 vezes maiores que os limites de detecção.

2.1.2 U-Pb

Concentrados de grãos de zircão foram extraídos de amostras de 1-10 kg moídas. A técnica de peneiramento foi empregada a fim de extrair a fração mais fina (inferior a 500 μm) e em seguida a concentração da fração mais

densa por concentração gravimétrica por uso de batéia. A separação magnética da fração mais densa foi realizada com o uso do separador isodinâmico Frantz seguinte, posteriormente, a separação manual dos grãos de zircão com o uso de lupa binocular. Os grãos separados foram então inseridos em *mounts* de resina epóxi, desgastados e polidos para a exposição de seus interiores e a conseguinte limpeza com banho de HNO_3 diluído a 3%, água Nanopure em ultrassom e em acetona para a eliminação de resíduos. A morfologia dos grãos de zircão foi analisada a partir de imageamento com microscopia eletrônica de varredura de retro-espalhamento e de catodoluminescência, JEOL QUANTA 450, no Laboratório de Geocronologia da Universidade de Brasília. Com base nas imagens geradas, foram selecionados locais pré-determinados para as análises, realizadas com sistema de ablação a laser.

As análises isotópicas de U-Pb foram realizadas no Laboratório de Geocronologia da Universidade de Brasília através de um espectrômetro de massa por plasma indutivamente acoplado *Neptune* HR-MC-ICP-MS (*Thermo-Finnigan*) acoplado com sistema de ablação a laser Nd:YAG UP213 (*New Wave Research*). Entre análises U-Pb em zircão foi utilizado o padrão interno internacional GJ-1 (Jackson *et al.*, 2004) a fim da correção da deriva do equipamento e o padrão externo 91500 (Wiendenbeck *et al.*, 1995, 2004) para a verificação da acurácia, de formas escalonadas entre as análises dos grãos de origem desconhecida. A ablação dos grãos foi determinada em *spots* de 30 μm , em configuração de 10 Hz a 2-3 J/cm². As massas analisadas referem-se ao ^{238}U , ^{208}Pb , ^{207}Pb , ^{206}Pb , $^{204}(\text{Pb+Hg})$ e ^{202}Hg .

Os dados brutos foram processados e reduzidos utilizando planilha do Microsoft Excel (Buhn *et al.*, 2009). Foi utilizado o software Isoplot 4.15 para confecção de diagramas de concórdia, histogramas de densidade de probabilidade e a geração de idades de média ponderada.

2.1.3 Sm-Nd

Os dados isotópicos de Sm-Nd foram analisados no Laboratório de Geocronologia da Universidade de Brasília, em um espectrômetro de massa po ionização termal multicoletor Finnigan MAT 262 em modo estático, e a metodologia aplicada de acordo com a descrita por Gioia & Pimentel (2000). Amostras pulverizadas de rocha total (aprox. 50 mg cada) foram misturadas a solução de *spike* ^{149}Sm - ^{150}Nd e dissolvidas por HF, HNO_3 e HCl em cápsulas Savillex. As técnicas de troca catiônica implantadas para a extração de Sm e Nd nas amostras usaram colunas de Teflon contendo resina LN-Spec. As amostras de Sm e Nd foram então submetidas a evaporação em filamentos de Re em montagem de filamentos duplos. As incertezas das razões Sm/Nd e $^{146}\text{Nd}/^{144}\text{Nd}$ são inferiores a $\pm 0,5\%$ (2σ) e $\pm 0,005\%$ (2σ), respectivamente, e baseadas em repetidas análises dos padrões internos BHVO-1 and BCR-1. As razões $^{143}\text{Nd}/^{144}\text{Nd}$ foram normalizadas a $^{146}\text{Nd}/^{144}\text{Nd}$ em valor de 0,7219. O modelo de De Paolo (1981) foi utilizado para o cálculo das idades modelo T_{DM} e as isócronas de Sm-Nd foram calculadas utilizando o software Isoplot 3/EX (Ludwig, 2003).

3 CAPÍTULO 3 - GEOLOGIA REGIONAL

A Faixa Brasília faz parte de um orógeno Neoproterozoico, que foi desenvolvido durante o evento Brasiliano entre os Cráticos Amazônico, São Francisco/Congo e Paranapanema, ocupando a porção centro-leste da Província Tocantins (Pimentel *et al.*, 2004b) e se estende por mais de 1000 km na direção N-S a oeste do Cráton São Francisco (Dardenne, 2000).

A Faixa Brasília (Figura 3.1) consiste basicamente em

- i) Espessa sequência de rochas sedimentares e metassedimentares na seção mais ao leste, depositadas e deformadas ao longo da margem oeste do Cráton São Francisco/Congo, representada pelos Grupos Bambuí, Paranoá, Vazante, Canastra, Ibiá, Araxá. Pimentel *et al.* (2001) sugeriram um modelo alternativo para a evolução destes grupos com base em estudos de isótopos de Nd e de proveniência, onde vários destes grupos são sin-orogênicos (*fore-arc*) e o Grupo Bambuí representa uma bacia de ante-país. (Rodrigues *et al.*, 2010; Pimentel *et al.*, 2011) Além disso, ocorrem sequências do tipo rifte caracterizadas pelos grupos Serra da Mesa, Araí e Natividade (Pimentel *et al.*, 2011; Fuck *et al.*, 1993 e Fuck 1994).
- ii) Maciço de Goiás do Arqueano/Paleoproterozoico, bloco siálico alóctone constituído principalmente em terrenos arqueanos da área de Goiás-Crixás (Pimentel *et al.*, 2011).
- iii) Núcleo metamórfico do orógeno conhecido como complexo granulítico Anápolis-Itauçu; associações de rochas muito similares são expostas no chamado Complexo Uruaçu (Della Giustina *et al.*, 2009).
- iv) Arco Magmático de Goiás composto por uma grande exposição de associações vulcana-plutônicas Neoproterozoicas. (Pimentel & Fuck, 1992).

As associações supracrustais na parte sul da faixa são marcadas por um empurrão de escala regional com vergência para leste em direção à plataforma São Francisco/Congo. Outra feição estrutural é o extenso sistema de zonas de cisalhamento do tipo *strike-slip* com *trend* NNE, que marca os limites da Faixa Brasília e das faixas de dobramentos Araguaia e Paraguaia, a oeste do Cráton. Essas feições lineares são conhecidas como Lineamento Transbrasiliano (Pimentel *et al.*, 2011).

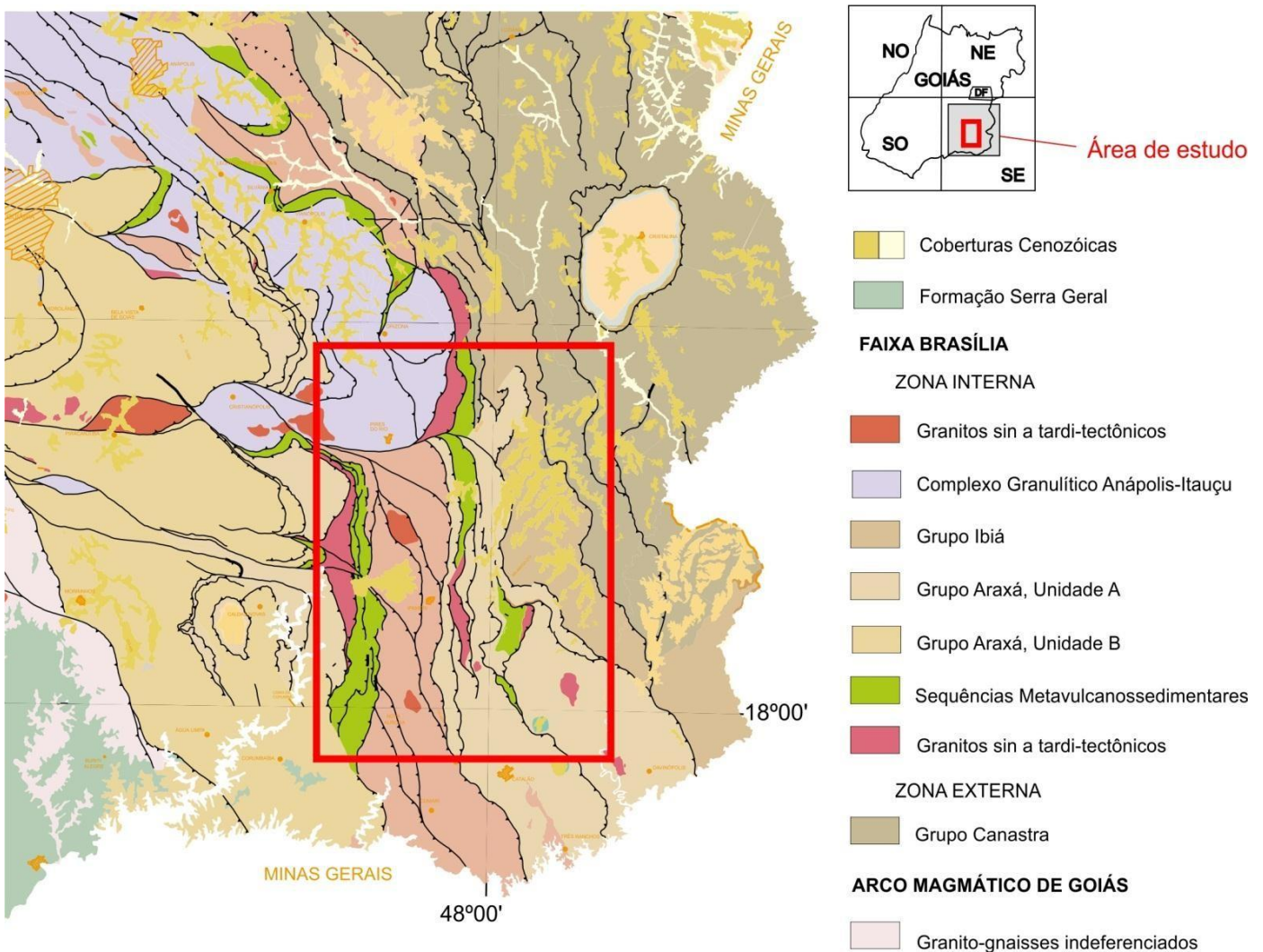


Figura 3.1 - Mapa geológico simplificado da porção sudeste de Goiás (adaptado de SIEG)

3.1 Associação Ortognáissica Migmatítica

A Associação Ortognáissica Migmatítica é uma unidade de provável idade Arqueana a Paleoproterozoica, constituída por uma geração de granitóides composta por tonalitos, com variações locais para granitos e granodioritos, além de migmatitos com enclaves de granulitos, de geoquímica calcio-alcalina de baixo potássio (CPRM, 2001).

Os enclaves granulíticos são interpretados como produtos de anatexia, parcial ou total, de rochas do Complexo Granulítico Anápolis-Itauçu. É difícil delimitar com precisão as ocorrências desses litotipos, pois ocorrem associados também granitóides mais juvenis, dos quais provavelmente parte é originária da própria fusão dos granitóides mais antigos. Devido a essa associação, os granitóides mostram as amplas variedades compostionais dessas misturas, ao invés de caracterizar os tonalitos dominantes na unidade. Corpos de tal natureza ocorrem em uma faixa de direção SE-NW. Na porção noroeste, os gnaisses formam lentes alongadas descontínuas, intercaladas em granulitos (CPRM, 2001).

3.2 O Complexo Anápolis-Itauçu

O complexo constitui a base de uma ampla área na parte centro-sul da Faixa Brasília, com exposição de rochas de alto grau e de granitos, separados dos metassedimentos do Grupo Araxá por zonas de cisalhamento de baixo e de alto ângulo pobemente expostas (Piuzana *et al.*, 2003a).

Grande parte deste complexo de alto grau é de idade Neoproterozóica, confirmados a partir de estudos geocronológicos mais recentes, ao contrário do que tradicionalmente era proposto por autores por fazer parte do embasamento siálico, de provável idade Arqueana (Pimentel *et al.*, 1999).

A exposição dessas rochas metamorfizadas em alto grau, na Faixa Brasília, está alçada tectonicamente e justaposta às rochas de mais baixo grau (Pimentel *et al.*, 2001).

De acordo com Pimentel *et al.* (2004), este complexo comprehende:

- i) Ortogranulitos, incluindo corpos máficos-ultramáficos acamados e granulitos de composição tonalítica a granodiorítica.
- ii) Granulitos aluminosos, leptinitos e granada gnaisses associados com mármore, rochas calcio-silicáticas, quartzitos e granulitos máficos finos.
- iii) Sequências vulcanossedimentares constituídas por anfibolitos, micaxistos, metavulcânicas félscicas, metacherts e formações ferríferas.
- iv) Intrusões graníticas alongadas segundo NW-SE.

Rochas deste complexo possuem uma associação similar exposta no chamado Complexo Uruaçu (Della Giustina *et al.*, 2009).

Assembléias mineralógicas de alguns granulitos contendo cordierita, espinélio, rutilo e zircão, além de safirina e quartzo em equilíbrio são sugeridas por Moraes *et al.* (2002) como evidência de um metamorfismo de ultra-alta-temperatura (UHT), a qual pode ter chegado a 1150 °C e pressões acima de 10 kbar. Texturas de retrogradação mostram que o resfriamento se deu em condições próximas às isobáricas (Piuzana *et al.*, 2003b). Trabalhos posteriores de Baldwin & Brown (2008), Della Giustina *et al.* (2009) e Reno *et al.* (2009) mostram idades do pico de metamorfismo entre aproximadamente 620 Ma nas porções ao sul e 650 Ma, nas áreas ao norte.

3.3 Sequências Supracrustais

3.3.1 Grupo Canastra

O Grupo Canastra constitui uma sequência regressiva de margem passiva com idade máxima de deposição de 1040 Ma pelo estudo de idades U-Pb em zircões (Silva *et al.*, 2012; Rodrigues *et al.*, 2010).

Esta sequência é composta principalmente por rochas metapelíticas e metapsamíticas metamorfizadas em fácies xisto verde incluindo clorita filito, metarritmito, quartzitos finos e micáceos e restritas intercalações de calcário e filito carbonático. Similaridades litológicas, tais como abundância de níveis psamíticos, presença rítmica de pelitos e níveis com associações carbonáticas, têm levado muitos autores a correlacionar os grupos Canastra e Paranoá (Rodrigues, 2008).

3.3.2 Grupo Araxá

O Grupo Araxá possui estratigrafia interna pobremente conhecida devido à intensa deformação, já que compõe lascas tectônicas apresentando arranjo litoestratigráfico interno próprio, refletindo ambientes tectônicos- sedimentares- ígneos diferentes, e está limitada por zonas de cisalhamento sub-horizontais e subverticais (Seer *et al.*, 2001).

O Grupo Araxá é representado por sequência ígnea máfica coberta por rochas metassedimentares. Esse conjunto foi metamorfizado sob condições de fácies anfibolitos há cerca de 630 Ma e foi intrudidos por granitos com assinatura geoquímica colisional a cerca de 637 Ma (Seer, 1999; Seer *et al.*, 2005).

As rochas metamáficas do Grupo Araxá são representadas por corpos de anfibolitos grossos a finos, clorita-anfibólito xistos e clorita xistos. Rochas ultramáficas, como serpentinitos e anfibólito-talco xistos podem ocorrer, assim como também depósitos locais de cromita podiforme, representando uma melange ofiolítica N-S (Seer *et al.*, 2001; Pimentel *et al.*, 2001; Pimentel *et al.*, 2011).

Já as rochas metassedimentares do Grupo Araxá, dominantemente pelíticas, são representadas por quartzo-mica xistos, mica xistos, granada-quartzo-mica xistos, granada-clorítioide-quartzo-mica xistos, calcoxistos, clorita-muscovita xistos, biotita-granada xistos, estaurolita xistos, e xistos feldspáticos, com poucas intercalações de paragnaisse e mármore, quartzitos e quartzitos micáceos. Provavelmente essas rochas tiveram seus sedimentos depositados em águas marinhas profundas. Os metassedimentos do Grupo Araxá, em sua porção leste, encontram-se intercalados com uma estreita faixa de rochas riolíticas/graníticas da Sequência Maratá (Seer *et al.*, 2001; Pimentel *et al.*, 2001, Pimentel *et al.*, 2011).

Os valores de idade modelo parecem apresentar uma distribuição bimodal, com um grupo de sedimentos entre 1,1 e 1,3 Ga, e outro entre 1,9 e 2,3 Ga. Essa bimodalidade provavelmente representa a influência de pelo menos duas fontes principais para os sedimentos do Grupo Araxá, de terrenos Paleoproterozoicos (<2,3 Ga) e terrenos mais jovens, provavelmente Neoproterozoicos (Pimentel *et al.*, 1998). Dados de U-Pb SHRIMP indicam que o Grupo Araxá foi depositado em um intervalo entre 1.0-0.8 Ga (Piuzana *et al.*, 2003a).

Os anfibolitos são derivados de protólitos basálticos toleíticos e gabróicos, e devido ao seu padrão de enriquecimento nos elementos incompatíveis, assemelham-se, em parte, a basaltos tipo E-MORB gerados em um contexto de bacia de retro-arco durante o Neoproterozoico. Esses fatores têm sido base para interpretação de que esses anfibolitos representam fragmentos de assoloce oceânico que foram tectonicamente colocados dentro dos metassedimentos do Grupo Araxá.

O padrão estrutural regional das unidades do Grupo Araxá é dominado por foliações de baixo ângulo associado com lascas de empurramento com transporte tectônico em direção ao Cráton São Francisco. Comcomitantemente há feições de estiramento com direção aproximadamente E-W, representadas por lineamentos que provavelmente corresponde a rampas laterais ou *wrench faults* originadas pelo deslocamento diferencial de

cunhas de empurrão (Strieder & Nilson, 1992). Em direção à área cratônica, as deformações tornam-se progressivamente menos intensas (Pimentel *et al.*, 1998).

3.3.3 Sequência Vulcanossedimentar de Maratá

A sequência Maratá é constituída por faixas de rochas metavulcanossedimentares, na direção N-S, que se estendem de maneira quase contínua desde Pires do Rio até Nova Aurora.

As idades modelo Sm-Nd (T_{DM}) são entre 1,6 e 2,0 Ga, e sugerem participação de crosta continental mais antiga nos magmas originais destas rochas, provavelmente Paleoproterozóicas (Pimentel *et al.*, 1999).

Esta sequência é composta na base por anfibolitos finos, metagabros finos com intercalações de metassedimentos químicos (gonditos) com a presença de metavulcânicas félsicas. Sobrepondo estas unidades ocorrem diferentes tipos de xistos, metapelitos, metagrauvacas, quartzitos micáceos e quartzo xistos (Dardenne *et al.*, 1991).

Os teores de SiO_2 apresentam composições equivalentes a dacitos e riolitos e moderados teores em álcalis mostram sua característica sub-alcalina. O excesso de Al_2O_3 em relação a álcalis+CaO confere a essas rochas caráter peraluminoso (Pimentel *et al.*, 1995)

3.3.4 Sequência vulcanosedimentar Veríssimo

Localizada entre as cidades de Ipameri e Campo Alegre, a Sequência Veríssimo é composta por um conjunto de rochas metavulcanosedimentares Paleoproterozoicas.

Formada por faixas estreitas e alongadas na direção N-S, esta pertence à base do Grupo Araxá em contato tectônico com o Grupo Ibiá e é cortada pelos granitos Sesmaria, Tambu e Encruzilhada. Seus contatos tectônicos com os Grupos Araxá e Canastra são falhas de cavagem N-S, de mergulhos baixos a médios para oeste (CPRM, 2001).

A base desta sequência é formada por clorita xistos, podendo apresentar porfiroblastos subcentimétricos de granada sobrepostos por sericita filitos com lentes de quartzito e filito carbonoso. Acima deste pacote encontram-se muscovita xistos com intercalações de clorita xistos e anfibolitos associados. Em seguida ocorrem quartzitos e quartzo xistos fortemente deformados, sendo observáveis dobras em bainha macroscópicas de escala regional e entre esses dois pacotes está inserido o Granito Encruzilhada. Por fim, o topo da sequência é constituído por granada xistos e biotita-muscovita gnaisses com porfiroclastos centimétricos de feldspato potássicos e porfiroclastos subcentimétricos estirados de plagioclásio. Comcomitantemente ocorrem rochas metavulcânicas ácidas com porfiroclastos de quartzo azul intercalados por quartzo milonitos feldspáticos (Dardenne *et al.*, 1994).

3.4 Granitos tipo-Ipameri

Próximo às cidades de Ipameri e Pires do Rio, há ocorrência de corpos graníticos sintectônicos metaluminosos e peraluminosos, do tipo "S", com texturas protomiloníticas, miloníticas e ultramiloníticas, relacionados à principal fase de deformação do Grupo Araxá. (Lacerda Filho *et al.*, 1995; Pimentel *et al.*, 1995). Encontram-se inseridos tectonicamente nos metassedimentos do Grupo Araxá ou superpostos por eles (Botelho & Moura, 1998) e possuem mineralizações de cassiterita associadas (Pimentel *et al.*, 1999).

3.4.1 Grupo Ibiá

O Grupo Ibiá é formado por metassedimentos detríticos metamorfizados em fácies xisto verde (Seer *et al.*, 2000), representados pelo metaparaconglomerado basal da Formação Cubatão e sobreposto por espesso pacote de xistos da Formação Rio Verde (Dias *et al.*, 2011).

A geocronologia do Grupo Ibiá mostra duas fontes distintas: uma Neoproterozoica primária e uma Paleoproterozoica secundária, com zircões euédricos que denotam uma fonte magmática extrusiva próxima. Sua idade de sedimentação mínima é de aproximadamente 639 ± 5 Ma (Dias *et al.*, 2011). Ao contrário, as idades encontradas na Formação Cubatão apontam uma idade de sedimentação mínima de 1154 ± 61 Ma (Dias *et al.*, 2011).

Sua relação com os grupos Canastra e Araxá é discutida, já que trabalhos mostram descontinuidade vertical e lateral em diferentes localidades. Tais peculiaridades têm sido interpretadas de duas formas: como uma discordância erosiva angular ou como um contato tectônico, devido às zonas de cisalhamento presentes entre os grupos (Figura 3.2). Outra problemática em relação ao contato entre o Grupo Ibiá e o Grupo Araxá é que pode ter natureza transicional, além da origem dos metassedimentos do Grupo Ibiá, que pode ser de origem vulcânica devido à presença abundante de plagioclásio e clorita (Seer *et al.*, 2000).

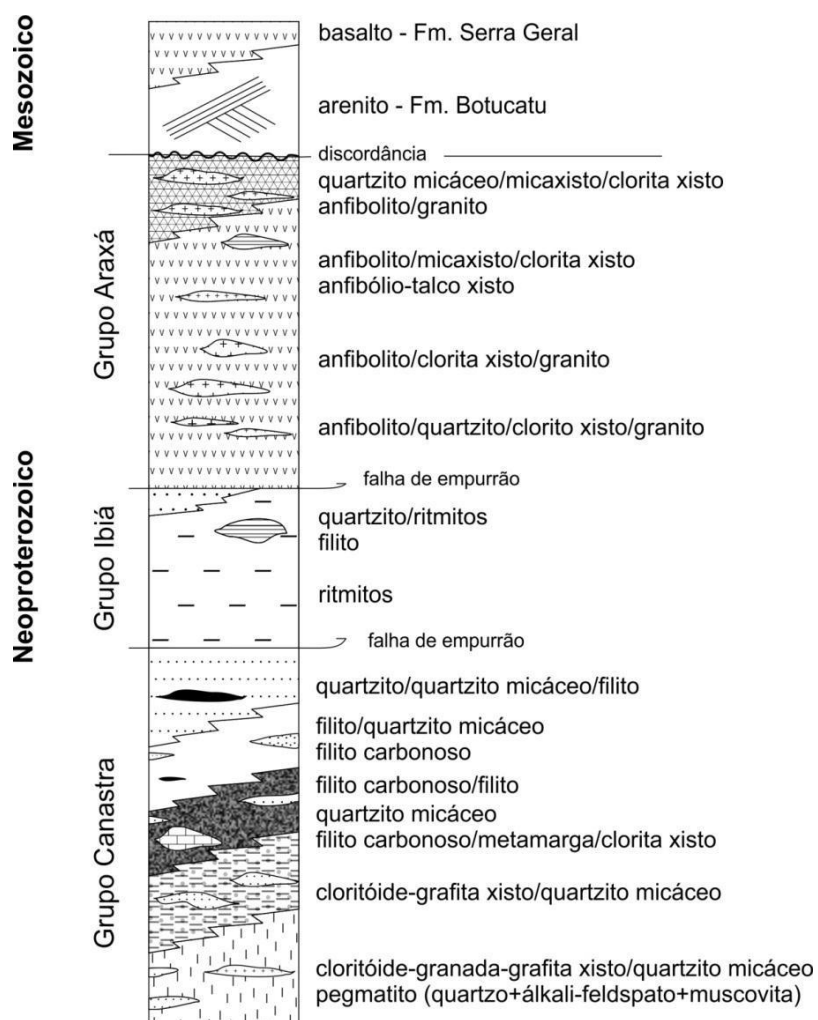


Figura 3.2 - Coluna estratigráfica dos Grupos Canastra, Ibiá e Araxá (modificado de Seer, 1999)

**FROM PASSIVE MARGIN TO CONTINENTAL COLLISION: GEOCHEMICAL AND ISOTOPIC CONSTRAINS FOR
E-MORB AND OIB-LIKE MAGMATISM DURING THE NEOPROTEROZOIC EVOLUTION OF THE SOUTHEAST
BRASÍLIA BELT**

Pedro F. Piauilino^{1*}; Natalia Hauser¹; Elton L. Dantas¹

¹ – Institute of Geosciences, University of Brasília, Brasília (DF) 70910-900, Brazil

* - Corresponding Author. Address: SQN 316 Bloco A apartment 601 – Asa Norte – Brasília/DF - 70775-010 – Brazil. + 55 61 3273-4046 / +55 61 99618-5235. E-mail addresses: pfpiaulino@gmail.com / pfpiaulino@hotmail.com

ABSTRACT

The Southeastern Brasília Belt of Central Brazil exhibits Neoproterozoic mafic rocks of amphibolite metamorphic grade that were emplaced in metasedimentary sequences related to the collision of the Amazonian and São Francisco cratons at the end of the Neoproterozoic. In the Pires do Rio-Catalão area, mafic rocks can be classified to be related to three main events: The first one, at ca. 980 Ma as recorded in U-Pb data for zircon, is related to low-K tholeiitic basalts and related alkali basalts. The low-K tholeiitic basalts have negative Rb, K, P and Ti anomalies in a primitive mantle-normalized trace element spider diagram and are LREE-enriched, similar to E-MORB source patterns. The related alkali basalts are characterized by higher La/Lu ratios, have negative Rb, K, Pb and Sr anomalies when normalized to primitive mantle, and have a chemical affinity to OIB. This event can be associated with a 1 Ga volcano-sedimentary sequence that is dominated by cratonic provenance. Sm-Nd isotopic data that give T_{DM} model ages between 1.26 and 1.4 Ga and $\epsilon Nd(t)$ values of +2.69 to +4.57 for uncontaminated MORB-like, and ca. +2.5 values for OIB-like basalts. The tectonic setting for this event would be into a continental extension of crustal thinning and mantle upwelling during passive margin development. The second mafic magmatic event, represented by Araxá Group syn-sedimentary basalts, can be related with an incipient forearc/back-arc extension at ca. 870 Ma. Although these rocks show E-MORB affinity as well, a distinct Nb-Ta negative anomaly, slightly lower $\epsilon Nd(t)$ values of +0.78 to +2.71 and older T_{DM} ages from 1.32 to 1.8 Ga suggesting a syn-subduction tectonic environment. The third event is represented by syn- to late-tectonic OIB-like basaltic/gabbroic magmatism at ca. 650 Ma, with younger T_{DM} ages at ca. 1.0 Ga and positive $\epsilon Nd(t)$ values of +1.82 to +2.57 that can be associated to regional continental collision and final closure of the Neoproterozoic ocean. These findings suggest that some tectonically superposed basins in Central Brazil might have individual association to occurrence of mafic magmatism along a timespan as wide as the long-lived evolution of the Brasília Belt (1.0-0.6 Ma). Furthermore, this scenario may be applicable to other ancient and modern scenarios worldwide.

Keywords: E-MORB; OIB; Neoproterozoic; Geochemistry; U-Pb; Sm-Nd; Brasilia Belt.

4.1 Introduction

Geochemical and isotope studies about mafic magmatism are broadly used to understand the generation, magmatic sources, geodynamic processes and in the last instance, the geotectonic setting of basalts and the metamorphosed rocks derived from them. Basalts from marginal basins worldwide usually show geochemical trends between mid-ocean ridge basalts (MORBs) and oceanic islands basalts (OIBs) end-members (Hickey-Vargas *et al.*,

2007). These signatures are controlled by several parameters, like the proximity to a plume or trench; the rate, geometry, and nature of ocean-ridge spreading; the composition, temperature and fertility of the mantle and the availability of fluids. Basalts can be present in any stage of the evolution, from the rift-drift to seafloor spreading to subduction initiation and final closure (Dilek & Furnes, 2014). Metamorphosed basic volcanic rocks, representing rests of ophiolites or basalts, are found in many orogenic belts (Donato, 1991). These rocks are often related with ocean-floor extension, but many basalts exhibit geochemical component that cannot be explained by spreading at a mid-ocean ridge (Wallin & Metacalf, 1998), maybe because they are influenced by processes related to subduction in convergent plate boundaries.

The generation of basalts in compressional settings comprehends oceanic islands, volcanic arcs and continental volcanoes environments, together with the development of associated basins. MORB and OIB geochemical end-members and its related transitional terms (e.g. back-arc basin basalts; BABBs) may occur as far separately as coeval magmatism. Debates and subsequent studies about “fingerprinting” characteristics and tectono-magmatic processes involved in many modern arch-trench systems and ancient ophiolites (as in Stern & Bloomer, 1992; Shervais, 2001; Dilek & Furnes, 2014; Pearce, 2014) investigate possible interpretations on evolution of orogenic belts.

The Brasília fold-and-thrust Belt is part of N-S Neoproterozoic orogeny along Central Brazil, developed during the convergence between the Amazonian and the São Francisco/Congo Cratons. Its passive margin sequence is characterized by a thick metasedimentary and metacarbonate Meso-Neoproterozoic rocks, developed along the São Francisco paleocontinent represented by Paranoá, Canastra and Vazante Groups; amphibolite-greenschist metamorphosed successions of intra-oceanic island arcs cycles ranging from 930-810 Ma (Mara Rosa and Arenópolis magmatic arcs) and a 670-630 Ma continental magmatic activity (Pimentel *et al.*, 2001; Laux *et al.*, 2004; Brito Neves *et al.*, 2014), with sequences of intrusive, volcanic and sedimentary rocks, represented mainly by the unit so-called Goiás Magmatic Arc and the Araxá Group interlayered with some volcano-sedimentary sequences as Maratá and Veríssimo Sequences. All geotectonic units are affected by a regional greenschist to amphibolite facies peak metamorphism that took place ca. 630-620 Ma, during the Brasiliano orogeny.

The regional geologic scenario for this work is located between tectonic sheets of passive margin (Canastra Group) and marginal basins (Araxá and Ibiá Groups; Maratá and Veríssimo metavolcano-sedimentary sequences) intruded by syn- to post-collisional granites, with the exposition of Anápolis-Itauçu high grade metamorphic core Complex. The basin is mainly composed by metavolcanic and siliciclastic rocks. Veríssimo Sequence is interpreted to be a Neoproterozoic metavolcano-sedimentary sequence composed by garnet-bearing chlorite schists, muscovite schists, phyllites, quartizes and occasionally interlayered metavolcanic acid rocks and metamafic rocks. Once attributed to be stratigraphic base of Araxá Group, the similar rock assemblage between Veríssimo Sequence and Araxá Group may induce to fair misleading when individualizing these units. Although the occurrence of mafic rocks is frequently quoted, few studies about the geological nature and age of the mafic volcanism in SE of Brasília Belt are available (e.g. Seer *et al.*, 2001; Piuzana *et al.*, 2003a; Valeriano *et al.*, 2003; Klein, 2008) along with the knowledge concerning the Veríssimo Sequence and Araxá Group roles as syn-orogenic basins and the geotectonical relation between them.

This study is focused on minor and trace, including rare-earth elements geochemical and isotope data (U-Pb and Sm-Nd) for amphibolites and host rocks within the Veríssimo Sequence and Araxá Group. The purpose of this study was to improve the geochemical, geochronological and isotopic knowledge about the mafic magmatism. We want to understand the magmatic and sedimentary sources, and the processes involved, during the evolution of the host basins. This work contributes to the understanding of the complex Neoproterozoic evolution of the southeast portion of the Brasilia Belt.

4.2 Regional Geologic Setting

Brasília Belt constitutes one of the Neoproterozoic orogenic belts within Tocantins tectonic province in Central Brazil, developed between the convergence and collision of Amazonian, São-Francisco-Congo and Paranapanema paleocontinents (Pimentel *et al.*, 2011). It constitutes more than 1100 km long folded and thrusted records of igneous associations and sedimentary sequences of island arcs and marginal basins related to extensional to collisional activity in West Gondwana during Neoproterozoic era.

Tectonically, Brasília Belt presents a general eastward vergence towards the São Francisco Craton (Pimentel *et al.*, 2011) and is sub-divided in two main segments, the northern part and the southern part, by the Pireneus Lineament – a WNW-ESE striking narrow zone of high strain (D’el Rey Silva *et al.*, 2011). Most of the sedimentary units in northern segment are well preserved; the southern segment, however, shows an intense deformation and metamorphism that obliterated the original stratigraphic relationships (Dardenne, 2000).

The southern segment of Brasília Belt exhibits different regional tectono-stratigraphic domains, from east to west (Fig. 4.1, Valeriano *et al.*, 2003): (a) the Cratonic Domain, which comprises Archean-Paleoproterozoic exposed São Francisco Craton basement along autochthonous and para-autochthonous pelitic-carbonatic covers of Neoproterozoic Bambuí Group and older minor metasedimentary successions; (b) the External Domain composed mainly by thrust systems of thick passive margin metasedimentary successions in low-metamorphic grade (Canastra, Paranoá and Vazante Groups) and subordinate Archean to Paleoproterozoic basement slivers; (c) the Internal Domain, represented by metasedimentary and metavolcanic rocks of deep-sea environment, deformed and metamorphosed under greenschist to amphibolite facies (Seer *et al.*, 2001), comprising Neoproterozoic Araxá and Ibiá Groups and Anápolis-Itauçu granilitic Complex; (d) exposures of Archean and Paleoproterozoic granite-greenstone and migmatite-gneissic microcontinent basement with Mesoproterozoic metavolcano-sedimentary rock assemblages composes the Goiás Massif; (e) and for last, the Goiás Magmatic Arc, which represents metasedimentary and metaplutonic associations with intra-oceanic island arc signature between the Amazonian and São Francisco paleocontinents with records of successive colliding magmatic arc systems. Provenance patterns for most extensive sedimentary record of South Brasília Belt are shown in Fig. 4.2.

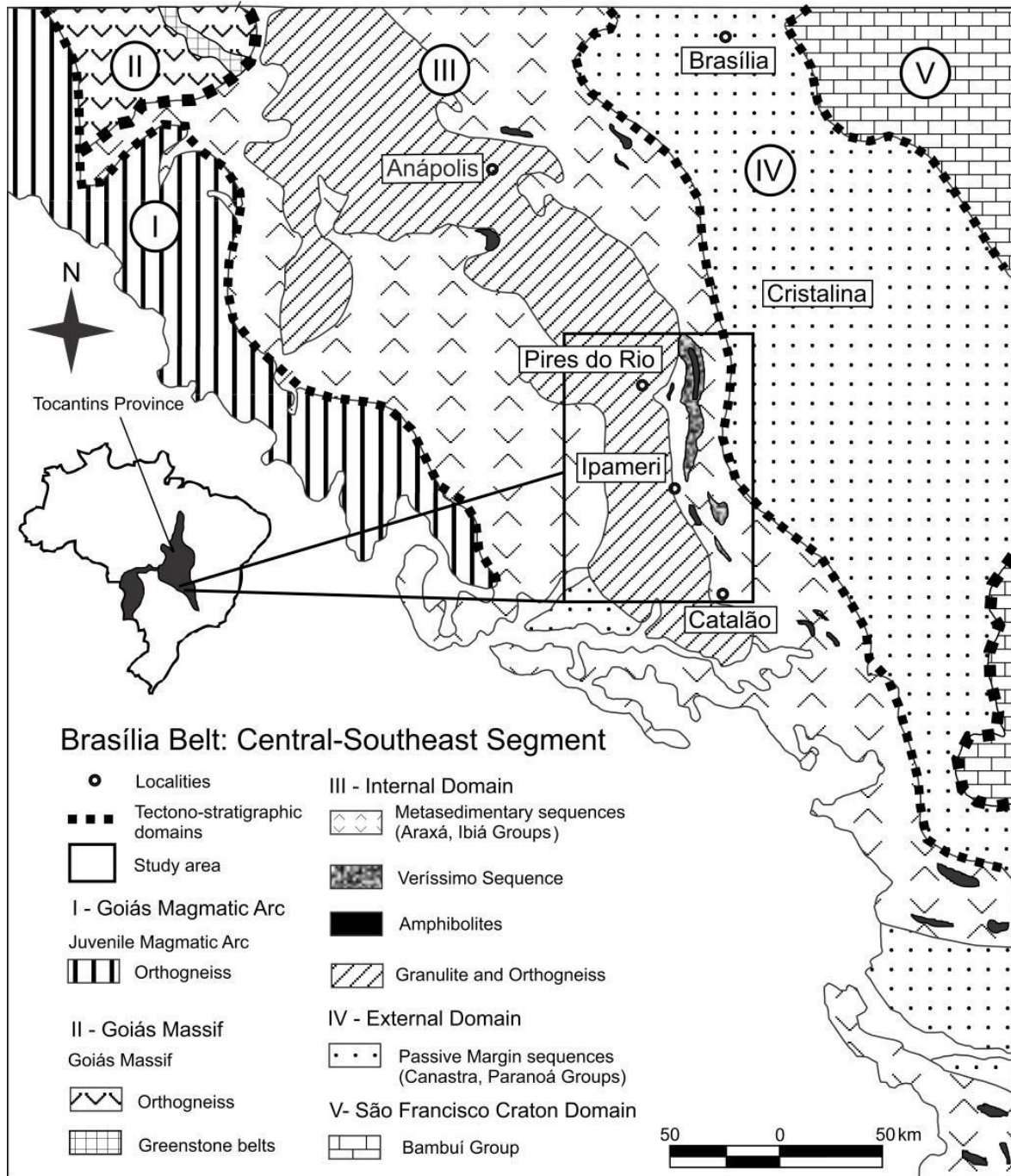


Figure 4.1 - Schematic tectonostratigraphic map of Southeast Brasília Belt. Rectangle shows the studied area (Adapted from Fuck et al., 1994).

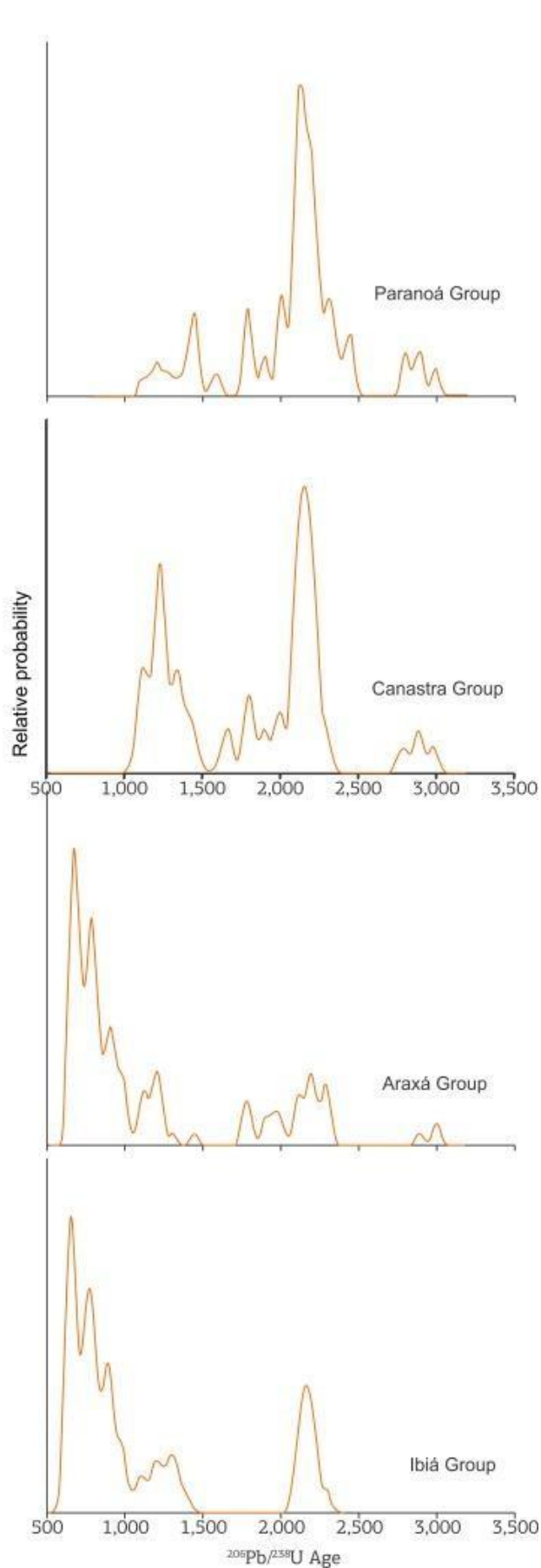


Figure 4.2 - Provenance patterns of most expressive sedimentary sequences in South Brasília Belt (from Pimentel et al., 2016).

The External Domain is represented in the studied area by Canastra Group. Considered as a lateral equivalent of Paranoá Group (Dardenne, 2000), has an extensive historical description, being characterized accordingly by its stratigraphy in different locations (Dias *et al.*, 2012) due to intense tectonism. Canastra Group is a typical platformal association of rocks formed by a regressive megacycle. This group shows Sm-Nd data providing T_{DM} ages lying between 1.5 and 2.3 Ga (Seer, 1999; Pimentel *et al.*, 2001, 2011; Rodrigues *et al.*, 2010; Dias *et al.*, 2011), suggesting Paleoproterozoic sources for these sediments probably from São Francisco Craton (Pimentel *et al.*, 2001, 2011, 2016). U-Pb data along the stratigraphic record show basal formations essentially 2000-2250 Ma detritical zircon grains with few Mesoproterozoic ages of maximum depositional age at ca. 1030-1040 Ma (Rodrigues *et al.*, 2010; Dias *et al.*, 2011; Pimentel *et al.*, 2011).

Within the Internal Domain, the metamorphic rocks of Araxá Group are represented by coarse-to-fine grained amphibolites bodies, chlorite-amphibole schists and chlorite schists. Ultramafic rocks, as serpentinites and amphibole-talc schists may occur, as well as local deposits of podiform chromite, representing a north-south ophiolitic mélange (Seer *et al.*, 2001; Pimentel *et al.*, 2001, 2011). Along the extensive occurrence, few studies about the mafic magmatism in Araxá Group were developed. Valeriano (1992) divided by their geochemistry peculiarities the amphibolites in Passos Nappe, southern-most part of Araxá Group, in two groups (high-TiO₂ and low-TiO₂), and by following Valeriano & Simões (1997) re-divided them in three particular groups: low-Ti non-fractionated, low-Ti fractionated and high-Ti. To the north, Seer *et al.* (2001) compared the amphibolite TiO₂ bimodal character near the city of Araxá with amphibolites in Passos Nappes as well the occurrences in Abadia dos Dourados (Brod *et al.*, 1992) and Abadiânia (Strieder & Nilson, 1992). Amphibolite rocks associated to Araxá Group show a tholeiitic MORB-like similarity, ranging from isotopic depleted mantle source, probably MORB source (Piuzana *et al.*, 2003a) to geochemical heterogeneous enriched mantle E-MORB sources (Valeriano *et al.*, 1992; Seer, 1999, 2000; Seer *et al.*, 2001; Valeriano *et al.*, 2003; Klein, 2008), associated to oceanic lithosphere extension, probably in a back-arc environment (Pimentel *et al.*, 1999, 2001; Seer *et al.*, 2001), although southern-most amphibolite rocks are as generated in a continental extension setting without oceanic floor generation (Valeriano & Simões, 1997; Valeriano *et al.*, 2003). U-Pb data yield crystallization ages between 838 ± 20 Ma (SHRIMP in zircon; Piuzana *et al.*, 2003a) and 958±45 Ma (ID-TIMS in rutile; Valeriano *et al.*, 2004). The metamorphic rocks associated to Araxá Group in Klein (2008) show Sm-Nd T_{DM} model ages at ca. 1.6 Ga, and $\epsilon_{Nd(t)}$ near-zero to positive values.

Metasedimentary rocks of the Araxá Group are petrographically subdivided in two sequences (Lacerda Filho *et al.*, 1999) containing micaceous quartzites and micaschists with also calc-schists, chlorite-muscovite schists, biotite- garnet schists, staurolite schists, feldspathic schists and a few paragneiss and marble intercalations. The Araxá Group was metamorphosed under amphibolite-greenschist facies conditions at around 630 Ma and was intruded by peralkalinous within-plate granites at ca. 830 Ma (Seer *et al.*, 2013); slightly peraluminous A-type granites at 798 Ma (Klein, 2008); and collisional geochemical signature granites at 637 Ma (Seer, 1999; Seer *et al.*, 2005, 2013). Differences along exposures of Araxá Group are pronounced in sedimentary detritical provenance studies. Central- north part has a dominant Neoproterozoic source in a bimodal provenance pattern ranging 0.84-0.64 Ga, with minor Paleoproterozoic input (Piuzana *et al.*, 2003a), whereas southern portions have more Archean to Paleoproterozoic and Mesoproterozoic- Neoproterozoic sources, with youngest zircons yielding ages from 1.0 to 0.9 Ga (Valeriano *et al.*, 2003, Klein, 2008). Deposition ages and tectonic environment of Araxá Group seems to have some discrepancies (Table 4.1), e.g., marginal basin with a short sedimentation time interval between 600 and 638 Ma (Piuzana *et al.*, 2003a); arc-related sediments with maximum age of deposition ca. 745 Ma (Navarro *et al.*, 2013) or sedimentation of distal passive margin-associated Araxá Group may have lasted 100-200 Ma (Valeriano *et al.*, 2003) in southern part, aged between ca. 950 and 640 Ma.

The Ibiá Group is composed by green-schist facies metamorphosed detritical sediments (Seer *et al.*, 2000), constrained by a basal para-conglomerate from the Cubatão Formation, deposited directly over Canastra Group, and superimposed by thick succession of schists with frequent carbonaceous interbeddings from the Rio Verde Formation (Dias *et al.*, 2011).

Both Araxá and Ibiá Groups show similar isotopic data (Rodrigues *et al.*, 2010), indicating multiple sources and bimodal distribution, with T_{DM} ages between 1.1 and 1.3 Ga (probably Neoproterozoic terrains), and another between 1.9 and 2.3 Ga Paleoproterozoic terrains (Pimentel *et al.*, 1998). The tectonic environment for the latter domain is widely discussed, as being early considered as distal margin passive to slope deposits (e.g. Pimentel & Botelho, 1998) but with further geochronological U-Pb and Sm-Nd data the correlation of these groups with different syn- orogenic basins have been proposed, as shown in Table 4.1.

		Geology	Tectonic setting	Amphibolite U-Pb age	Metasedimentary U-Pb age (max. sed. age)	Metasedimentary Sm-Nd T_{DM} age
Volcano-sedimentary sequences	Maratá Sequence	fine-grained amphibolites, metagabbros interbedded with chemical meta-sediments (gondites), felsic metavolcanic rocks (rhyolites), metapelites, metagraywackes, micaceous quartzites and quartz schists ³	Extensional event ¹¹	-	731 Ma ¹⁵	1.6 - 2.0 Ga ⁴
	Veríssimo Sequence	chlorite schists, sericite phyllites with quartzites lenses and carbonaceous phyllites, muscovite schists, chlorite schists, amphibolites, quartzites and quartz schists, garnet schists, biotite-muscovite gneisses, felsic metavolcanic rocks ³	Extensional continental rift ¹¹	-	-	1.77-1.86 Ga ¹¹
Araxá	North-Central	garnet-feldspar-biotite-muscovite schist, kyanite-garnet-biotite-muscovite schist, garnet quartzite and chlorite-muscovite schist ⁷	Marginal basin ⁷ , Forearc/back-arc basin ⁵	838 ± 20 Ma (SHRIMP in zircon) ⁷	North-Central: 660-640 Ma ⁷	1.0-1.26 and 1.79-2.2 Ga ⁵
	West	calc-chlorite-biotite schists, calc-chlorite-biotite feldspathic schists, calc-garnet-biotite-quartz feldspathic schists, garnet-chlorite schists, hornblend-garnet feldspathic schists, graphite schists, meta-limestone lenses, micaceous quartzites and subordinated amphibolite lenses ¹⁴	Arc-related ¹⁴	815-886 Ma (SHRIMP and ID-TIMS in zircon) ¹⁰	West: 745 Ma ¹⁴	1.12-1.46 and 1.76-2.18 Ga ¹⁴
	South	Muscovite-chlorite schists ± chloritoid, biotite-muscovite-quartz schists, garnet-muscovite-chlorite schists, chlorite-quartz schists, graphite schists, sericite schists, and hematite-sericite schists ⁹	continental extension, passive margin ^{6, 9}	958 ± 46 Ma (ID-TIMS in rutile) ⁹	South: 907 Ma ⁹	1.77-2.0 Ga ¹¹ ; 1.95 Ga ⁶
Ibiá		paraconglomerate, calcschists, calcphyllites and fine-grained quartzites ¹²	flysch-type ¹ , back-arc basin ¹² , pre- to syn-collisional ¹³	-	Cubatão Fm. - ca. 936 Ma ¹² Rio Verde Fm. - 750-640 Ma ¹²	1.16-1.46 and 1.58-2.1 Ga ¹²

1- Campos Neto *et al.*, 1984; 2 - Pimentel *et al.*, 1992; 3 - Dardenne *et al.*, 1994; 4 - Pimentel *et al.*, 1999; 5 - Pimentel *et al.*, 2001; 6 - Seer *et al.*, 2001; 7 - CPRM, 2001; 8 - Piuçana *et al.*, 2003a; 9 - Valeriano *et al.*, 2003; 10 - Laux *et al.*, 2004; 11 - Klein, 2008; 12 - Rodrigues *et al.*, 2008; 13 - Dias *et al.*, 2011; 14 - Navarro *et al.*, 2013; 15 - Sabaraense, 2017

Table 4.1 - Summary chart of isotopic data and tectonic setting interpretations for geological units whithin Pires do Rio – Catalão region.

Between thrust sheets of Araxá Group, there are two metavolcano-sedimentary sequences, known as Maratá Sequence and Veríssimo Sequence, tectonically individualized by low-angle thrust faults. Maratá Sequence is composed by fine-grained amphibolites, metagabbros interbedded with chemical meta-sediments (gondites), with presence of felsic metavolcanic rocks equivalent to dacites and rhyolites, and moderate alkali percentage shows sub-alkalic, peraluminous character (Lacerda Filho *et al.*, 1995). Above, occur different compositional schists – metapelites, metagraywackes, micaceous quartzites and quartz schists (Dardenne *et al.*, 1991). Their Sm-Nd T_{DM} ages lie between 1.6 and 2.0 Ga, and indicate the participation of older continental crust in the parental magma of this sequence, probably from Paleoproterozoic (Pimentel *et al.*, 1999). U-Pb in zircon grains of rhyolites indicate crystallization age of 794 ± 10 Ma (Pimentel *et al.*, 1992) and 791 ± 8 Ma (Klein, 2008).

Veríssimo Sequence is formed by straight and N-S elongated bodies and was once considered as belonging to the base of Araxá Group (Dardenne *et al.*, 1994) in tectonic contact with the Ibiá Group by low to medium dip thrusting faults to the west (CPRM, 2001). This sequence is made of garnet-bearing chlorite schists, sericite phyllites with quartzites lenses, carbonaceous phyllites, muscovite schists interbedded with chlorite schist and associated amphibolites, quartzites and quartz schists and metavolcanic acid rocks characterized by blue quartz (Dardenne *et al.*, 1994).

An N-S 25-km wide orthogneiss belt composed by granitoids associated often with granulites and related schists occur thrusted between the Maratá metavolcano-sedimentary sequence and over Araxá Group. This unit was divided into different geochemical and geochronological domains, which indicates a ca. 1.2 Ga exotic fragment of a possible exotic Mesoproterozoic arc; a ca. 790 Ma domain formed in active continental margin arc in subduction zone; and a ca. 640 Ma domain, in a transitional continental arc and extension rift environment, with juvenile Neoproterozoic with subordinated Meso- to Paleoproterozoic crustal reworking source (Klein, 2008).

Exposed above Araxá Group thrust sheets, there is an orogen metamorphic core known as granulitic Anápolis-Itauçu Complex. Mineralogic assemblages of some granulites may contain cordierite, spinel, rutile and zircon, beside balanced sapphirine and quartz and is suggested by Moraes *et al.* (2002) as evidence of ultra-high-temperature metamorphism at ca. 620Ma for southern part (Baldwin & Brown, 2008; DellaGiustina *et al.*, 2010). Mafic rocks within these complex yield U-Pb crystallization ages between 760 and 630 Ma, and Sm-Nd isotopic data attest strongly contaminated signature, indicating that these mafic rocks were emplaced into older continental crust (Della Giustina *et al.*, 2011).

4.3 Local Geology and Petrography

The study area is located between Pires do Rio and Catalão cities, southeast of Goiás state, Central Brazil. On the threshold between Internal and External Domains of Brasília Belt, it is a west-dipping thrust system developed during the compressional phase of Brasiliano orogeny, with most of N-S to NW-SE discontinuities (Fig. 4.3). Syn- orogenic basins such as Veríssimo and Maratá metavolcano-sedimentary sequences along with metasedimentary Araxá and Ibiá Groups are in tectonic contact with Canastra Group passive margin metasediments and a large orthogneiss belt, as tectonic sheets separated mostly by thrust faults and sometimes transcurrent faults (Klein, 2008). Besides that, there are restricted amphibolites outcrops, syn- to late-tectonic granodioritic to granitic plutons intruded in Araxá Group (Pimentel & Botelho, 1998) and the exposure of high-grade metamorphic rocks of Anápolis-Itauçu complex thrust sheet on northwestern-most part of the area. Due to the intense deformation and tectonic transport, higher metamorphic-grade rocks are placed over lower metamorphic-grade rocks. Although field observations on such geological contacts are severely obliterated by weathering and thick soil development, mapping was assisted by airborne geophysical gamma-ray spectrometry and magnetometry surveys.

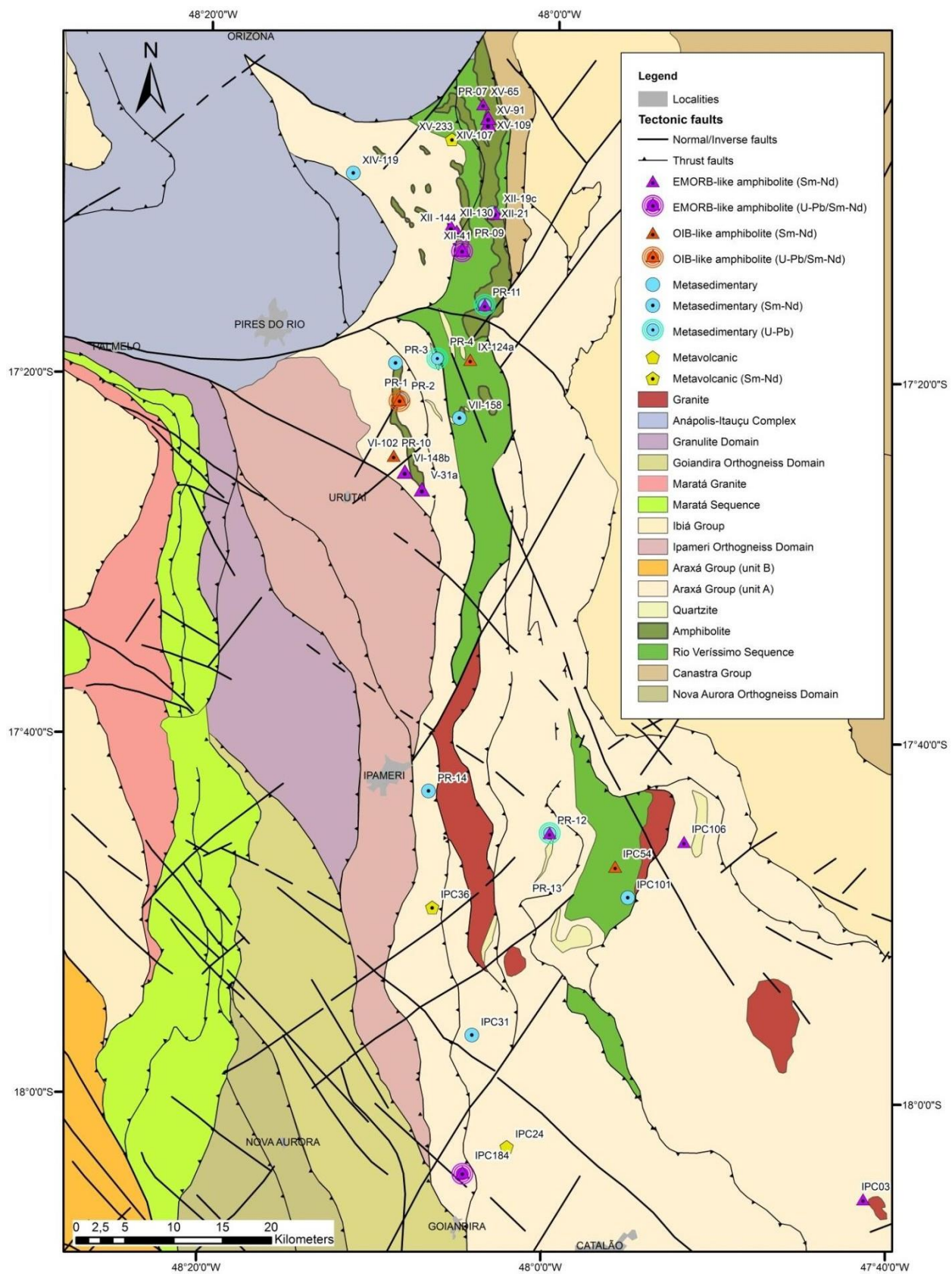


Figure 4.3 - Geological map of Pires do Rio – Catalão área

4.3.1 Amphibolites

The amphibolite rocks occur in Pires do Rio-Catalão area as elongated N-S bodies associated to both Araxá Group and Veríssimo Sequence. Besides the outcrops are not locally continuous, they are exposed as centimetric to metric sparse blocks, usually weathered, nevertheless few fresh specimens may be found.

Petrographically, the amphibolite samples are fine-to-coarse grained melanocratic metamafic rocks composed by hornblende, plagioclase and quartz, and locally garnet, leading to interpretation of basaltic to gabbroic protoliths (Fig. 4.4). The amphibole grains and elongated plagioclase are usually oriented marking the anisotropic texture. This is more commonly found at the borders of the bodies, whereas isotropic texture can be rarely found in center-most portions. Metamorphic segregation between mafic and felsic minerals may also occur.

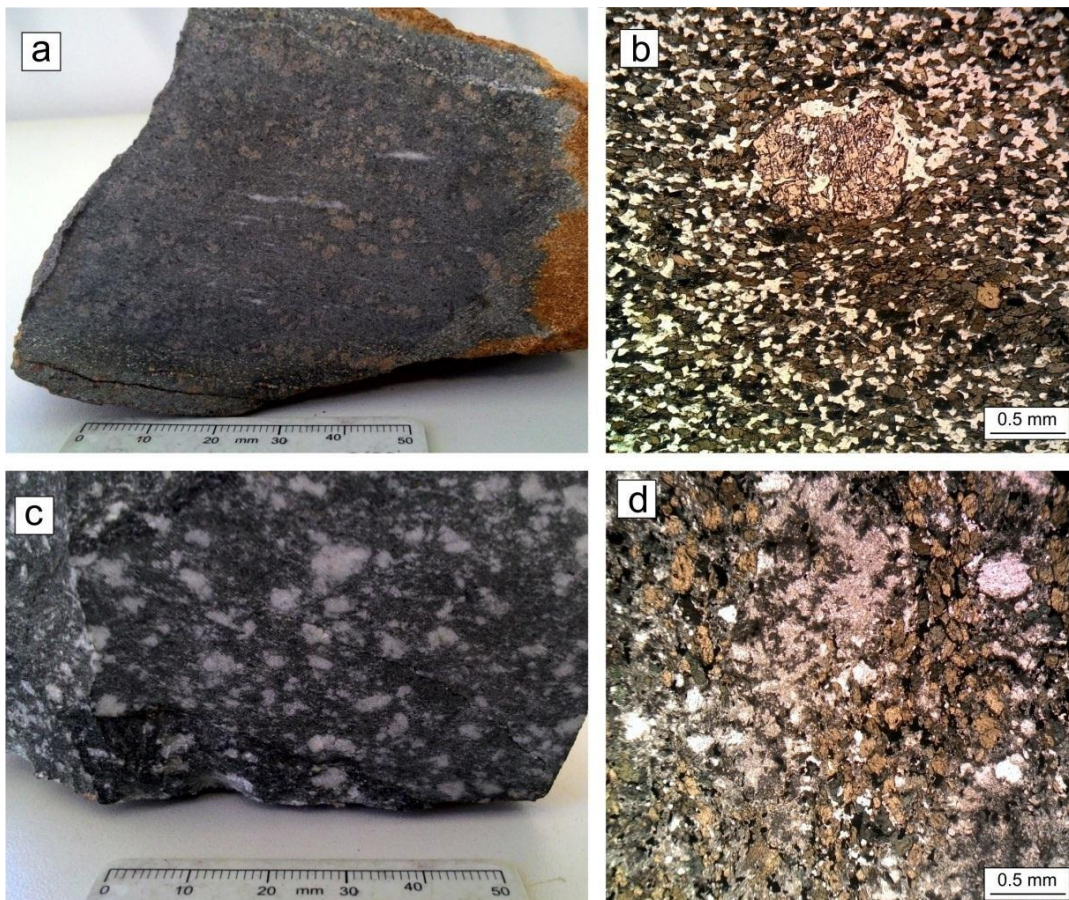


Figure 4.4 - Major macroscopic and microscopic amphibolite lithologies found in Pires do Rio – Catalão area. Images a and b show basaltic protoliths, whereas images c and d are representative for gabbroic protoliths.

In thin sections, hornblende is fine- to medium-coarsed grains in nematoblastic texture, usually associated with fine-grained to porphyritic actinolite, which can be interpreted as retrometamorphic result of hornblende. Garnet is found as pre- to syn-tectonic poikiloblasts with mostly quartz inclusions, sometimes oriented (Fig. 4.5a), and sparsely amphibole and opaque minerals, wrapped around the external foliation and presenting some reabsorption textures. Plagioclase occurs in more abundance in transitional to more magmatic evolved samples, as disseminate small grains within matrix to millimetric porphyroclasts weathered to epidote group minerals, but some grains maintain some visible relic lamellar twinning (Fig. 4.5b). The main accessory mineral is titanite, but rutile, carbonate, apatite, magnetite, ilmenite, pyrite and chalcopyrite may also occur. Quartz has undulose extinction and is disseminated as small grains, or recrystallized clusters due to possible metamorphic segregation, sometimes filling small veins which follow the

preference direction. The metamorphism reached amphibolite facies, nevertheless the mineral assemblage on thin sections show a greenschist retro-metamorphism paragenesis.

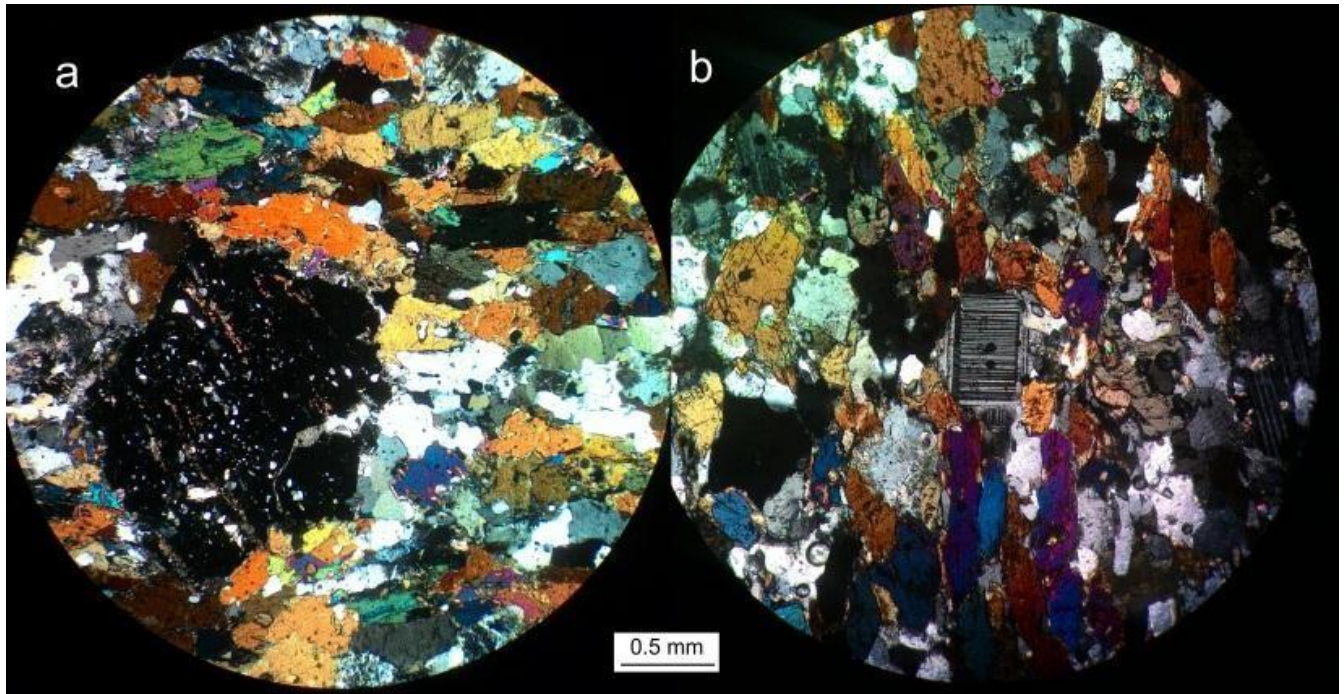


Figure 4.5 - (a) syn-tectonic garnet with oriented quartz inclusions (diagonal), and quartz stress shadows in oriented amphibole matrix (horizontal); (b) Plagioclase with lamellar twinning.

4.3.2 Supracrustal rocks from Veríssimo Sequence and Araxá Group

Araxá Group and Veríssimo sequences represent the host rocks for studied amphibolites. Araxá Group is characterized in Pires do Rio-Catalão area by the shallow marine deposits lower unit proposed by Lacerda Filho *et al.* (1999). It is composed by muscovite-chlorite schists \pm chloritoid, biotite-muscovite-quartz schists, garnet-muscovite-chlorite schists, chlorite-quartz schists, graphite schists, sericite schists, and hematite-sericite schists and micaceous quartzite. Feldspathic and calc-schists may also occur, preferentially in western-most portions.

Veríssimo Sequence is characterized by garnet-bearing chlorite schists, sericite fillites with associated quartzite and carbonaceous fillite, muscovite schists and biotite-muscovite feldspathic schists with often tourmaline (Klein, 2008). However, there was no possible to differentiate between Araxá Group and Veríssimo Sequence in petrological aspects, since both show similar mineralogy in thin sections and do not show any clear distinguishing characteristic.

In thin sections (Fig. 4.6), they are characterized by lepidoblastic texture made by well-developed grains of oriented chlorite and muscovite, preferentially following the main foliation. The textures vary from coarsely-grained schists to milotinic to ultramylonitic, and can often show S-C foliation, crenulation to chevron-like folds. The matrix is composed by microgranular quartz with undulose extinction and muscovite, but quartz may also be found as recrystallized veins and bands by metamorphic segregation. The presence of garnet is common, as syn-tectonic porphyroblasts wrapped around foliation, usually associated to chlorite, and rarely show recrystallized rims. Oriented quartz inclusions are often seen and do not follow the preferred foliation direction. Small anedral grains of biotite are also common, but have a small weight contribution in thin sections. They are mostly brownish colored with strong

pleochroism, which may be indicative of Ti-biotite. Feldspar occurs as porphyroclasts, strongly weathered to epidote group minerals, but some grains are possible to see some characteristic gemination. Occasionally, some Araxá Group schists show small carbonate grains.

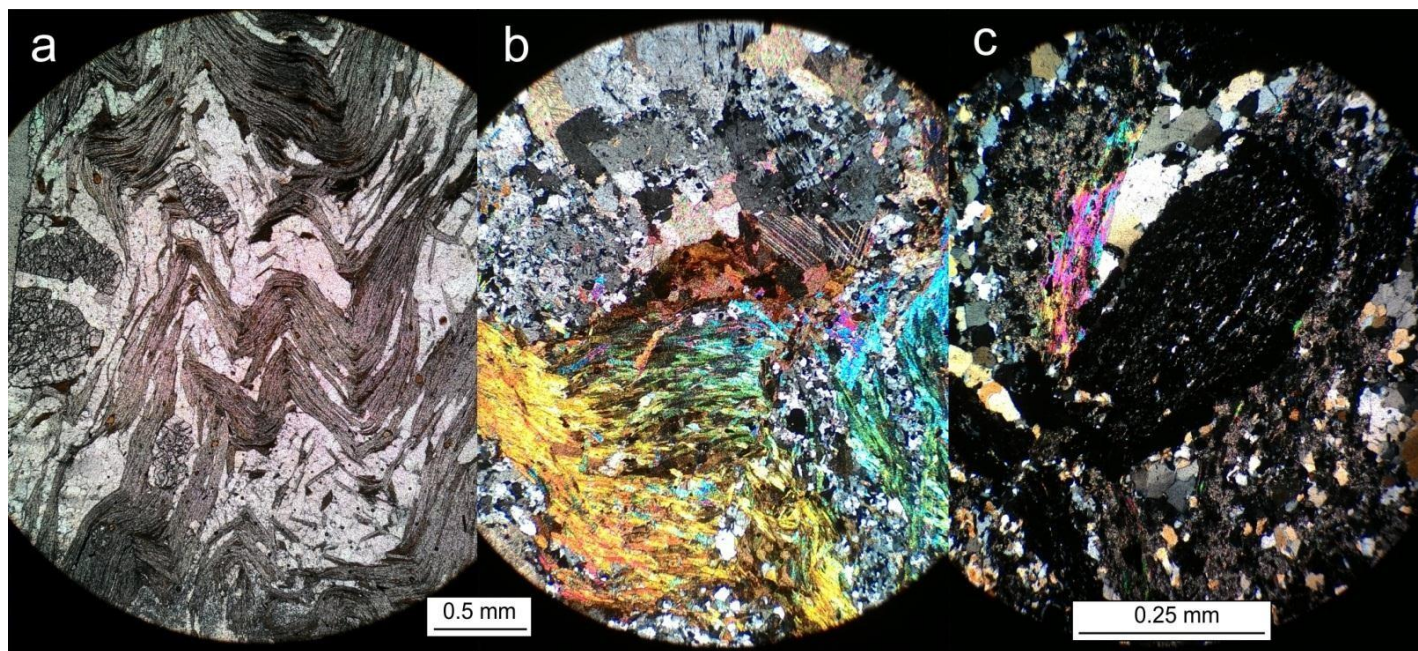


Figure 4.6 - (a) Folded chlorite schist; (b) calc-feldspar-chlorite schist; and (c) syn-tectonic garnet with reabsorption textures, recrystallized rim and quartz stress shadows.

As surrounding rocks for the amphibolite outcrops, mainly metasedimentary and metavolcanic supracrustals rocks from Araxá Group and Veríssimo Sequence were collected in order to improve the relation between mafic magmatism within the supracrustal basin sequence.

4.4 Analytical Procedures

4.4.1 Major, Trace and Rare-Earth Element geochemistry

Whole-rock samples from Pires do Rio-Catalão region were analyzed for major elements using ICP-AES, with an analytical error of $\pm 2\%$ for concentrations 50 times greater than the detection limits. Trace- and rare-earth elements (REE) were analyzed by ICP-MS, with an analytical error of $\pm 5\%$ for concentrations 50 times greater than the detection limits. In both cases, whole-rock samples were fused with LiBO₂, and digested and diluted in HNO₃. Analytical work was carried out by Acme Analytical Laboratories, Inc.

4.4.2 U-Pb

4.4.2.1 Separation and preparation procedures

Zircon concentrates were extracted from 1-10 kg rock samples by panning at different sizes (100 to 400 μm), and by magnetic separation using a Frantz isodynamic separator. After separation, the grains were placed on epoxy mounts, polished to approximately half thickness, and characterized by back-scattered electron and cathodoluminescence imaging using a JEOL QUANTA 450 scanning electron microscope at the Laboratory of Geochronology of University of Brasília. The images provided the basis for selecting locations for laser ablation analysis. The mounts were cleaned with 3% HNO₃ solution before analysis.

4.4.2.2 U-Pb analysis

U-Pb isotopic analyses were performed on zircon grains using a Thermo-Fisher Neptune HR-MC-ICP-MS coupled with a Nd:YAG UP213 New Wave laser ablation system, also at the Laboratory of Geochronology of the University of Brasília. The U-Pb analyses on zircon grains were carried out by the standard-sample bracketing method (Albarède *et al.*, 2004) using the GJ-1 standard zircon (Jackson *et al.*, 2004) in order to quantify the amount of ICP-MS fractionation. The tuned masses were 238, 207, 206, 204 and 202. The integration time was 1 second and the ablation time was 40 second. A 30 µm spot size was used and the laser setting was 10 Hz and 2-3 J/cm². Two to four unknown grains were analyzed between GJ-1 analyses. $^{206}\text{Pb}/^{207}\text{Pb}$ and $^{206}\text{Pb}/^{238}\text{U}$ ratios were time corrected. On smaller zircon grains (about 50 µm), single-spot laser-induced fractionation of the $^{206}\text{Pb}/^{238}\text{U}$ ratio was corrected using the linear regression method (Košler *et al.*, 2002). The raw data were processed off-line and reduced using an Excel worksheet (Buhn *et al.*, 2009). During the analytical sessions the zircon standard 91500 (Jackson *et al.*, 2004) was also analyzed as an external standard.

Common ^{204}Pb was monitored using the ^{202}Hg and ($^{204}\text{Hg}+^{204}\text{Pb}$) masses. Common Pb corrections were not done due to very low signals for ^{204}Pb (< 30 cps) and high $^{206}\text{Pb}/^{204}\text{Pb}$ ratios. Reported errors are propagated by quadratic addition $[(2\text{SD}^2+2\text{SE}^2)/2]$ (SD = standard deviation; SE = standard error) of external reproducibility and within-run precision. External reproducibility is represented by the standard deviation obtained from repeated analyses (n=20, ~1.1 % for $^{207}\text{Pb}/^{206}\text{Pb}$ and up to ~2 % for $^{206}\text{Pb}/^{238}\text{U}$) of the GJ-1 zircon standard during the analytical sessions, and the within-run precision is the standard error calculated for each analysis. Concordia diagrams (2 σ error ellipses), probability density plots and weighted average ages were calculated using the Isoplot-3/Ex software (Ludwig, 2003).

4.4.3 Sm-Nd

Sm-Nd isotopic data were measured at the Geochronology Laboratory of University of Brasília, on a multi-collector Finnigan MAT 262 mass spectrometer in static mode and following the methodology described by Gioia & Pimentel (2000). Whole-rock samples (ca. 50 mg powdered) were mixed with $^{149}\text{Sm}-^{150}\text{Nd}$ spike solution and dissolved in HF, HNO₃ and HCl in Savillex capsules. Cation exchange techniques were implanted for Sm and Nd extractoin of whole-rock samples using Teflon columns containing LN-Spec resin (HDEHP-di-ethylhexil phosphoric acid supported on PTFE powder). Sm and Nd samples were loaded onto Re evaporation filaments in a double filament assembly. Uncertainties for Sm/Nd and $^{143}\text{Nd}/^{144}\text{Nd}$ ratios are better than $\pm 0.5\%$ (2 σ) and $\pm 0.005\%$ (2 σ), respectively, based on repeated analyses of intern rock standards BHVO-1 and BCR-1. $^{143}\text{Nd}/^{144}\text{Nd}$ ratios were normalized to $^{146}\text{Nd}/^{144}\text{Nd}$ of 0.7219. De Paolo (1981) model was used to calculate TDM ages. Sm-Nd isochrones were calculated using the Isoplot-3/Ex software (Ludwig, 2003).

4.5 Results

4.5.1 Geochemistry

4.5.1.1 Amphibolites

Although mafic rocks from Pires do Rio-Catalão area were submitted to amphibolite facies metamorphism and some of them display high weathering processes, 18 samples were analyzed for major, minor, trace and rare-earth elements (Table 2). For comparison, 2 samples from Klein (2008) were also considered. These samples are characterized by 46.4-53.5 wt% SiO₂ with low Al₂O₃ variation (13.12-16.8 wt%) and high Fe₂O₃ values, between 10.73 to 16.85 wt%, TiO₂ (1.01-3.42%) beside low K₂O values (>1 wt%), presenting slight to moderate alteration values, with LOI ranging from 0.6 to 2.7. Samples with LOI values above 3 were discarded for major elements analysis. They show basaltic low-K tholeiitic trend protolith, where 15 samples show subalkaline affinity, and 5 samples are interpreted as having a transitional/alkaline behavior (Fig. 4.7).

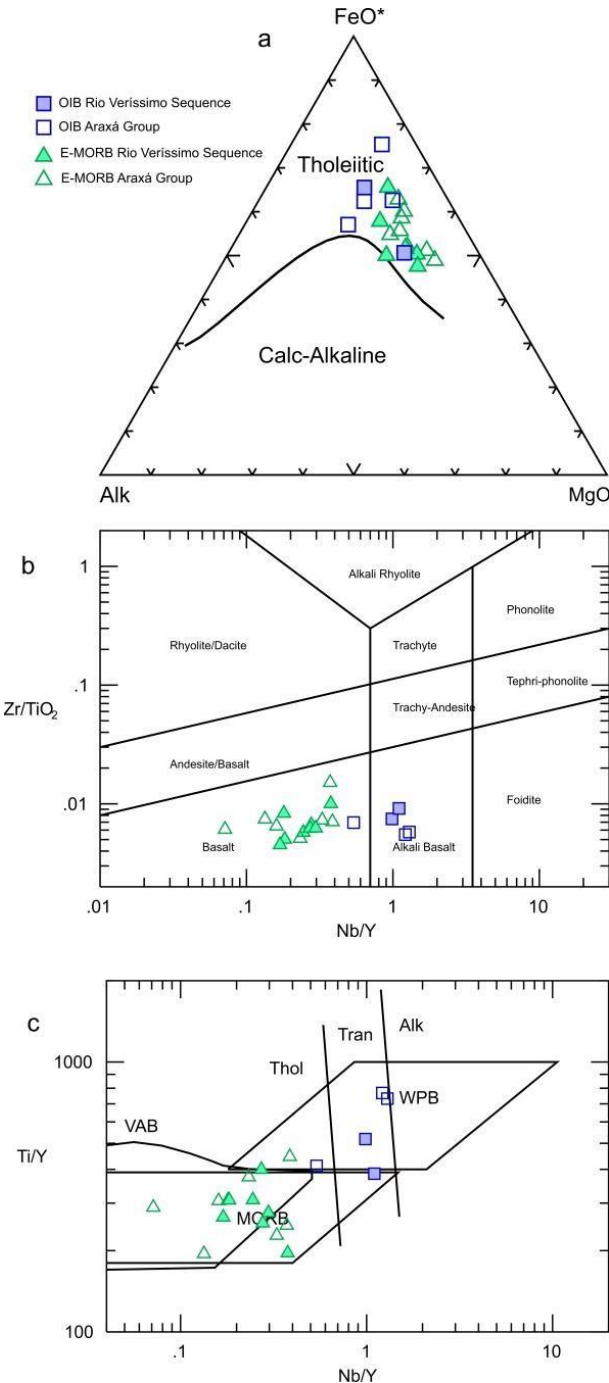


Figure 4.7 - (a)- AFM diagram (Irvine & Baragar, 1979) showing the tholeiitic affinity. (b)- Zr/TiO₂-Nb/Y diagram and (c) - Ti/Y-Nb/Y diagram (Pearce, 1982) plots evidence MORB and OIB-like samples.

TiO₂ was used as a discriminant for mafic rocks of south Brasília Belt due to their incompatibility and immobility during metamorphism and alteration processes (Dilek & Furnes, 2011). It was also used by Valeriano (1992); Brod *et al.* (1992); Valeriano & Simões, (1997); Strieder, (1994); Seer *et al.*, (2001). In this sense, two main groups of amphibolites were discriminated. Low-Ti amphibolites (TiO₂ 1.01-2.35 %wt) related to subalkaline rocks, showing higher SiO₂ (48.94%wt. average) and MgO (6.87%wt. average) contents; and high-Ti amphibolites (TiO₂ = 2.46-3.77 %wt), showing lower values of SiO₂ (46.45%wt average) and MgO (5.75%wt average), characterizing the alkaline rocks. Mg number varies from 19.22 to 45.98, which may be indicative of magma differentiation in high degree. The TiO₂ values are inversely proportional to Mg number, but directly proportional to Nb, Y, and Zr incompatible elements.

These two groups are also evidenced in chondrite-normalized rare-earth element patterns (Fig. 4.8a). Both groups show different degrees of LREE (Light Rare Earth Elements) enrichment and do not present any significant Eu anomaly. Alkaline high-Ti amphibolites show higher Σ REE, and MREE (Medium Rare-Earth Elements) concentrations and La/Lu ratios when compared to subalkaline low-Ti amphibolites, displaying more pronounced slope. In multi-element diagram normalized to primitive mantle (Fig. 8c, d), both groups show some patterns heterogeneity. However, high-Ti amphibolites have pattern similar to OIB reference sample (Sun & McDonough, 1989), with preferentially negative anomalies of Pb and LILEs (Large Ion Lithophile Elements) such as Rb, Ba, K and Sr in most samples. Subalkaline low-Ti amphibolites show trace elements pattern similar to E-MORB reference sample (Sun & McDonough, 1989) with a near horizontal slope with slightly LREE enrichment in chondrite-normalized diagram, and positive anomalies in Cs, Rb, Ba, U and Sr, locally stronger Pb and P anomalies, with small negative anomalies in HFSE (High Field Strong Elements).

In MORB-normalized diagram (Fig. 4.8b), Sun & McDonough, 1989 *in* Pearce, 2014) it is clearer an individualization between amphibolite samples MORB-like from Veríssimo Sequence and Araxá Group. The latter show a pronounced Nb-Ta negative anomaly distinguishable from other sample groups. OIB-like also show a transitional behavior whereas Veríssimo Sequence shows more similarity to reference data in both MORB- and OIB- like samples.

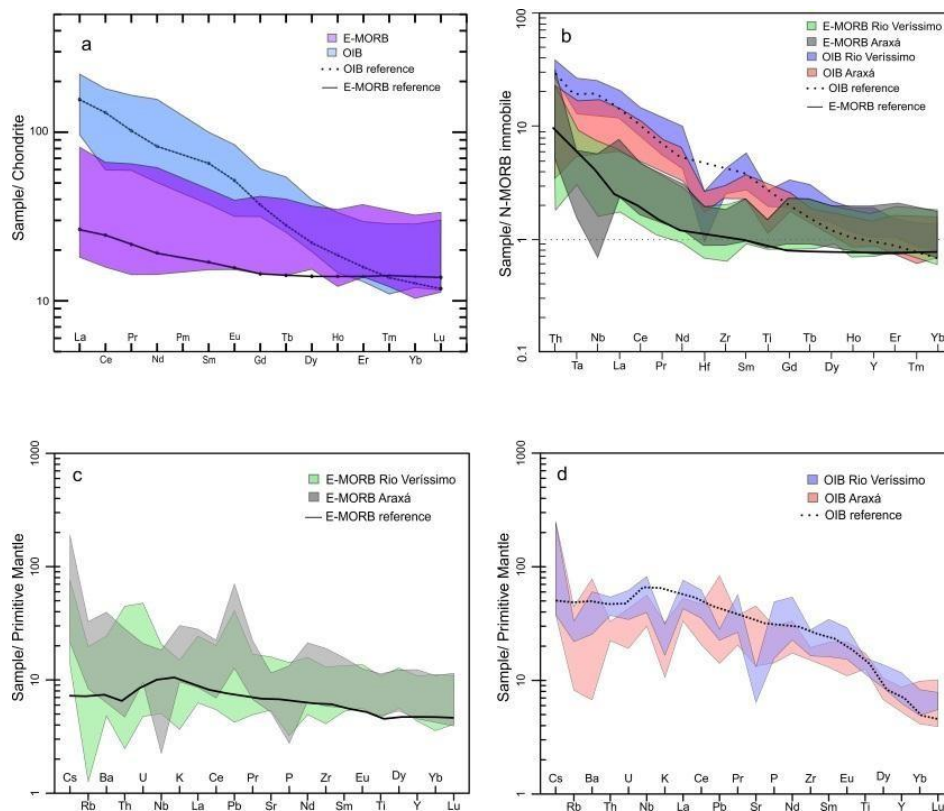


Figure 4.8 - Amphibolite samples chondrite-normalized (Sun & McDonough, 1989) (a), N-MORB normalized (Sun & McDonough, 1989) and(b) primitive mantle-normalized (Sun & McDonough, 1989) (c, d).

4.5.1.2 Supracrustal rocks from Veríssimo Sequence and Araxá Group

Nine samples from supracrustal rocks were analyzed along with 4 samples compiled from Klein (2008), where 4 samples are interpreted as volcanic-related (2 from Araxá Group and 2 related to Veríssimo Sequence), and 10 as metasedimentary rocks (6 from Araxá Group and 3 from Veríssimo Sequence)(Table 4.3).

Due to severe weathering and high grade metamorphism imposed in these rocks, major elements were not analyzed and interpreted. Minor and trace-elements of metasedimentary rocks from both Araxá Group and Veríssimo

metasedimentary sequence show a considerable variation between more juvenile sources to more evolved sources. This geochemical behavior is well observed in Th/Sc-Zr/Sc diagram (after McLennan *et al.*, 1990) , in which all samples plot between mantle-derived and upper continental crust provenance; and V-Ni-Th diagram shows the influence of mixed mafic and felsic sources in metasedimentary rocks from both units (Fig. 4.9b).

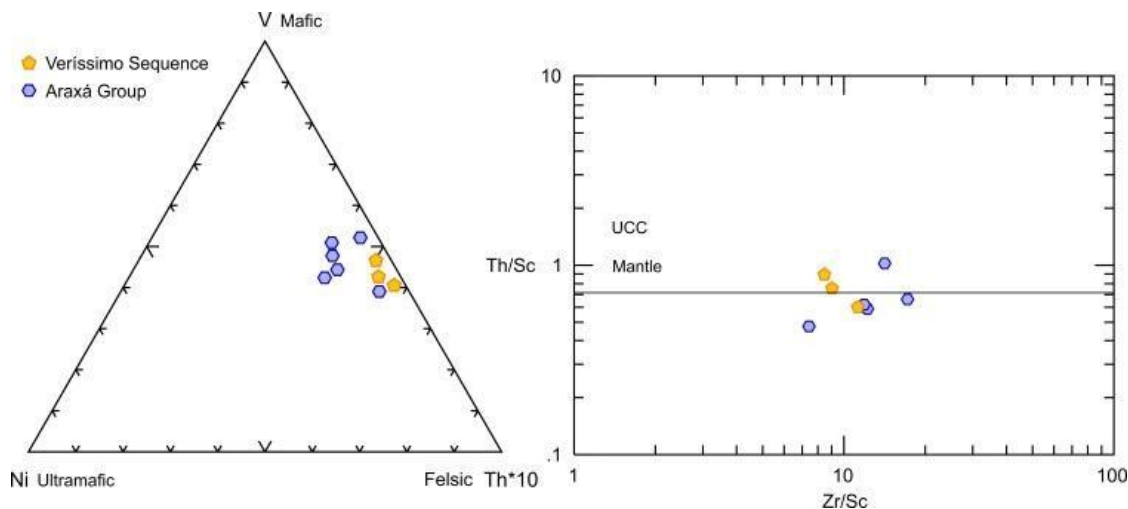


Figure 4.9 - V-Ni-Th diagram (left) and Th/Sc-Zr/Sc diagram (right) plotting metasedimentary samples with possible mixing between felsic and mafic sources.

REEs pattern normalized to chondrite (Sun & McDonough, 1989) for metasedimentary rocks from Araxá Group and Veríssimo Sequence show LREE enrichment when compared to HREE, with strong Eu negative anomaly, which can be compared to sedimentary rocks that have been affected by intracrustal differentiation (McLennan *et al.*, 1993).

Multi-element spidergram normalized to Upper Continental Crust (Taylor & McLennan, 1985) evidence Ba, Nb-Ta and Sr negative anomalies (Fig. 4.10) that can suggest influence of minor volcanic arc provenance. Nevertheless, the less spreading of Araxá Group patterns in geochemical patterns along with slightly higher Zr/Sc and Th/Sc ratios may be an indicative of more extensive sedimentary processes.

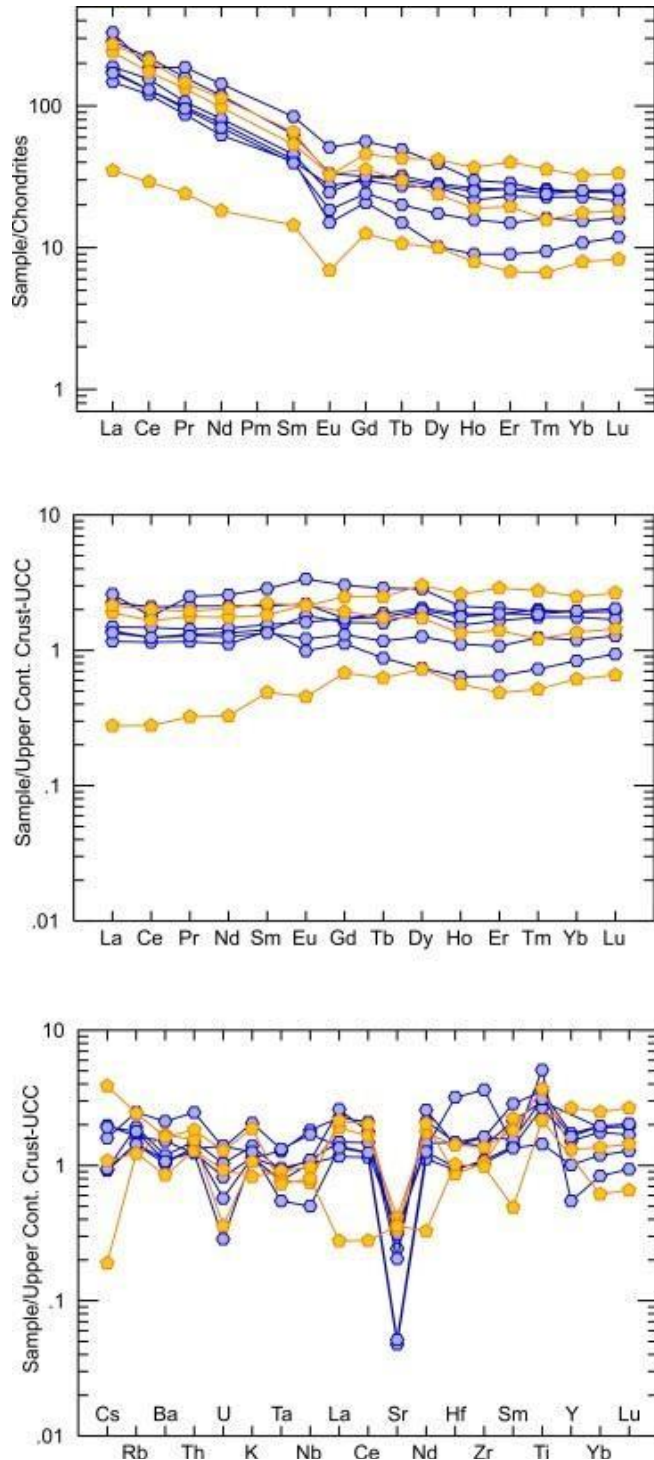


Figure 4.10 - From top to bottom: REE pattern for chondrite-normalized and upper continental crust-normalized. Bottom most diagram show minor and trace-elements normalized to upper continental crust. Symbols as in Fig. 4.9.

Metavolcanic rock samples also show different geochemical behavior between these units. Veríssimo Sequence metavolcanic rocks are characterized by higher overall minor, trace and rare-earth elements such as La, Ce, Nb, Y, Zr. On the other hand, Araxá Group is comparatively distinguished by higher values of Rb, Sc, V, Ni and Cu. On multi-element diagram normalized to primitive mantle (Sun & McDonough, 1989), Araxá Group show major Nb-Ta and La-Ce negative anomalies that are not present in Veríssimo Sequence metavolcanic samples, showing instead Cs, K, P and Ti negative anomalies (Fig. 4.11).

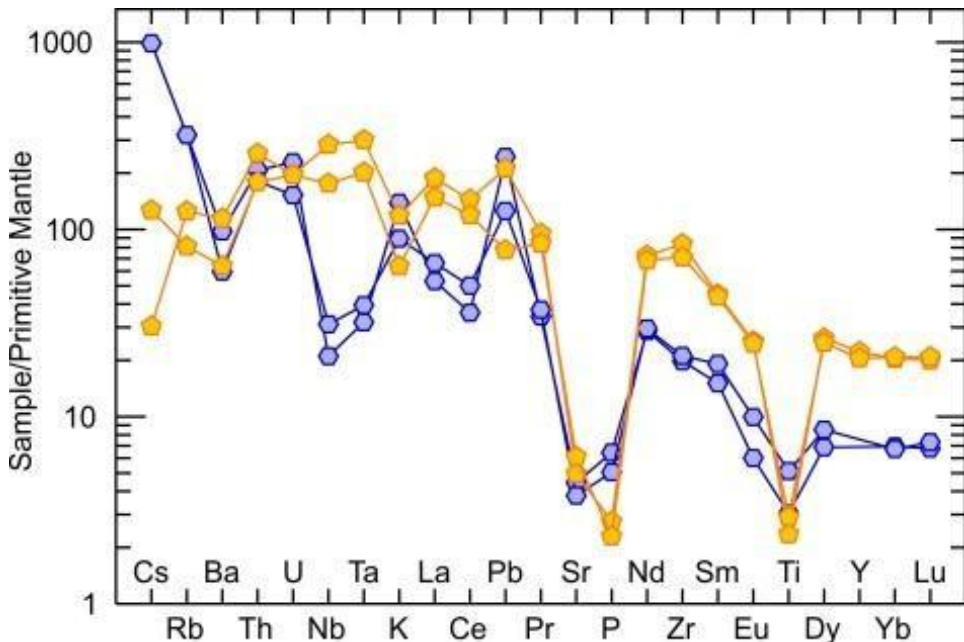


Figure 4.11 - Metavolcanic rock samples normalized to primitive mantle. Symbols as in Fig. 4.9.

4.5.2 U-Pb age data

Isotopic U-Pb composition of zircon crystals of three amphibolites were analyzed (Table 4.4): E-MORB-like (PR-09) from Veríssimo Sequence; E-MORB-like (IPC184) from Araxá Group; and OIB-like (PR-01a) intruded in Araxá Group. Were investigated zircon grains morphology and U-Pb results, since early Precambrian zircon often imprints a complex evolution history (e.g. Kröner *et al.*, 2014). All samples show complex internal structures of lighter and darker domains in zircon imaging (Fig. 4.12) interpreted as zircon recrystallization/regrowth and/or Pb-loss during post-emplacement metamorphic and tectonic events.

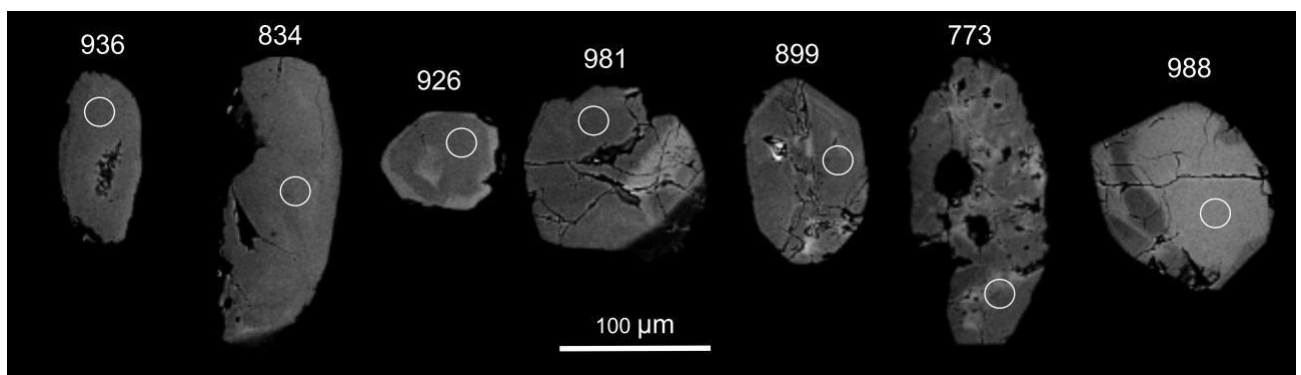


Figure 4.12 - Zircon backscattered images of sample PR-09 and associated U-Pb age exemplifying complex internal structures represented by lighter and darker domains.

4.5.2.1 Sample PR-09:

Sample PR-09 is characterized by E-MORB signature comprising medium- to fine-grained amphibolite with garnet porphyroblasts, roughly foliated, in a slightly more elevated topography in Veríssimo Sequence.

The zircon crystals from this sample are 100-250 µm, rounded short bipyramidal shapes, with color varying from transparent to pinky and brownish shades. Most of the crystals show in backscattered electron image irregular zoning, fractures and a variable amount of mineral inclusions (Fig. 4.12).

U-Pb analyses were obtained from 28 zircon grains, 9 were discarded because of analytical errors and 6 zircon grains showed 95-105% concordance values, enabling Concordia age at 979.4 ± 17 Ma (Fig. 4.13a). Small population of discordant $^{207}\text{Pb}/^{206}\text{Pb}$ ages from Neoarchean/Paleoproterozoic is found and it is here interpreted as inherited grains, reworked from the cratonic area eastern of the study area.

4.5.2.2 Sample IPC184:

Sample IPC 184 is a sparse block of amphibolite within Araxá Group, next to tectonic contact with the orthogneiss unit. The sample represents E-MORB-like amphibolites from Araxá Group. From 43 zircon grains, 12 were discarded due to high analytical errors and only 5 showed 95-105% of concordance. Most concordant zircon ages vary from 813-875 Ma, allowing to obtain a Concordia age of 870.7 ± 4.1 Ma (Fig. 4.13b). Minor $^{207}\text{Pb}/^{206}\text{Pb}$ discordant populations of Meso- to Paleoproterozoic ages for inherited zircon grains and younger discordant ages are attributed to Pb-loss.

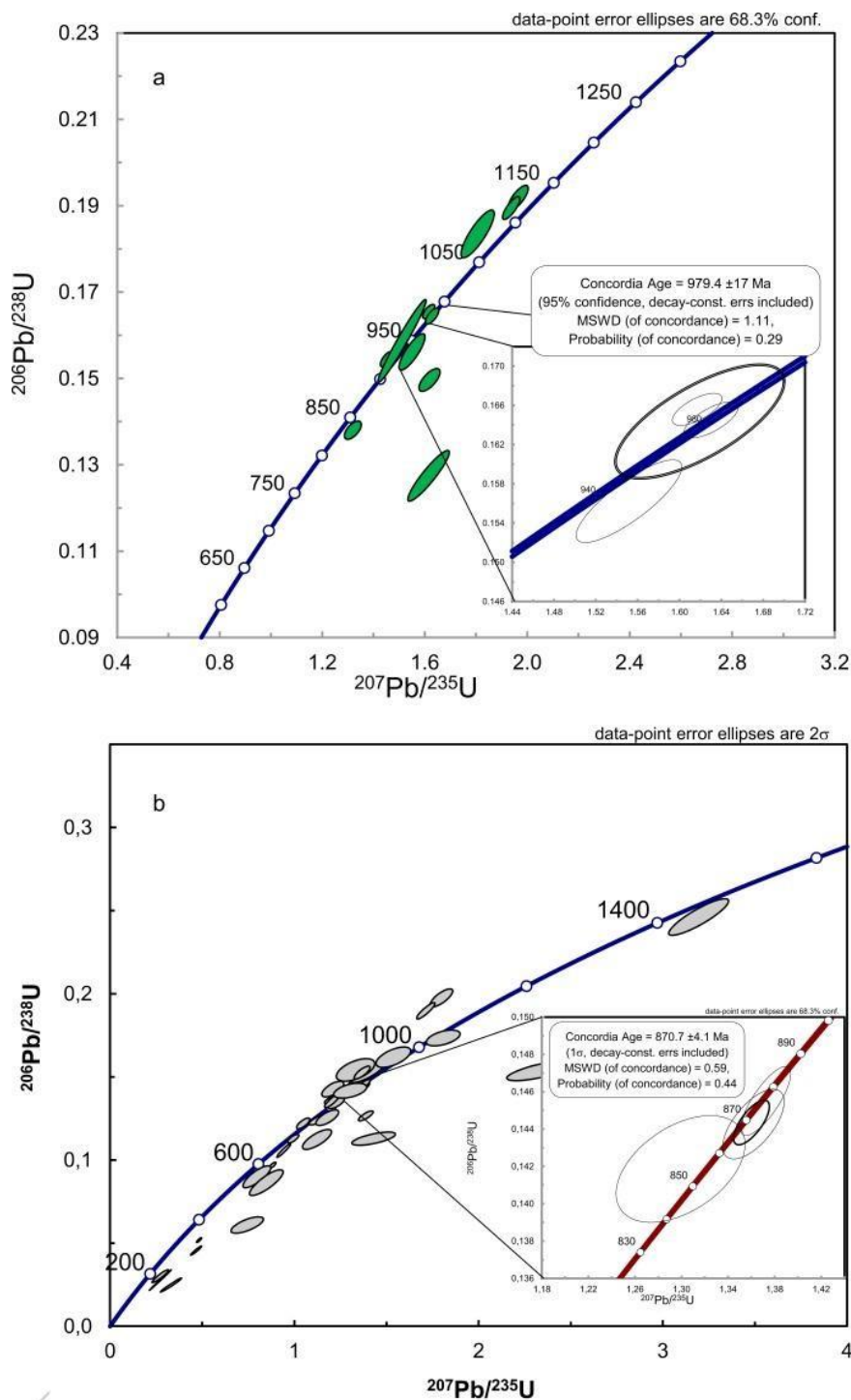


Figure 4.1 - Concordia ages for (a) PR-09 Veríssimo Sequence MORB-like and (b) IPC 184 Araxá Group MORB-like.

4.5.2.3 Sample PR-10

Sample PR-10 is a small block of gabbroic amphibolite within Veríssimo Sequence, and presents an OIB affinity. From 29 zircon grains, 13 were not used for age calculations and 8 showed 95-105 % of concordance. PR-10 sample concordant zircon age is of 819.7 ± 6.3 Ma (Figure 4.14), and more discordant Neoproterozoic population presents ages between 728.9 to 823.3 Ma, due to Pb-loss.

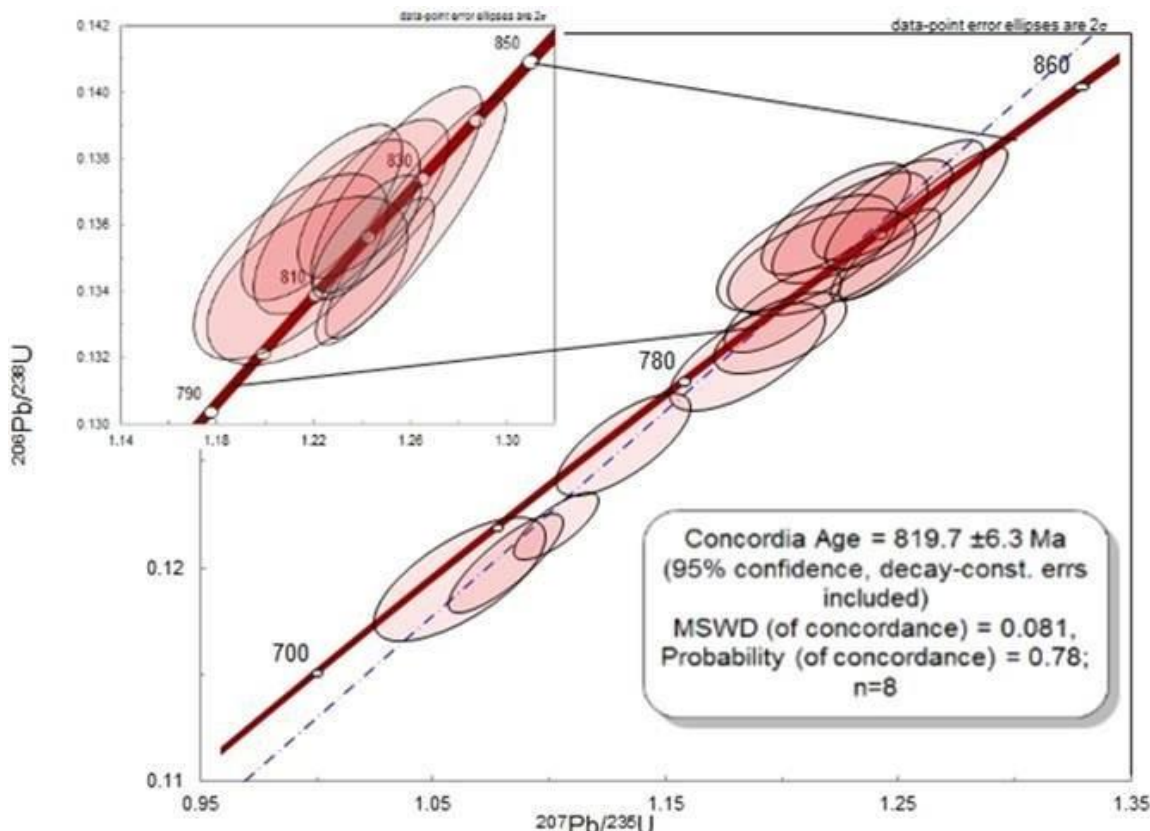


Figure 4.13 - Concordia age of sample PR-10 Grupo Araxá OIB-like.

4.5.2.4 Sample PR-01a:

OIB-like sample PR-01a from Araxá Group is interpreted as a gabbroic amphibolite, characterized by elongated milimetric plagioclase crystals, in a medium to fine grained amphibolite matrix. It is associated with a considerable intrusive body in Araxá Group, next to orthogneiss domain and Anápolis-Itauçu Complex tectonic contacts.

The crystals from this sample are 150-200 µm transparent to pink, and the backscattered electron images show two groups (Fig. 4.14): one represented by slightly rounded crystals, homogeneous with few inclusions and less fractured; the other more broken and fractured is represented by more elongated prismatic crystals, zoned, with more inclusions. The latter group is related to zircon grains inheritance, with older and more discordant ages.

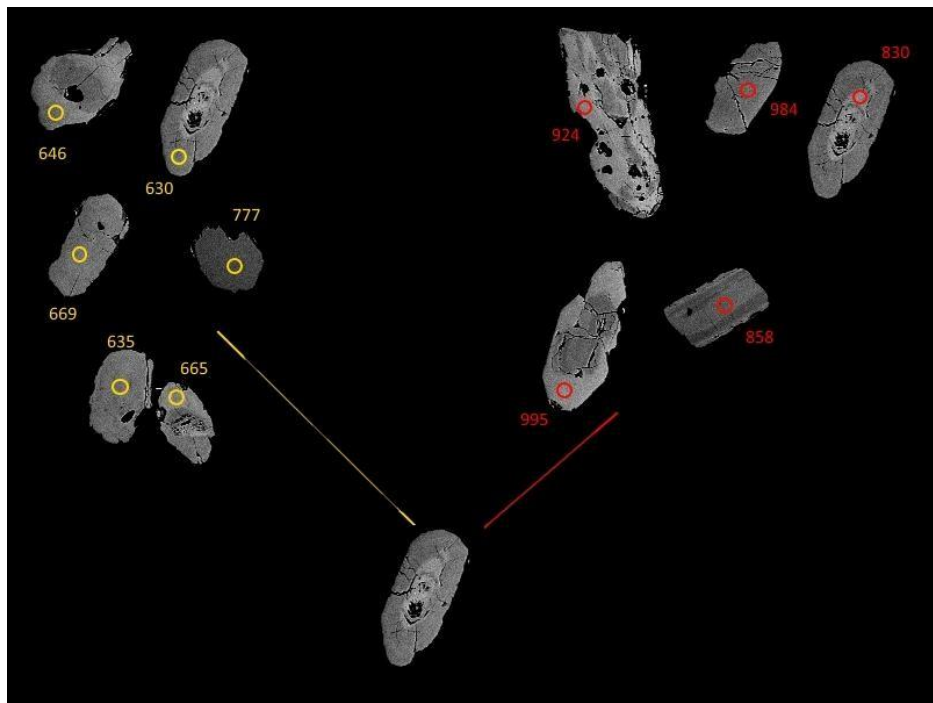


Figure 4.14 - Zircon grains from OIB sample PR-01a and its respective analized U-Pb ages.

U-Pb analyses were performed on 30 zircon grains, which 9 were discarded because of high analytical errors and 11 have concordance between 95-105%. Zircon grains have an expressive Neoproterozoic population of 618-697 Ma (42.86%), and yield Concordia age of 651.7 ± 6.5 Ma (Fig. 4.15).

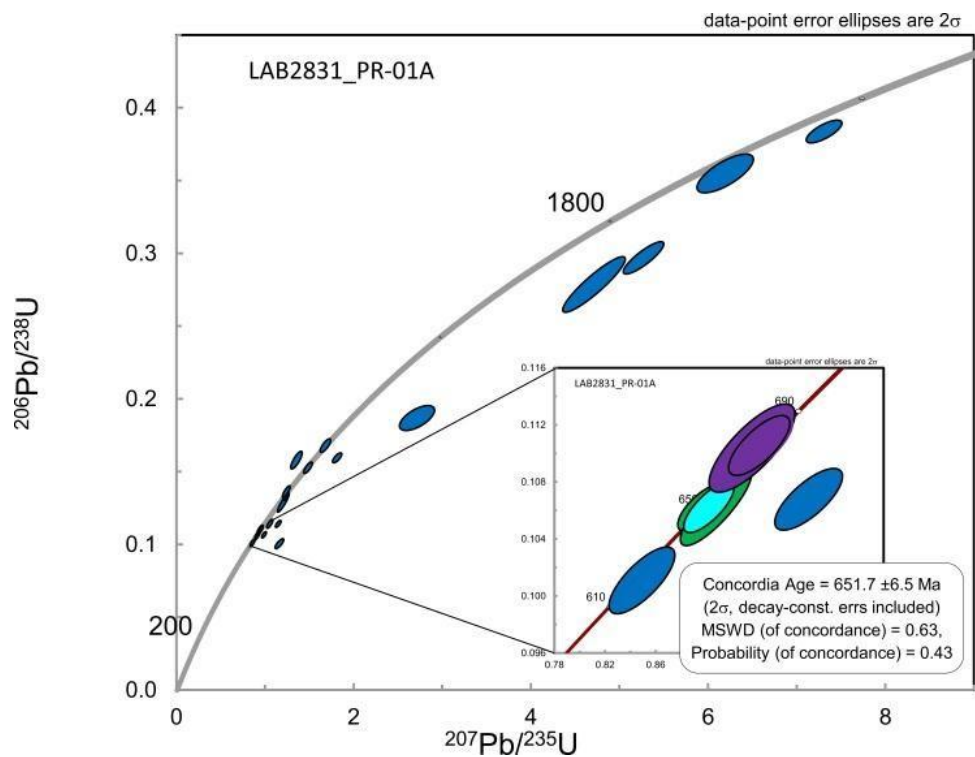


Figure 4.15 - Concordia age for PR-01a OIB-like amphibolite.

The youngest Neoproterozoic population show overall low Th/U ratios ($\text{Th}/\text{U} < 0.1$) that commonly could be related to metamorphic zircons. Nevertheless, cathodoluminescence imaging of internal structures from rim and core of these grains show zonation correlated to magmatic processes (Fig. 4.16), such as zircon overgrowth over inherited older cores and thus may represent recycling of zircon grains from previous geologic events. The substantial percentage population of ca. 650 Ma zircon grains over the total amount analyzed, and the presence of older but concordant U-Pb ages also constrain a magmatic affinity, being interpreted as the age of crystallization.

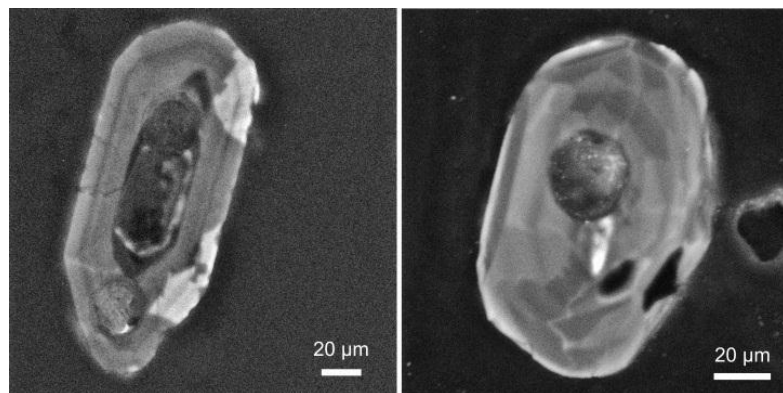


Figure 4.16 - Cathodoluminescence imaging from low Th/U ratios zircon crystals of OIB-like amphibolite. Magmatic zonation and overgrowth are remarkable and allow an igneous provenance for these crystals.

4.5.3 U-Pb provenance data

For provenance analysis of metasedimentary rocks, probability density plots of U-Pb data (Table 5) from 3 distinct stratigraphic position samples of the studied area are shown (Fig. 4.20). All samples show two groups of zircon grains based on morphology and internal structures: one represented by overall small zircon grains (150-200 μm), subrounded and showing homogeneous internal structures in backscattered and cathodoluminescence image, with incipient metamorphic rims; and other group represented by elongated grains of 150-300 μm , essentially broken and fractured, with higher amount of inclusions and showing oscillatory or convolute zoning, with some pronounced rim overgrowth over previous cores. Morphology from zircon grains and U-Pb data did not exhibit any clear correlation.

4.5.3.1 PR-04:

Is a NW-SE quartzite ridge from Veríssimo Sequence, stratigraphically above chlorite schist and near tectonic contact with Araxá Group, in central portion of the study area. 65 zircon grains were analyzed from this sample, from which 36 zircon grains show 95 to 105% of U-Pb concordance.

Two main population grains are evidenced (Fig. 4.17): one between 938 and 1536.9 Ma, representing 41.67% of analyzed zircon grains; an older population between 1715 and 2190.3 Ma, representing 50% of analyzed zircon grains; few Archean zircons from 2.7 and 3.1 Ga, 8.33% of total analyzed zircon grains. The weighted average age of the youngest peak ($n=4$) indicates a maximum depositional age of 1015 ± 66 Ma.

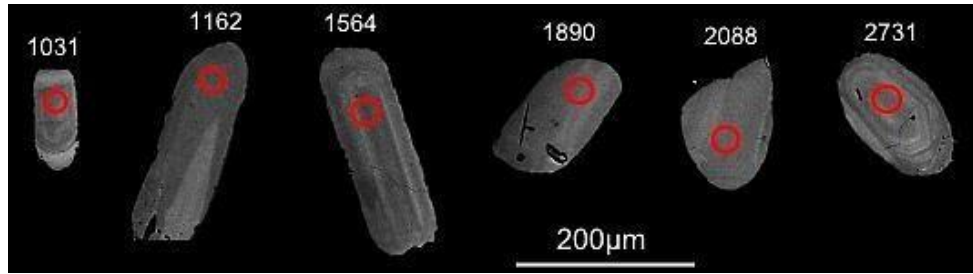


Figure 4.17- Representative zircon grains from main populations of sample PR-04 and its analyzed ages (circles, in Ma).

4.5.3.2 PR-11b:

Surrounding outcropped of amphibolite with E-MORB like affinity in Veríssimo Sequence, correspond to a chlorite schist located south of main amphibolite body of this sequence. 15 from 28 zircon grains analyzed have 95-105% U-Pb concordance. It is evidenced three main zircon grains populations (Fig.4.18): a 1206.9-1341.6 Ma population, corresponding to 17.86% of total; a 1726.6-2074 Ma population (28.57%); and few Archean zircon grains, from 2.1 and 2.9 Ga, 7.14% from all analysis. Youngest peak show a weighted average age of 1220 ± 20 Ma for maximum depositional age.

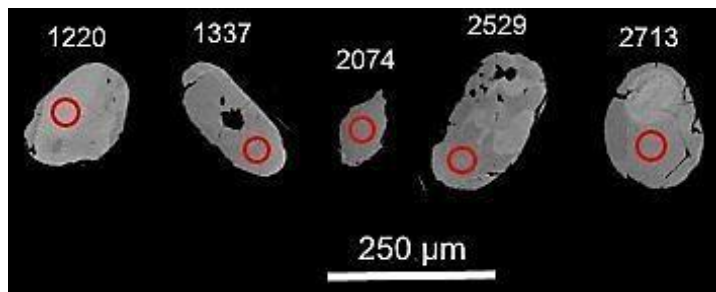


Figure 4.18 - Representative zircon grains from main populations of sample PR-11b and its analyzed ages (circles, in Ma).

4.5.3.3 PR-12b:

The chlorite schist PR-12b sample is interlayered with amphibolite outcrop, related to Araxá Group tectonic sheet, in an intermediate stratigraphic level between Veríssimo Sequence and orthogneiss unit. It shows zircon grains with morphologies similar to PR-11b. From 73 analyzed zircon grains which 42 data present concordant values between 95-105%. Three main zircon grain populations were observed in this sample (Fig.4.19): a younger population between 900 and 1300 Ma, comprising main peaks with ages of 959.4-1003.5 Ma (5.48%); a group of 1078.5-1346 Ma (19.18%) grains; a greater population (28.77%) with ages between 1735.5 and 2163.6 Ma; and few Neoarchean zircon grains, aged 2.6-2.7 Ma (4.1%). The younger population allow to define a maximum depositional age of 976 ± 17 Ma.

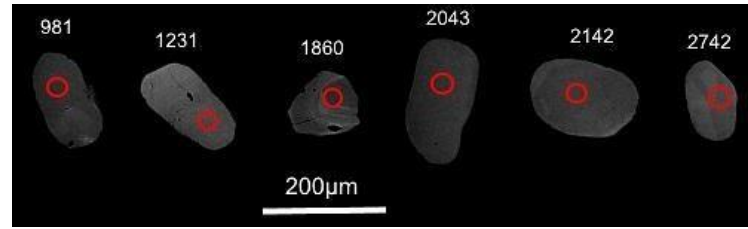


Figure 4.19 - Representative zircon grains from main populations of sample PR-12b and its analyzed ages (circles, in Ma).

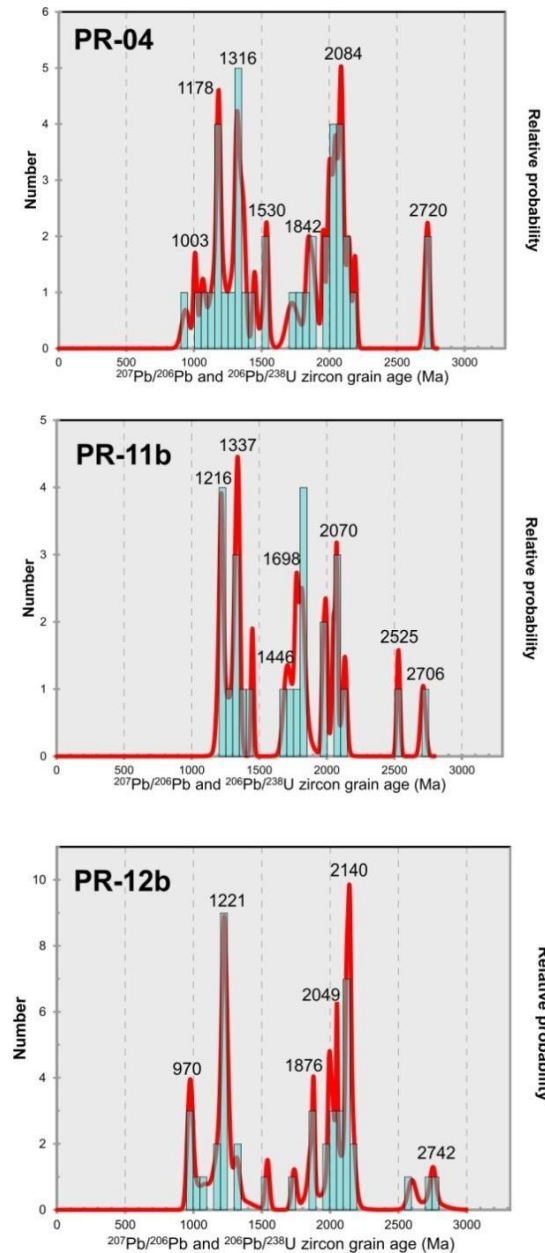


Figure 4.20 - Probability density plots for analyzed metasedimentary samples.

4.5.4 Sm-Nd results:

4.5.4.1 Amphibolites:

The initial $^{143}\text{Nd}/^{144}\text{Nd}$ ratios were recalculated using the interpreted U-Pb crystallization age for the analyzed amphibolites and then extrapolated to similar geological and geochemical groups (Table 6).

Sample	Sm (ppm)	Nd (ppm)	$^{143}\text{Nd}/^{144}\text{Nd}$ (measured)	$\pm 2\sigma$	$^{143}\text{Nd}/^{144}\text{Nd}$ (initial)	$^{147}\text{Sm}/^{144}\text{Nd}$	$\epsilon_{(0)}$	$\epsilon(t)$	$T_{\text{DM}}(\text{Ga})$	t (Ga)
Veríssimo Sequence										
E-MORB amphibolites										
XV-109	4.537	17.300	0.512530	(16)	0.511594	0.1585	-2.11	+2.69	1.40	0.98
PR-09	5.154	21.052	0.512217	(2)	0.511265	0.1480	-8.21	-2.11	1.84	0.98
XII-41	4.857	20.146	0.512152	(7)	0.511292	0.1457	-9.48	-3.09	1.92	0.98
XII-19c	3.977	13.510	0.512751	(5)	0.511349	0.1780	+2.20	+4.57	1.26	0.98
XII-144	5.382	17.977	0.512646	(13)	0.511637	0.1810	+0.16	+2.13	-	0.98
PR-11	3.928	12.785	0.512801	(5)	0.511705	0.1857	+3.18	+4.57	-	0.98
XV-65	2.306	7.470	0.512727	(7)	0.511625	0.1866	+1.74	+3.01	-	0.98
XV-91	2.478	7.728	0.512846	(3)	0.511319	0.1938	+4.06	+4.43	-	0.98
OIB amphibolites										
IX-124a	7.243	32.591	0.512388	(3)	0.511330	0.1343	-4.88	+2.95	1.26	0.98
IPC54	14.800	70.710	0.512296	(12)	0.511591	0.1265	-6.67	+2.14	1.30	0.98
Metasedimentary										
PR-04	0.946	4.929	0.511868	(6)	0.511107	0.1160	-15.02	-4.91	1.79	0.98
IPC101	2.090	8.560	0.512007	(11)	0.511039	0.1475	-12.31	-6.15	2.26	0.98
Metavolcanic										
XV-233	20.568	104.710	0.512330	(20)	0.511629	0.1187	-6.01	+3.78	1.16	0.98
Araxá Group										
E-MORB amphibolites										
VI-123	6.689	26.369	0.512521	(3)	0.511666	0.1534	-2.28	+2.55	1.32	0.87
V-31a	4.918	18.482	0.512572	(14)	0.511622	0.1608	-1.29	+2.71	1.35	0.87
XII-130	3.518	12.629	0.512582	(8)	0.511710	0.1684	-1.09	+2.06	1.51	0.87
IPC106	3.770	13.890	0.512509	(11)	0.511540	0.1641	-2.52	+1.11	1.59	0.87
VI-148b	3.957	14.857	0.512474	(9)	0.511640	0.1610	-3.20	+0.78	1.60	0.87
IPC03	3.960	13.840	0.512604	(22)	0.511708	0.1730	-0.66	+1.98	1.58	0.87
PR-12a	2.438	8.310	0.512607	(13)	0.511851	0.1774	-0.60	+1.55	1.80	0.87
XII-144	5.382	17.977	0.512646	(13)	0.511637	0.1810	+0.16	+1.91	-	0.87
IPC184	3.540	10.500	0.512733		0.511865	0.2038	+1.85	+1.07	-	0.87
OIB amphibolites										
PR-10	9.807	49.079	0.512427	(2)	0.511912	0.1208	-4.12	+3.85	1.03	0.82
VI-102	8.003	38.536	0.512428	(9)	0.511910	0.1255	-4.10	+3.37	1.08	0.82
PR-01a	6.835	26.903	0.512586	(3)	0.511932	0.1536	-1.01	+2.57	1.18	0.65
Metasedimentary										
IPC31	9.040	52.600	0.511753	(8)	0.511071	0.1039	-17.26	-5.64	1.75	0.98
PR-02	4.036	22.610	0.511786	(15)	0.510865	0.1079	-16.62	-5.50	1.77	0.98
PR-03	5.529	29.231	0.511833	(11)	0.510857	0.1143	-15.70	-5.39	1.84	0.98
PR-12b	4.492	24.866	0.511660	(9)	0.510728	0.1092	-19.08	-8.12	2.00	0.98
PR-14	0.943	3.432	0.511923	(19)	0.510615	0.1660	-13.95	-10.13	-	0.98
Metavolcanic										
IPC36	6.480	33.950	0.511829	(8)	0.511059	0.1174	-15.78	-6.97	1.87	0.87
IPC24	7.760	38.950	0.511787	(6)	0.510997	0.1204	-16.60	-8.13	1.98	0.87

Table 4.2 - Sm-Nd data for rocks in Pires do Rio – Catalão area.

The enriched E-MORB-like samples from Veríssimo Sequence, recalculated to U-Pb age of ca. 980 Ma, show T_{DM} varying from 1.40 to 1.92 Ga and $\epsilon_{\text{Nd}(t)}$ values between +4.57 to -3.09. Data are correspondent to average data from Goiás Magmatic Arc, which is indicative of juvenile Neoproterozoic sources. Sm-Nd isochron age from E-MORB

like amphibolites from Veríssimo Sequence gave an age of 987 ± 34 Ma (MSWD = 2.7), matching with U-Pb data for this suite (Fig.4.21).

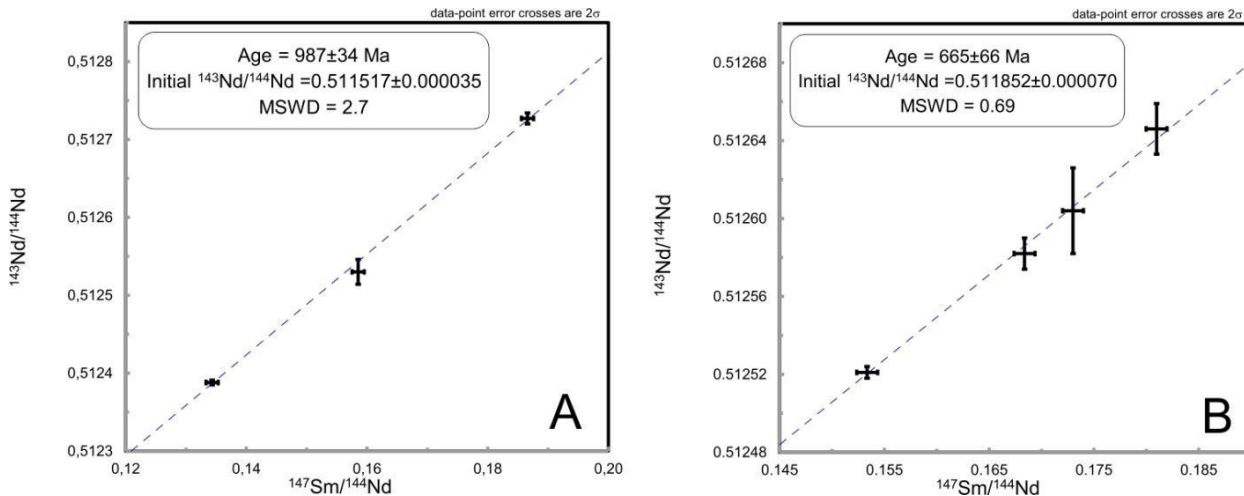


Figure 4.21 - Sm-Nd isochron ages for MORB-like amphibolites from Veríssimo Sequence (A) and Araxá Group (B).

OIB-like samples from Veríssimo Sequence is here assumed as coeval to E-MORB magmatic event within this unit, and thus were recalculated to 980 Ma as well. They show T_{DM} ages at 1.26-1.30 Ga and positive $\epsilon_{\text{Nd(t)}}$ values between +2.14 and +2.95.

Araxá Group amphibolites with an E-MORB affinity were recalculated taking in consideration U-Pb age of ca. 870 Ma. They show a range in T_{DM} ages, from 1.32 to 1.80 Ga and $\epsilon_{\text{Nd(t)}}$ positive values from +2.55 to +0.78 respectively. Deviation of data might be caused by observed wider geochemical patterns which include transitional geochemical affinities, variable degrees of system fractionation or even crustal reworking. In Nd evolution diagram (Fig. 4.19), the samples show a flatter slope when compared to Veríssimo Sequence, but Araxá MORB-like amphibolites show isochron age of 665 ± 66 Ma (MSWD = 0.69) (Fig. 4.21), that high-amphibolite facies metamorphism may have influenced the system opening for this unit, since the age achieved is near from the peak of metamorphism in South Brasília Belt instead of yielded isotopic U-Pb ages for these rocks.

OIB-like amphibolite samples intruded in Araxá Group yield younger T_{DM} ages between 1.03-1.18 Ga when compared to OIB-like of Veríssimo Sequence, and similiar positive $\epsilon_{\text{Nd(t)}}$ of +1.82 to +2.57.

4.5.4.2 Supracrustal rocks from Veríssimo Sequence and Araxá Group:

The Sm-Nd analyses on supracrustals rocks from Veríssimo Sequence and Araxá Group were obtained in 13 samples, from those 10 samples are metasedimentary rocks and 3 samples are metavolcanic rocks. All metasedimentary samples were recalculated to the maximum depositional age of 980 Ma, and metavolcanic samples where recalculated to the metabasic rocks ages of each unit.

Metasedimentary rocks from Araxá Group show T_{DM} ages ranging from 1.16 to 3.22 Ga and $\epsilon_{\text{Nd(t)}}$ from +3.78 to -10.13. Two samples analysed from Veríssimo sequence, show T_{DM} ages of 1.79 and 2.26 Ga and $\epsilon_{\text{Nd(t)}}$ of -4.91 and -6.15. In $\epsilon_{\text{Nd(t)}}$ evolution diagram (Fig. 4.22), both metasedimentary rocks plot between older Paleoproterozoic sources from São Francisco Craton and Goiás Magmatic Arc, displaying significant mixture from these sources, but with a major influence of São Francisco Craton provenance.

Metavolcanic sample, XV-233 from Veríssimo Sequence, has younger T_{DM} age of 1.16 Ga and positive $\epsilon Nd_{(t)}$ value of +1.87 for the ca. 980 Ma magmatism. It is differently from Araxá Group metavolcanic rocks, that is characterized by high negative $\epsilon Nd_{(t)}$ values and higher T_{DM} ages, correlated to associated metasedimentary record of this unit.

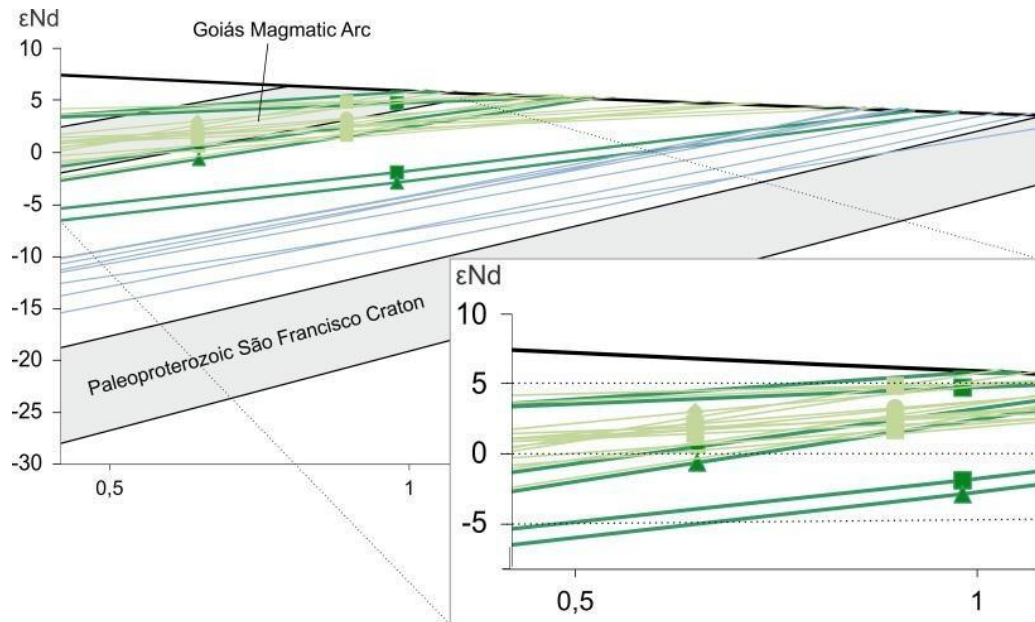


Figure 4.22 - Nd evolution diagram. Light green - Veríssimo Sequence; dark green - Araxá Group; light blue - supracrustal rocks.

4.6 Discussions

4.6.1 Tectonic setting of mafic magmatism

Geochemical fingerprint for ancient oceanic lithosphere are useful for determination of tectonic environment and geologic processes involved in mafic magmatism generation. The use of immobile element proxies within geochemical systematics for identification and classification of mafic rocks are broadly recommended (as in Dilek & Furnes, 2011; Pearce, 2008, 2014), due to metamorphism and alteration during generation, emplacement and exposure during its evolution history.

The Th-Nb proxy in Th/Yb-Nb/Yb diagram (Pearce, 2008, 2014) is indicative of crustal input (enrichment by crustal contamination, subduction, and alteration by crustal fluids or crustal recycling). Although Th-Nb enrichment is markedly visible in MORB-normalized multi-element and Th/Yb-Nb/Yb diagrams (Fig. 4.23), most of samples show low Th/Nb ratios, which can be interpreted as high degree of melting caused by extensional decompression and subsequent asthenosphere upwelling. Transitional basalts and some MORB-like samples from Araxá Group show high La/Nb and Th/Nb high ratios that, due to its near-vertical trend display (Th enrichment) in Th/Yb-Nb/Yb diagram, can be interpreted as magma-crust interaction or a volcanic arc affinity. Th enrichment relatively to Nb may be achieved also because of element mobility during melting and presence of high-temperature aqueous fluid in amphibolite facies metamorphism, and more susceptible when rocks are interlayered with volcano-sedimentary or mélange sediments (Pearce, 2008), in which may be the case for Pires do Rio-Catalão area, where rocks reached high amphibolite facies and plot samples above the MORB-OIB array.

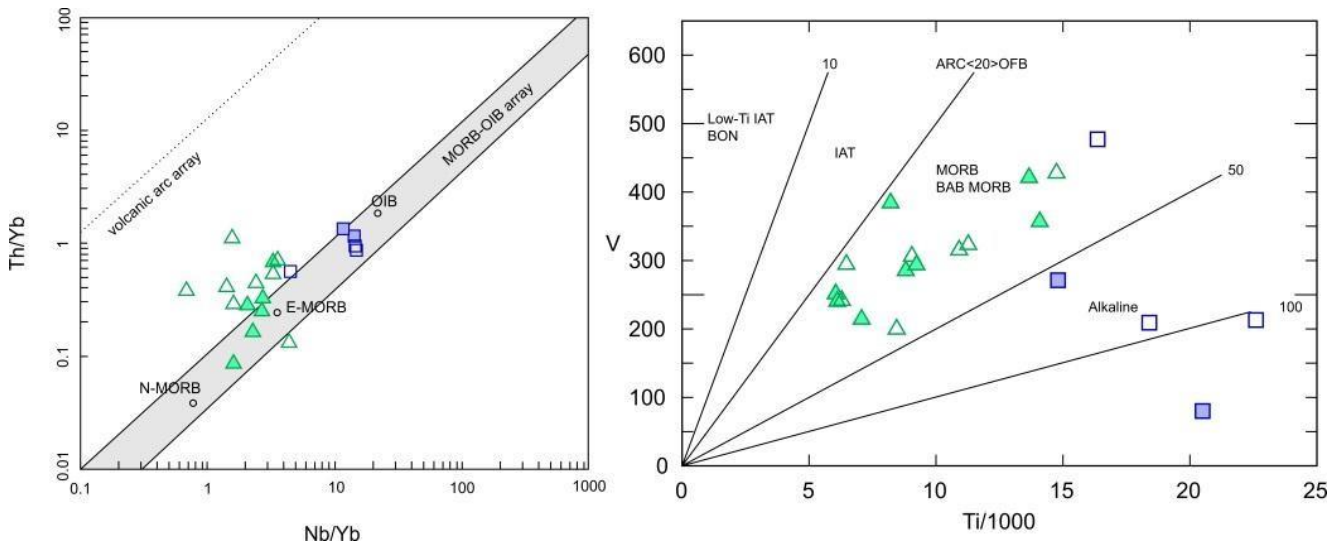


Figure 4.23 - Th/Yb-Nb/Yb diagram and V-Ti diagram for amphibolite samples. Symbols as in Fig. 4.7.

In V-Ti diagram (Fig. 4.23), MORB-like samples from both units plot within MORB and slab-distal BAB/FAB field in a supra-subduction zone. Subduction process generates an extensional event on fore-arc, intra-arc to back-arc environment, due to hinge rollback and sinking of new slab edge. Subduction fluids produce a high melting and latter an enrichment of the mantle wedge, as well as a possible attenuation on the continental lithosphere.

4.6.1.1 *E-MORB amphibolites from Veríssimo Sequence and Araxá Group*

Although Veríssimo Sequence and Araxá Group MORB-like amphibolites have an overall slight LILE and LREE enrichment with flat MREE and HFSE pattern, distinctive characteristics between them are remarkable. The amphibolites from Veríssimo Sequence do not show pronounced Th and Pb enrichment or the Nb-Ta negative anomaly that was observed in the amphibolites emplaced in Araxá Group. It is evidence that the amphibolites from Veríssimo Sequence could be emplaced in a subduction-unrelated setting at approx. 980 Ma, as seen in U-Pb geochronology and Sm-Nd isochron.

Southeastern Brasilian Belt amphibolites are often related to continental extension/lithospheric thinning and to the possible beginning of ocean floor generation, and are marked by pelagic and hemi-pelagic sediments from continent margin of São Francisco-Congo Craton, locally related to ophiolitic melâne. LILE and LREE enrichment can be related to magma-crust processes as the influence of less-depleted subcontinental lithospheric mantle (Dilek & Furnes, 2011) and crustal contamination. This can be supported by older T_{DM} ages reflecting the influence of mantle overflowing of older magmatic sources related to São Francisco-Congo cratonic lithosphere. Similarly, E-MORB character is also explained where cooler, shorter melting columns hence less degree of melting and thus generate an enriched source (Pearce, 2014). This model is supported by Bowen diagrams (Fig. 4.24; Dilek & Furnes, 2011) and V-Ti diagram (Fig. 4.23), where MORB-like samples are plotted within fields characterized as subduction-unrelated continental margin in TiO_2 , SiO_2 and MgO contents and V/Ti ratio. TiO_2-Yb proxy for melting depth (Pearce, 2008, 2014) show a diagonal trend between deep melting OIB compositions and shallow melting MORB (plume-ridge interaction), trending to Primitive Mantle composition (Fig. 4.25). This can be an indicative of mantle upwelling during crustal thinning in an extensional tectonic setting

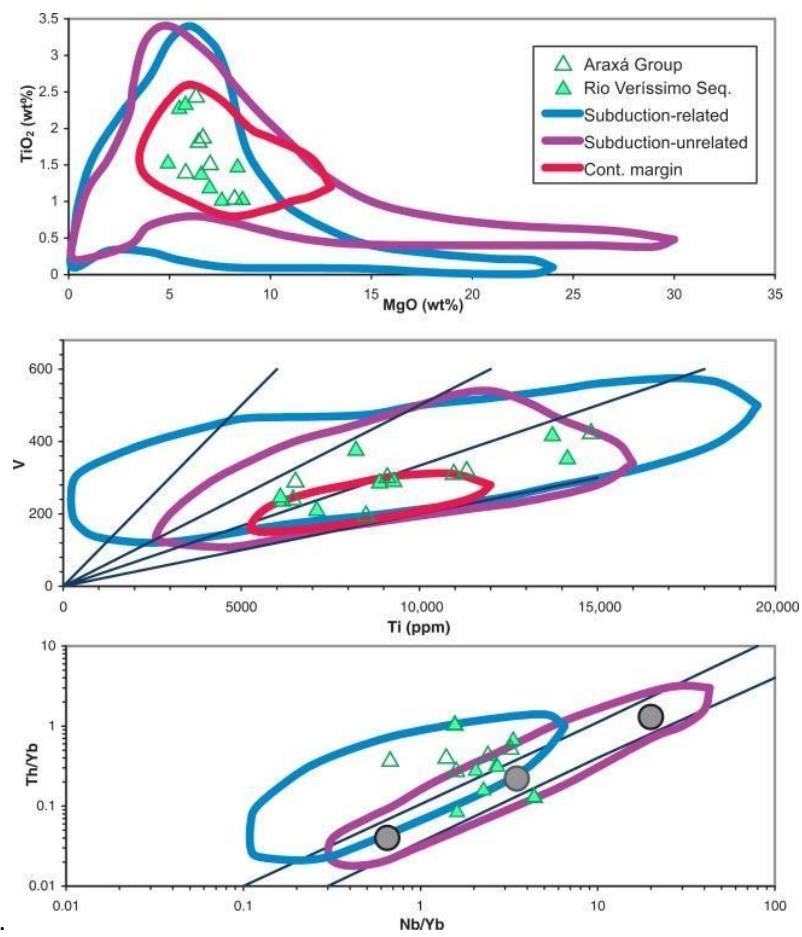


Figure 4.24 - Bowen diagrams (after Dilek & Furnes, 2011), showing the possible subduction-unrelated correlation for Veríssimo Sequence MORB-like basalts.

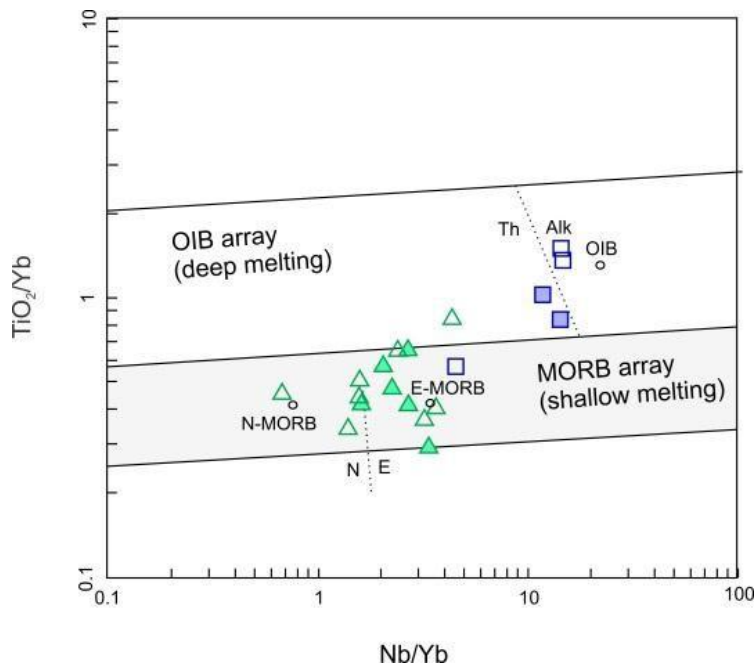


Figure 4.25 - TiO_2/Yb - Nb/Yb diagram showing a possible diagonal trend between MORB and OIB for amphibolite in Pires do Rio – Catalão area. Symbols as in Fig. 4.7

The Nb-Ta negative anomaly, similar to those of basalts erupted in volcanic arcs, along with LILE and LREE enrichment presented by MORB-like amphibolites of Araxá Group, may be characteristics of subduction-related origin influenced by slab-derived fluids and melts. In this setting, the Nb and Ta behave as immobile elements and generate the distinctive negative anomaly geochemical fingerprint whereas LILE and LREE are mobile during slab subduction thus increased in suprasubduction zones when compared to N-MORB. Pb and Sr positive anomalies in samples are also distinctive of suprasubduction zones (Dilek & Furnes, 2011).

Forearc/back-arc basin hypothesis for Araxá Group is also supported by slightly positive (+0.78 to +2.71) $\varepsilon_{\text{Nd(t)}}$ values and T_{DM} ages of 1.32- 1.80 Ga that may reflect an mixed enriched MORB source possibly with magmas related to Paleoproterozoic São Francisco Craton. The U-Pb age for MORB-like amphibolite (IPC184 at ca. 870 Ma) is compatible with a subduction-related marginal basin development, analogous to ca. 890-830 Ma mafic magmatism from some sequences within Goiás Magmatic Arc (Laux *et al.*, 2004, 2005), and often related to Araxá Group tectonic sheets.

Beside the possible crustal contamination and/or metamorphic influence, Zr/117-Th-Nb/16 diagram (Wood, 1980) shows a possible discrimination between Araxá and Veríssimo amphibolites. The Araxá amphibolites are plotted in the within arc-basalts field whereas Veríssimo amphibolites are plotted in the E-MORB field (Fig. 4.26), supporting both hypotheses for tectonic environment of these units.

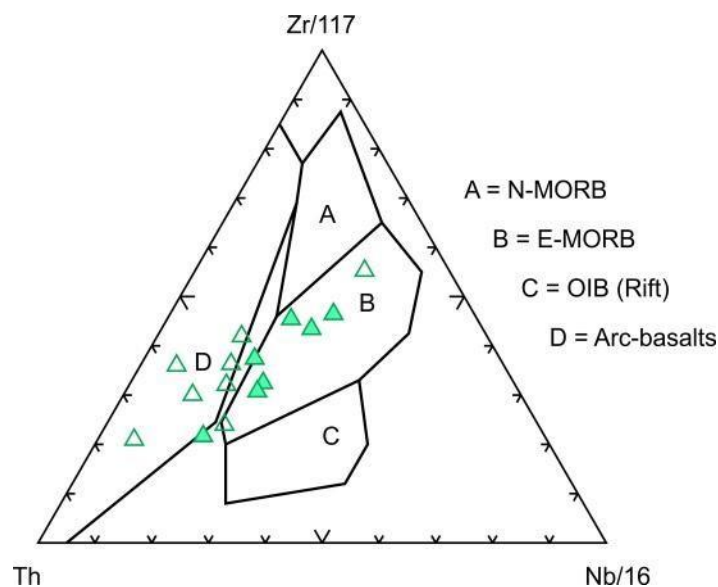


Figure 4.26 - Zr-Th-Nb diagram (Wood et al., 1980) for MORB-like samples. Araxá Group samples plot preferentially in arc-basalts field, whereas Veríssimo Sequence samples plot in E-MORB field. Symbols as in Fig. 4.7

4.6.1.2 OIB-like amphibolites

OIB-type magmatism can occur by local extensions during orogeny collapse, lithospheric thinning, mantle upwelling following slab break-off, dewatering of lithospheric mantle hydrous phases, melting of deeply-subducted continental crust or sub-lithospheric convection (Kheirkhah *et al.*, 2014). OIB-like samples show most LREE enrichment compared do HREE, high Nb/Yb and TiO₂/Yb ratios, but variable trace elements pattern, except for flat Nb-Ta patterns relative to Primitive Mantle normalization. U-Pb zircon analysis of Araxá Group constrained the age of the amphibolite sample PR-10 at 819.7±6.3 Ma, representing an coeval magmatism with E-MORB, while sample PR- 01a at ca. 650 Ma. These younger ages was obtained into homogeneous crystals with magmatic zonation over

inherited older cores that, besides low Th/U ratios, does resemble magmatic overgrowth (e.g. Lopes-Sánchez *et al.*, 2015) and thus are interpreted as crystallization age. Nevertheless, OIB-like magmatism occur in both Araxá and Veríssimo metasedimentary sequences, and can be found in different stratigraphic positions within Araxá Group, as in Valeriano & Simões (1997), and along exposures of Anápolis-Itauçu Complex, where mafic magmatism and anatexis were partially coeval (Piuçana *et al.*, 2003b; Della Giustina *et al.*, 2011). Presented constrains for 650 Ma OIB-like magmatism are compatible with later stages of collisional magmatism of Brasília Belt, in a continental environment.

This does not exclude the possibility of others OIB-like magmatic events over the development of the basin, with older crystallization ages, as interpreted here for Veríssimo Sequence OIB-like basalts (i.e. synchronous to MORB-like basalts at ca. 980 Ma), since they show T_{DM} ages of ca. 1.3 Ga, whereas OIB-like intruded at 650 Ma have younger T_{DM} ages (1.0 Ga) and this Sm-Nd model age disparity can hypothetically reflect the 300 Ma timespan between different OIB-like magmatic sources at distinct tectonic settings.

4.6.2 Araxá and Veríssimo supracrustal rocks

Geologic sedimentary records are usually studied to understand magmatic, sedimentary and tectonic processes involving history and processes related to plate convergence and continental crustal growth (Draut & Clift, 2012). However, arc-continent collision zones may have complex interpretations, above all from ancient accreted orogens, since arc-related basins can occur in variable tectonic settings based on paleogeography, geometries of collision, structural characteristics, evolution of the arc itself, sedimentary influx, preservation potential, and so many others geological constrains.

The analyzed metasedimentary rocks from Araxá Group and Veríssimo Sequence show similarities and differences from a geochemical and isotopic provenance point of view for its potential sources. Both geological units exhibit LREE enrichment and flat HREE pattern, with substancial Eu negative anomaly ($\text{Eu/Eu}^*=0.48-0.77$), normalized to chondrite, which is interpreted as intracrustal differentiation of sedimentary sources, evaluated by high Th/Sc and La/Sc contents. High Th/U and Zr/Sc ratios may be indicative for more severe weathering and sediment recycling (McLennan, 1993), and is more evidenced for Araxá Group samples. An upper continental crust and/or a dissected mature arc source is interpreted as main geochemical provenances, and corroborated by Th/Sc vs. Zr/Sc and La-Th-Sc diagrams.

Both sedimentary sequences show also two main provenance sources in isotopic data. One, characterized by immature, ca. 1.2-1.5 Ga volcanoclastic input that can be related to intermediate to felsic arc dissection, which source is here interpreted as Nova Aurora Domain (Klein, 2008) exposed southwestern of the studied area, and the other is represented by siliciclastic continental flux, evidenced by older detrital zircon grains populations ranging from 1.7-2.9 Ga, from São Francisco-Congo Craton passive margin to the east. This mixed source of sedimentary input is clear in Sm-Nd data, where supracrustal rocks of Pires do Rio-Ipameri area are characterized by negative $\epsilon\text{Nd}_{(t)}$ values and T_{DM} ages of ca. 1.75-2.26 Ga, and plot slightly above Paleoproterozoic crustal rocks from São Francisco-Congo Craton, thus evidencing the require of younger volcanoclastic source.

Nevertheless, Veríssimo is characterized by more variable major, trace and rare-earth elements contents, consequently more variable ratios. This can be explained due to more localized provenance with minor effects of weathering, sedimentary recycling and sorting when compared to Araxá Group, where a broader and well-mixed provenance is inferred. A more localized, arc-like provenance source is evaluated by high Ba/La ratios, along with an increasing trend of V and Sc.

Metavolcanic rocks give essential constrain to possible geotectonic environments concerning the individualization of Veríssimo Sequence and Araxá Group basins. Veríssimo metavolcanic rocks show an overall enrichment of minor, trace and rare-earth elements, and negative anomalies of Cs, K, P and Ti compared to primitive mantle. Along with positive Nb-Ta anomaly, young T_{DM} age of 1.16 Ga and positive $\epsilon Nd(t)$ value of +3.78, Veríssimo silicic volcanism can be related to extensional continental environment, in a volcanic rifted margin context.

Araxá Group metavolcanic samples from Klein (2008) show higher values of Sc, Rb, V, Ni and Cu, along with negative Nb-Ta anomaly that lead to a geochemical arc-signature interpretation. T_{DM} age at ca. 1.8 Ga, negative $\epsilon Nd(t)$ value at -5.64 and U-Pb age of 720 Ma shows a possibly continental setting of crustal recycling during subduction process.

Araxá Group tectonic environment was always a point of discussion along knowledge evolution of Brasília Belt. Many researches associate metasediments and mafic intrusions of Araxá Group as distal sedimentary facies of passive margin (as in Valeriano & Simões, 1997; Valeriano, 1999; Valeriano *et al.*, 2004; 2008) and the occurrence of amphibolite rocks are related to lithosphere thinning but no oceanic crust generation. On the other hand, Araxá Group is hence interpreted as sediments over oceanic crust possibly from a back-arc basin (as in Pimentel *et al.*, 1999; 2001; 2011; Seer *et al.*, 2001 Piuzana *et al.*, 2003), represented by a long, roughly N-S ophiolitic mélange (Strieder & Nilson, 1992).

Convergent margins can show extension or contraction, as well as be strain-neutral, that is mostly manifested in back-arc regions and can occur multiples times in arc evolution. Back-arc sedimentation records are dominated by volcanic and volcanoclastic products of the arc, with less sediment flux of pelagic and hemipelagic clays, biogenic material and resedimented carbonates. The lack of Neoproterozoic zircon grains in southernmost Araxá Group can also be explained in the back-arc model, when arc rifting occurs trenchward (i.e. fore-arc) from the volcanic front the extension causes a subsidence on the remnant arc and creates a barrier to the sedimentation of volcanic-related sediments to the forearc (Clift, 1995). Remnants of backarc basins are unlikely to be preserved in orogens, and when, it is plutons and ophiolite crustal sections along with deformed, offscraped fragments within the accretionary prism. Nevertheless, in arc-continent collisional backarc basins that contain large sediment volumes by virtue of proximity to a continent would significant siliciclastic sediment volumes be preserved in geologic records, as Macquarie arc in southeastern Australia, Alisitos arc terrane in Baja California, and many other examples (Draut & Clift, 2013 and references therein).

Despite that, Araxá Group has a vast geographical mapped area and for some of these authors may not represent a unique tectonic setting and is highly recommended to be revised, as seen in different geochronological data between northwestern and southeastern rocks mapped as Araxá Group (Piuzana *et al.*, 2003a and Valeriano *et al.*, 2004, respectively) in South Brasília Belt. Lastly, this discussion is pertinent, since relationships between metaigneous rocks and Araxá metasediments are still far from clear and remain controversial due to tectonic imbrications (Pimentel *et al.*, 2016).

4.7 Conclusions

Based on the new geochemical, chronological and isotope data, we suggest:

The Veríssimo Sequence (980 Ma) is inserted in an extensional tectonic environment, where crustal thinning and mantle upwelling allowed the emplacement of both MORB- and OIB-like basalts. Sedimentation is characterized as a volcano-sedimentary sequence, with deposition of sediments derived from western margin of São Francisco Craton and with a minor input of volcanoclastic material from seaward Nova Aurora Domain.

Stratigraphically above, Araxá Group mafic magmatism present subduction-related patterns of forearc/back-arc bimodal (E-MORB and OIB) basalts yielding ca. 870-820 Ma, probably generated due to extension processes in continental crust but without any significant change in sedimentary provenance.

Gabbroic OIB-like rocks intruded in Araxá Group yield 650 Ma and are coeval with the exhumation of metamorphic core Anápolis-Itauçu Complex. This mafic magmatism is here inferred as final stages of collisional event, in a continental environment. Geological processes linked to its generation (e.g. lower crust delamination) require more studies and techniques that are beyond the scope of this work.

Although geochemical and isotopic Sm-Nd and U-Pb data separates MORB- and OIB-like basalts both temporally and genetically, it does not attenuate discussions concerning magmatic sources, tectonic processes and the proper individualization of superposed tectonic sheets which represent ancient marginal basins. More quantity of geochemical and isotopic data is highly recommended in order to assuage biased and misleading further interpretations, and the application of other geological, geochemical and isotopic systematics to investigate possible fingerprints and so correlate with previous studies and others settings where amphibolite outcrops are described, since Brasília Belt exhibit complex evolution of overlapped geological events in a wide timespan.

4.8 References

- Albarède, F., Telouk, S. Blichert-Toft, J., Boyet, M., Agranier, A., Nelson, B., 2004. Precise and accurate isotopic measurements using multiple-collector ICPMS. *Geochimica et Cosmochimica Acta*, 68, 2725–2744.
- Baldwin, J.A. & Brown, M. (2008). Age and duration of ultrahigh-temperature metamorphism in the Anápolis–Itauçu Complex, Southern Brasilia Belt, central Brazil - constraints from U–Pb geochronology, mineral rare earth element chemistry and trace-element thermometry. *Journal of Metamorphic Geology*, 26, 213–233.
- Brito Neves, B.B, Fuck, R.A., Pimentel, M.M (2014). The Brasiliano collage in South America: a review. *Brazilian Journal of Geology*, 44(3), 493-518.
- Brod, J.A., Leonardos, O.H., Meneses, P.R., Albuquerque, M.A.C., Almeida, R., Blanco, S.B., Cardoso, F.B.F, Romão, P.A., Tallarico, F.H.B., Thomsen, F.P.R. (1992). Geoquímica da Sequência Vulcano-Sedimentar de Abadia dos Dourados e Complexo Chapada das Perdizes, Triângulo Mineiro – MG. *Rev. Esc. Minas de Ouro Preto*, 45(2), 164-166.
- Buhn, B., Pimentel M.M., Matteini M., Dantas E.L., 2009. High spatial resolution analysis of Pb and U isotopes for geochronology by laser ablation multi-collector inductively coupled plasma mass spectrometry (LA-MC-ICPMS). *Annals of the Brazilian Academy of Sciences*, 81, 99–114.
- Campos, J. E. G., Dardenne, M. A., Freitas-Silva, F. H., & Martins-Ferreira, M. A. C. (2013). Geologia do Grupo Paranoá na porção externa da Faixa Brasília. *Brazilian Journal of Geology*, 43(3), 461–476.

CPRM, (2001). Programa Levantamentos Geológicos Básicos do Brasil. Goiânia – Folha SE.22-X-B. Escala 1:250.000. Estado de Goiás. (Eds) José Domingos Alves Baêta Júnior – Brasília: CPRM, 2001. *Explanatory text*, p. 11-12.

D'el-Rey Silva, L. J. H., de Oliveira, . L., Pohren, C. B., Tanizaki, M. L. N., Carneiro, R. C., Fernandes, G. L. D. F., Aragão, P. E. (2011). Coeval perpendicular shortenings in the Brasília belt: Collision of irregular plate margins leading to orocinal bending in the Neoproterozoic of central Brazil. *Journal of South American Earth Sciences*, 32(1), 1–13.

Dardenne M.A., Fuck R.A., D'el Rey Silva L.H., Pimentel, M.M.. (1994). Mapa Geológico - Projeto Rio Veríssimo. Brasília, *Undergraduate Final Essay*, Institute of Geosciences, University of Brasília.

Dardenne M.A., Fuck R.A., Meneses P.R., Pimentel, M.M.. (1991). Mapa Geológico - Projeto Sucuri. Brasília, Brasília, *Undergraduate Final Essay*, Institute of Geosciences, University of Brasília.

Dardenne, M.A., (2000). The Brasília Fold Belt. In: Cordani, U.G., Milani, E.J., Tomas Filho, A., Campos, D.A. (Eds.), Tectonic Evolution of South America. Proceedings of the XXXI International Geological Congress, Rio de Janeiro, pp. 231–263.

De Paolo, D.J. (1981). A neodymium and strontium isotopic study of the Mesozoic calc-alkaline granitic batoliths of the Sierra Nevada and Peninsular Rangers, California, *Journal of Geophysical Research*, 86, 10470-10488.

Della Giustina, M.E.S., Pimentel, M.M., Ferreira Filho, C.F., Hollanda, M.H.B.M. (2011). Dating coeval mafic magmatism in the Anápolis-Itauçu Complex, Central Brazil. *Lithos*, 124, 82-102.

Della Giustina, M.E.S.; Claudinei, G.O.; Pimentel, M.M.; Buhn, .B. (2009). Neoproterozoic magmatism and high-grade metamorphism in the Goiás Massif: New LA-MC-ICMPS U–Pb and Sm–Nd data and implications for collisional history of the Brasília Belt. *Precambrian Research* 172 (2009) 67–79.

Dias, H. P. A., Noce, C. M., Pedrosa-Soares, A. C., Seer, H. J., Dussin, I. A., Valeriano, C. M., & Kuchenbecker, M. (2011). O Grupo Ibiá (Faixa Brasília Meridional): evidências isotópicas Sm-Nd e U-Pb de bacia colisional tipo flysch. *Geonomos*, 19(2), 90–99.

Dilek, Y., & Furnes, H. (2011). Ophiolite genesis and global tectonics: Geochemical and tectonic fingerprinting of ancient oceanic lithosphere. *Bulletin of the Geological Society of America*, 123(3–4), 387–411.

Dilek, Y., & Furnes, H. (2014). Ophiolites and their origins. *Elements*, 10(2), 93–100.

Donato, M.M. (1991). Geochemical recognition of a captured back-arc basin metabasaltic complex, southwestern Oregon. *Journal of Geology*, 99, 711-728.

Draut, A. E., & Clift, P. D. (2013). Differential preservation in the geologic record of intraoceanic arc sedimentary and tectonic processes. *Earth-Science Reviews*, 116(1), 57–84.

Draut, A.E. & Clift, P.D. (2012). Basins in arc-continent collisions. In: Busby, E. and Azor, A. (Eds.) *Tectonics of Sedimentary Basins: Recent Advances*, First Edition, Blackwell Publishing Ltd. 347-368

Ferreira Filho, C.F., Kamo, S.L., Fuck, R.A., Krogh, T.E., Naldrett, A.J. (1994). Zircon and rutile U-Pb geochronology of the Niquelândia layered mafic and ultramafic intrusion, Brazil: constraints for the timing of magmatism and high grade metamorphism. *Precambrian Research*, 68, 241-255.

Fuck, R.A., Jardim De Sá, E.F., Pimentel, M.M., Dardenne, M.A., Soares, A.C.P., (1994). As faixas de dobramentos marginais do Cráton do São Francisco; síntese dos conhecimentos. In: Dominguez, J.M.L., Misi, A. (Eds.), *O Cráton do São Francisco*. SBG-SGM-CNPq, Salvador, pp. 161–185.

Gioia, S.M.C.L. & Pimentel, M.M. (2000). The Sm-Nd isotopic method in the Geochronology Laboratory of the University of Brasília. *Anais da Academia Brasília de Ciências*, 72(2), 219-245.

Guimarães E.M., (1997). Estudos de proveniência e diagênese com ênfase na caracterização dos filossilicatos dos Grupos Paranoá e Bambuí, na região de Bezerra-Cabeceiras (GO). Doctorate thesis. Geosciences Institute, University of Brasília, 270p.

Hickey-Vargas, R., Savov, I. P., Bizimis, M., Ishii, T., & Fujioka, K. (2013). Origin of Diverse Geochemical Signatures in Igneous Rocks from the West Philippine Basin: Implications for Tectonic Models. *Back-Arc Spreading Systems: Geological, Biological, Chemical, and Physical Interactions*, (June 2016), 287–303.

Irvine, T. N. & Baragar, W. R. A., (1971). A guide to the chemical classification of the common volcanic rocks. *Canadian Journal Earth Sciences*. 8, 523-548.

Jackson, S.E., Pearson, N.J., Griffina, W.L., Belousova, E.A., 2004. The application of laser ablation-inductively coupled plasma-mass spectrometry to in situ U-Pb zircon geochronology. *Chemical Geology*, 211, 47–69.

Junges, S.L., Pimentel, M.M., Dantas, E.L., Laux, J.H. (2003). New ID-TIMS U-Pb ages in the western portion of the Mara Rosa Arc: two hundred million years of arc building. In: 4th South American Symposium on Isotope Geology, Salvador, 2003. Short Papers, Salvador, CBPM, IRD, v1:198-201.

Kheirkhah, M., Neill, I., & Allen, M. B. (2015). Petrogenesis of OIB-like basaltic volcanic rocks in a continental collision zone: Late Cenozoic magmatism of Eastern Iran. *Journal of Asian Earth Sciences*, 106, 19–33.

Klein, P.B.W., (2008). Geoquímica de Rocha Total, Geocronologia de U-Pb e Geologia Isotópica de Sm-Nd das Rochas Ortognáissicas e Unidades Litológicas Associadas da Região Ipameri – Catalão (Goiás). Doctorate thesis, Institute of Geosciences, University of Brasília.

Košler, J., Fonneland, H., Sylvester, P., Tubrett, M., Pedersen, R.B., 2002. U–Pb dating of detrital zircons for sediment provenance studies, a comparison of laser ablation ICP-MS and SIMS techniques. *Chemical Geology*, 182, 605–618.

Kröner, A., Wan, Y., Liu, X., & Liu, D. (2014). Dating of zircon from high-grade rocks: Which is the most reliable method? *Geoscience Frontiers*, 5(4), 515–523.

Lacerda Filho, J.V.; Camargo, M.A.; Wildner, W. (1995). Granitoide Sintectônico de Maratá. In: SIMPÓSIO DE GEOLOGIA DO CENTRO-OESTE, 5, *Anais Goiânia: SBG-Núcleos Centro-Oeste e Brasília*, 1995.p.66-67.

Laux, J. H. Pimentel M.M., Dantas E.L., Armstrong R., Armele A., Nilson A.A. (2004). Mafic magmatism associated with the Goiás magmatic arc in the Anicuns region, Goiás, Central Brazil: Sm-Nd isotops and new ID-TIMS and SHRIMP U-Pb data, *Journal of South American Earth Sciences*, 16, 599-614.

Laux, J. H., Pimentel, M.M., Dantas, E. L., Armstrong, R., Junges, S.L. (2005) – Two Neoproterozoic crustal accretion events in the Brasília Belt, Central Brazil. *Journal of South American Earth Sciences*, 28, 183-198.

Lopez-Sánchez, M. A., Aleinikoff, J. N., Marcos, A., Martínez, F. J., & Llana-Fúnez, S. (2016). An example of low-Th/U zircon overgrowths of magmatic origin in a late orogenic Variscan intrusion: the San Ciprián massif (NW Spain). *Journal of the Geological Society*, 173(2), 282–291.

Matteini, M., Dantas, E.L, Pimentel, M.M., Alvarenga, C.J.S., Dardenne, M.A., (2012). U-Pb and Hf isotope study on detritial zircons from the Paranoá Group, Brasília Belt, Brazil: Constraints on depositional age at Mesoproterozoic – Neoproterozoic transition and tectonomagmatic events in the São Francisco Craton. *Precambrian Research*, 206-207, 168-181.

McLennan, S.M., Hemming, S., McDaniel, D.K., Hanson, G.N. (1993) Geochemical approaches to sedimentation, provenance, and tectonics. In: Johnsson, M.J., and Basu, A. (Eds.), *Processes Controlling the Composition of Clastic Sediments*: Boulder, Colorado. *Geological Society of America Special Paper*, 284.

McLennan, S.M., Taylor, S.R., McCulloch, M.T. and Maynard, J.B. (1990). Geochemical and Nd-Sr Isotopic Composition of Deep-Sea Turbidites - Crustal Evolution and Plate Tectonic Associations. *Geochimica et Cosmochimica Acta*, 54(7): 2015-2050.

Moraes, R.; Brown, M.; Fuck, R.A.; Camargo, M.A.; Lima, T.M.(2002). Characterization and P-T evolution of melt-bearing ultrahigh-temperature granulites: an example from the Anápolis–Itauçu Complex of the Brasília Fold Belt, Brazil. *Journal of Petrology*, 43, 1673–1705.

- Navarro, G. R. B., Zanardo, A., & Da Conceição, F. T. (2013). O grupo araxá na região sul-sudoeste do estado de goiás. *Geologia USP - Série Científica, São Paulo*, 13(2), 5–28.
- Pearce, J. A. (2008). Geochemical fingerprinting of oceanic basalts with applications to ophiolite classification and the search for Archean oceanic crust. *Lithos*, 100(1–4), 14–48.
- Pearce, J. A. (2014). Immobile element fingerprinting of ophiolites. *Elements*, 10(2), 101–108.
- Pimentel, M. M. (2016). The tectonic evolution of the Neoproterozoic Brasília Belt, central Brazil: a geochronological and isotopic approach. *Brazilian Journal of Geology*, 46(June), 67–82.
- Pimentel, M. M., Dardenne, M. A., Fuck, R. A., Viana, M. G., Junges, S. L., Fischel, D. P., Dantas, E. L. (2001). Nd isotopes and the provenance of detrital sediments of the neoproterozoic Brasília belt, central Brazil. *Journal of South American Earth Sciences*, 14(6), 571–585.
- Pimentel, M. M., Rodrigues, J. B., DellaGiustina, M. E. S., Junges, S., Matteini, M., & Armstrong, R. (2011). The tectonic evolution of the Neoproterozoic Brasília Belt, central Brazil, based on SHRIMP and LA-ICPMS U-Pb sedimentary provenance data: A review. *Journal of South American Earth Sciences*, 31(4), 345–357.
- Pimentel, M. M.; Jost, H.; Fuck, R. A. (2004) O embasamento da Faixa Brasília e o arco Magmático de Goiás. In: Mantesso-Neto, V., Bartorelli, A., Carneiro, C. DAL RÉ; (Eds) Brito-Neves, B. B. *Geologia do Continente Sul-Americano: evolução da obra de Fernando Flávio Marques de Almeida*. São Paulo: Beca, 355–368.
- Pimentel, M.M. & Fuck, R.A. (1992). Neoproterozoic crustal accretion in Central Brazil. *Geology*, 20:375–379.
- Pimentel, M.M., Fuck, R.A. & Botelho, N.F., (1999). Granites and the geodynamic history of the neoproterozoic Brasília belt , Central Brazil :a review. *Lithos*, 46, pp.463–483.
- Pimentel, M.M., Fuck, R.A. & Fischel, D.P., (1999). Estudo Isotópico Sm-Nd Regional da Porção Central Da Faixa Brasília, Goiás: Implicações para Idade e Origem dos Granulitos do Complexo Anápolis-Itauçu e Rochas Metassedimentares Do Grupo Araxá. . *Revista Brasileira de Geociências*, 29(2), pp.271–276.
- Pimentel, M.M., Rodrigues, J.B., Della Giustina, M.E.S., Junges, S.L., Matteini, M., (2011). The tectonic evolution of the Neoproterozoic Brasília Belt, central Brazil, based on SHRIMP and LA-ICPMS U–Pb sedimentary provenance data: A review. *Journal of South American Earth Sciences*, 31(4), pp.345–357.
- Pimentel, M.M.; Dardenne, R. A.; Viana, M. G.; Junges, S. L.; Fischel, D. P.; Seer, H. J.; Dantas, E. L. (2001). Nd isotopes and the provenance of detrital sediments of the Neoproterozoic Brasília Belt, central Brazil. *Journal of South American Earth Sciences*, 14, pp.571–585.
- Piuzana D., Pimentel M.M., Fuck R.A., Armstrong R.A. (2003b). Neoproterozoic granulite facies metamorphism and coeval granitic magmatism in the Brasilia Belt, Central Brazil: regional implications of new SHRIMP U-Pb and Sm-Nd data. *Precambrian Research*, 125:245–273.
- Piuzana, D., Pimentel, M. M., Fuck, R. A., & Armstrong, R. (2003a). SHRIMP U-Pb and Sm-Nd data for the Araxá Group and associated magmatic rocks: Constraints for the age of sedimentation and geodynamic context of the southern Brasília Belt, central Brazil. *Precambrian Research*, 125(1–2), 139–160.
- Rodrigues, J.B., Pimentel, M.M., Dardenne, M.A., Armstrong, R.A. (2010). Age, provenance and tectonic setting of the Canastra and Ibiá Groups (Brasília Belt, Brazil): Implications for the age of a Neoproterozoic glacial event in central Brazil. *Journal of South American Earth Sciences*, 29(2), pp.512–521.
- Seer, H.J. (1999). Evolução tectônica dos Grupos Araxá, Ibiá e Canastra na sínfoma de Araxá, Araxá, Minas Gerais. *Doctorate thesis*. Geosciences Institute, University of Brasília, 270p.
- Seer, H.J., Brod, J.A., Fuck, R.A., Pimentel, M.M., Boaventura, G.R., Dardenne, M.A. (2001). Grupo Araxá em sua Área Tipo : Um Fragmento de Crosta Oceânica Neoproterozóica na Faixa de Dobramentos Brasília. *Revista Brasileira de Geociências*, d(3), pp.385–396.

Seer, H.J., Brod, J.A., Valeriano, C.M., Fuck, R.A. (2005). Leucogranitos Intrusivos no Grupo Araxá : Registro de um Evento Magmático durante Colisão Neoproterozóica na Porção Meridional da Faixa Brasília. *Revista Brasileira de Geociências*, 35(1), pp.33–42.

Shervais, J. W. (2001). Birth, death, and resurrection: The life cycle of suprasubduction zone ophiolites. *Geochemistry, Geophysics, Geosystems*, 2(1), 45.

Stern, R. J. & Bloomer, S. H. (1992). Subduction zone infancy: Examples from the Eocene Izu-Bonin-Mariana and Jurassic California arcs. *Geological Society of America Bulletin*, 104, 1621-1636.

Strieder A. J. & Nilson A. A., (1992). Mélange ofiolítica nos metassedimentos do Grupo Araxá de Abadiânia (GO) e implicações tectônicas regionais. *Revista Brasileira de Geociências*, 22: 204-215.

Strieder, A. J. & Suita, M.T.F., (1999). Neoproterozoic geotectonic evolution of Tocantins Structural Province, Central Brazil. *Geodynamics*, 28, pp.267–289.

Sun, S.S. and McDonough, W.F. (1989). Chemical and isotopic systematics of oceanic basalts; implications for mantle composition and processes. In: *Magmatism in the ocean basins*. Saunders, A.D. and Norry, M.J. (Editors), *Geological Society of London*, London. 42: 313-345.

Taylor, S.R. and McLennan, S.M. (1985). *The Continental Crust; Its composition and evolution; an examination of the geochemical record preserved in sedimentary rocks*. Blackwell, Oxford. 312.

Valeriano, C. M., Machado, N., Simonetti, A., Valladares, C. S., Seer, H. J., & Simões, L. S. A. (2004). U-Pb geochronology of the southern Brasília belt (SE-Brazil): Sedimentary provenance, Neoproterozoic orogeny and assembly of West Gondwana. *Precambrian Research*, 130(1–4), 27–55.

Valeriano, C.M. & Simões, L.S.A. (1997). Geochemistry of Proterozoic mafic rocks from the Passos Nappe (Minas Gerais, Brazil): tectonic implications to the evolution of the southern Brasília Belt. *Revista Brasileira de Geociências*, 27(1), 99-110.

Valeriano, C.M. (1992). Evolução tectônica da extremidade sul meridional da Faixa Brasília, região da represa de Furnas, Sudoeste de Minas Gerais. *Doctorate thesis*. Geosciences Institute, University of São Paulo. 258p

Wallin, E.T. & Metacalf, R.V. (1998). Supra-subduction zone ophiolite formed in an extensional forearc: Trinity Terrane, Klamath Mountains, California. *Journal of Geology*, 106, 591-608.

Wood, D.A. (1980). The application of a Th-Hf-Ta diagram to problems of tectonomagmatic classification and to establishing the nature of crustal contamination of basaltic lavas of the British Tertiary volcanic province. *Earth Planet, Sci. Lett.*, 50, 11-3

4.9 Appendix

Table 4.3 - Coordinates (UTM) from rock samples

SAMPLE	X	Y	UNIT	TYPE
PR-01	802599	8077161	Grupo Araxá	Amphibolite
PR-07	811170	8107413	Seq. Veríssimo	Amphibolite
PR-09	809013	8092507	Seq. Veríssimo	Amphibolite
PR-10	802007	8071378	Grupo Araxá	Amphibolite
PR-11	811354	8086846	Seq. Veríssimo	Amphibolite
PR-12	817993	8032690	Grupo Araxá	Amphibolite
XV-65	811175	8107403	Seq. Veríssimo	Amphibolite
V-31a	804903	8067950	Grupo Araxá	Amphibolite
VI-148b	803142	8069764	Grupo Araxá	Amphibolite
XII-19c	812372	8096301	Grupo Araxá	Amphibolite
XII-41	809009	8092492	Seq. Veríssimo	Amphibolite
XII-130	807867	8094842	Seq. Veríssimo	Amphibolite
XII -144	808467	8094336	Grupo Araxá	Amphibolite
XV-91	811680	8105367	Seq. Veríssimo	Amphibolite
XV-109	811689	8106033	Seq. Veríssimo	Amphibolite
IPC54	824711	8029241	Seq. Veríssimo	Amphibolite
IPC03	850127	7995135	Grupo Araxá	Amphibolite
IPC106	831781	8031778	Grupo Araxá	Amphibolite
IPC184	809039	7997921	Grupo Araxá	Amphibolite
IX-124A	809881	8081207	Seq. Veríssimo	Amphibolite
VI-102	802017	8071378	Grupo Araxá	Amphibolite
XII-21	812100	8096243	Seq. Veríssimo	Amphibolite
XIV-107	808239	8103634	Seq. Veríssimo	Metavolcanic
PR-13	816036	8026428	Grupo Araxá	Metavolcanic
IPC24	813599	8000531	Grupo Araxá	Metavolcanic
IPC36	805971	8025096	Grupo Araxá	Metavolcanic
XV-233	807981	8103820	Seq. Veríssimo	Metavolcanic
PR-02	802893	8077195	Grupo Araxá	Supracrustal
PR-03	802193	8080888	Grupo Araxá	Supracrustal
PR-04	806479	8081359	Grupo Araxá	Supracrustal
PR-14	805579	8037005	Grupo Araxá	Supracrustal
VII-158	808753	8075229	Seq. Veríssimo	Supracrustal
XIV-119	797867	8100361	Grupo Araxá	Supracrustal
IPC101	826007	8026074	Grupo Araxá	Supracrustal
IPC31	810005	8011969	Grupo Araxá	Supracrustal

Table 4.4 - Geochemical data from amphibolite samples

Sample	MORB-like												OIB-like		
	PR-09	PR-11	PR-12a	XII-130	IPC03 ¹	XV-65	XII-21	VI-148b	XV-109	VI-123	XIII-144	VI-102	IPC54 ¹	PR-01a	
SiO ₂	53.50	45.77	49.29	47.52	46.47	47.11	46.96	50.4	50.3	49.39	45.55	45.33	45.21	40.76	
TiO ₂	1.54	1.47	1.08	1.05	1.88	1.01	2.35	1.82	1.18	1.41	2.46	3.07	3.42	2.73	
Al ₂ O ₃	14.73	15.46	14.49	15.80	14.98	16.16	15.68	14	15.65	15.86	13.12	17.84	14.83	17.72	
Fe ₂ O ₃	12.56	13.95	11.10	10.73	14.33	11.36	14.15	14.4	11.65	11.85	16.65	13.04	18.05	19.42	
MnO	0.28	0.22	0.20	0.18	0.25	0.17	0.18	0.28	0.18	0.19	0.25	0.19	0.17	0.25	
MgO	4.93	8.37	7.60	8.22	6.66	7.59	5.80	6.45	6.99	5.81	6.32	4.20	4.81	4.16	
CaO	8.21	8.38	11.62	12.55	10.08	11.55	10.24	10.4	9.86	10.81	11.28	8.87	3.70	6.44	
Na ₂ O	1.33	3.09	1.55	1.59	1.90	2.23	3.09	1.5	2.46	2.20	2.14	3.67	2.81	1.24	
K ₂ O	0.42	0.15	0.41	0.29	0.58	0.28	0.41	0.66	0.38	0.80	0.50	0.97	0.94	0.32	
P ₂ O ₅	0.15	0.13	0.06	0.08	0.16	0.07	0.23	0.2	0.14	0.29	0.21	0.49	1.07	0.31	
LOI	2.1	2.7	2.3	1.7	2.3	2.1	0.6	1.4	2.21	1.1	1.2	2.0	4.7	6.3	
TOTAL	99.74	99.69	99.7	99.71	99.59	99.63	99.69	101.56	101.06	99.71	99.71	99.67	99.71	99.65	
Ti	9232	8813	6475	6294.75	11271	6054.95	14088.3	10911.1	7074.22	8452.95	14748	18404.7	20503.6	16367	
Cr	292	438	511	301.052	321.7	184.737	171.053	130	90	164.21	-	b.d.l	6.84	146	
Ba	95	41	59	48	90	138	170	133.5	118	44	143	397	421	47	
Ce	27.8	14.0	13.3	12.3	20.1	11.4	27.5	34.6	32.1	37.5	39.8	60.3	110.8	36.6	
Co	87.4	76.9	62.2	77.2	-	76.2	62.4	190	141	79.9	56.4	61.4	-	71.2	
Cr ₂ O ₃	0.020	0.030	0.035	0.044	-	0.027	0.025	0.03	0.02	0.024	0.018	<0.002	-	0.010	
Cs	0.4	0.6	0.6	0.6	1.5	0.5	<0.1	0.17	0.11	<0.1	<0.1	1.4	0.3	0.3	
Dy	5.63	5.11	4.04	3.91	5.11	4.23	5.60	9.03	6.26	6.66	7.02	4.98	10.10	7.71	
Er	3.59	3.29	2.56	2.17	3.03	2.29	3.53	6.17	4.18	3.66	3.29	2.15	4.56	4.88	
Eu	1.30	1.17	0.89	0.95	1.42	0.95	1.81	1.99	1.19	1.97	2.11	2.98	4.89	1.84	
Ga	19.5	16.3	17.2	17.0	21.5	15.3	20.9	20.1	18.3	22.0	21.4	21.5	27.2	25.7	
Gd	4.89	4.43	3.36	3.85	4.54	3.01	6.14	8.56	5.32	6.50	6.89	6.50	12.48	6.71	
Hf	3.4	2.4	1.8	2.5	2.9	1.4	4.1	4.1	3.8	5.4	4.3	3.6	1.9	4.9	
Ho	1.17	1.09	0.82	0.81	1.13	0.69	1.30	1.97	1.35	1.25	1.23	0.83	1.89	1.59	
La	16.7	6.9	5.9	6.3	8.7	4.7	11.7	19.3	14.6	16.7	14.8	27.3	52.4	22.9	
Lu	0.60	0.52	0.38	0.29	0.44	0.30	0.56	0.85	0.6	0.51	0.41	0.29	0.58	0.75	
Nb	5.4	7.0	1.6	3.3	7.0	3.6	9.6	7.5	13.6	12.7	12.8	29.2	58.6	21.4	
Nd	18.3	10.4	8.7	9.0	13.8	7.5	18.6	22.4	15	24.7	28.8	39.0	73.2	23.5	
Ni	<20	133	42	78	-	135	69	86	99	81	99	26	-	53	
Pr	4.34	2.22	1.86	2.06	2.80	1.51	4.07	4.82	3.75	5.08	6.12	8.11	15.72	5.64	
Rb	6.6	12.5	12.7	5.5	13.4	7.0	6.3	8.5	3.6	5.3	7.0	16.5	21.1	5.2	
Sc	39	40	44	38	45	38	40	46	34	34	37	18	23	53	
Sm	4.20	3.18	2.52	2.88	4.00	2.38	5.28	5.93	4.41	5.84	6.97	7.29	15.30	5.78	
Sr	114.1	246.5	182.6	139.9	161.2	272.1	336.2	109	296	189.1	243.2	953.0	134.5	283.3	
Ta	0.6	0.5	0.2	0.7	0.5	0.5	0.7	0.7	1	1.1	0.7	1.8	3.5	1.2	
Tb	0.88	0.83	0.62	0.60	0.84	0.54	1.06	1.5	0.94	1.12	1.12	0.94	2.03	1.23	
Th	3.8	0.5	0.9	0.6	1.3	0.5	0.9	2.22	2.8	2.4	0.4	1.9	4.6	2.8	
Tm	0.56	0.55	0.35	0.39	0.44	0.31	0.55	0.86	0.61	0.47	0.44	0.28	0.64	0.74	
U	1.0	0.1	0.2	<0.1	0.3	<0.1	0.2	0.44	0.59	0.4	0.3	0.4	1.3	0.9	
V	296	285	294	244	323	251	359	315	214	202	430	209	80	477	
W	400.3	146.3	159.8	217.7	-	200.8	112.5	1110	666	226.1	1.8	193.6	-	121.6	
Y	30.0	28.6	22.4	20.6	30.1	19.7	35.3	56.1	36.1	34.1	33.1	24.0	53.2	39.7	
Yb	3.46	3.09	2.38	2.08	2.92	1.76	3.60	5.38	4.08	3.48	2.93	2.04	4.09	4.85	
Zr	128.0	84.1	65.7	68.0	95.9	50.6	145.8	135	118	212.6	173.0	168.7	312.2	189.5	
Cu	48.8	116.4	59.7	64.8	30.4	119.1	67.1	60	85	69.8	86.3	25.5	7.6	167.2	
Pb	2.9	0.4	0.9	1.4	2.3	<0.1	0.3	2	<2	1.7	1.8	1.0	1.6	5.9	
Zn	34	47	30	27	65	20	29	122	95	36	41	50	186	28	

Table 4.5 - Geochemical data from supracrustal rock samples

Sample	Metasedimentary										Metavolcanic		
	IPC31 ¹	X-13	PR-01b	PR-02	PR-03	PR-12b	VII-158	XIV-107	XIV-119a	IPC101 ¹	XV-233	IPC36 ¹	IPC24 ¹
SiO ₂	53.76	57.42	53.42	36.40	58.33	65.88	57.37	64.51	59.50	57.45	61.40	68.65	65.03
TiO ₂	1.49	1.34	1.77	2.54	1.55	0.72	1.84	0.63	1.07	1.08	0.51	0.66	1.11
Al ₂ O ₃	20.41	18.88	21.20	29.87	18.29	15.35	21.25	13.49	19.38	22.31	15.05	14.22	15.87
Fe ₂ O ₃	9.97	11.12	12.21	14.96	11.04	7.42	9.10	9.98	9.05	5.36	8.85	5.01	8.42
MnO	0.38	0.08	0.05	0.04	0.14	0.03	0.09	0.30	0.11	0.03	0.23	0.07	0.09
MgO	2.69	2.05	1.06	0.75	0.43	1.15	1.49	0.10	3.24	1.71	0.19	1.33	1.70
CaO	1.04	0.82	0.32	0.02	0.03	0.02	0.29	1.91	0.57	0.07	1.62	1.41	0.63
Na ₂ O	2.32	0.56	0.58	0.40	0.57	0.23	0.76	5.37	0.61	0.84	7.17	1.83	0.96
K ₂ O	3.86	3.88	3.86	6.94	4.69	4.24	2.78	1.91	3.59	6.30	3.57	4.18	2.69
P ₂ O ₅	0.12	0.05	0.17	0.02	0.03	0.08	0.15	0.05	0.02	0.01	0.06	0.14	0.11
LOI	3.5	3.5	5.1	7.7	4.6	4.6	4.6	1.4	2.5	4.7	3.4	2.0	3.0
TOTAL	99.66	99.70	99.72	99.63	99.72	99.77	99.72	99.65	99.64	99.86	>102.00	99.59	99.61
Cr	-	129.9999	136.836	198.418	123.156	82.104	102.6315	-	95.7894	20.53	<10	-	82.14
Ba	832	605	567	1164	652	590	467	446	928	896	798	682	416
Ce	134.1	73.5	113.7	79.6	94.4	79.5	106.1	211.8	128.7	17.8	256.0	63.7	88.8
Co	-	40.9	64.1	15.3	89.5	93.9	31.8	64.7	75.6	-	142.0	-	-
Cr ₂ O ₃	-	0.019	0.020	0.029	0.018	0.012	0.015	<0.002	0.014	0.007	<0.01	-	0.006
Cs	7.3	3.5	3.4	5.9	3.5	7.1	4.0	1.0	0.7	14.3	0.2	7.8	7.8
Dy	7.17	6.78	9.96	2.58	6.91	4.42	6.05	18.30	10.60	2.54	19.30	5.05	6.27
Er	4.26	3.81	4.73	1.49	4.28	2.47	3.22	10.37	6.63	1.12	10.75	3.15	3.56
Eu	1.93	1.59	2.96	0.87	1.42	1.07	1.91	4.12	1.88	0.40	4.24	1.01	1.67
Ga	28.0	26.4	30.2	44.3	25.0	19.5	32.2	35.2	23.9	27.8	41.1	20.8	21.0
Gd	6.54	6.11	11.52	4.27	6.50	4.95	7.32	18.90	9.42	2.58	19.60	5.12	6.35
Hf	8.6	5.4	8.2	18.5	8.6	5.6	8.2	17.9	5.0	5.9	24.8	6.7	7.4
Ho	1.49	1.23	1.69	0.51	1.42	0.89	1.07	3.49	2.08	0.45	3.79	1.08	1.33
La	67.8	35.0	78.0	41.7	44.7	40.4	56.8	101.9	64.3	8.3	129.0	36.4	45.4
Lu	0.62	0.54	0.65	0.30	0.65	0.41	0.46	1.54	0.85	0.21	1.48	0.50	0.54
Nb	45.5	25.9	26.8	42.5	27.5	12.5	24.3	125.4	18.6	20.0	202.0	15.0	22.2
Nd	55.2	29.0	66.7	35.1	37.9	32.8	45.5	92.5	53.0	8.5	98.2	38.8	40.0
Pr	15.06	8.25	17.76	9.32	10.15	9.06	12.60	23.23	13.81	2.29	26.20	9.46	10.29
Rb	183.8	161.9	160.4	277.4	215.2	199.8	138.5	51.5	137.1	272.4	79.4	202.8	202.8
Sc	22	28	25	40	26	14	23	1	22	22	1	13	19
Sm	9.60	6.22	12.86	6.38	6.97	6.05	8.19	19.46	10.03	2.20	19.95	6.70	8.50
Sn	5	4	4	8	1	3	4	8	<1	4	11	4	4
Sr	84.8	16.7	71.5	115.1	109.1	18.0	144.4	128.6	117.3	124.8	104.5	93.6	79.9
Ta	2.8	1.7	2.1	2.9	2.0	1.2	2.0	8.2	1.7	1.6	12.2	1.3	1.6
Tb	1.20	1.02	1.84	0.56	1.13	0.75	1.12	2.94	1.59	0.40	3.27	0.85	1.11
Th	13.2	13.3	14.7	26.4	16.1	14.3	13.8	15.2	16.6	19.6	21.6	17.6	15.4
Tm	0.66	0.58	0.64	0.24	0.61	0.41	0.40	1.63	0.91	0.17	1.68	0.48	0.55
U	0.8	2.3	1.6	3.8	2.9	3.9	2.6	4.1	1.0	3.6	4.1	4.8	3.2
V	135	175	151	312	190	102	128	9	134	139	<5	60	108
W	-	190.7	355.5	11.6	417.1	426.3	206.9	465.2	497.8	-	916.0	-	-
Y	38.8	33.4	37.9	12.0	36.0	22.2	28.8	93.2	58.6	11.6	101.0	30.0	34.0
Yb	4.18	3.87	4.30	1.84	4.30	2.62	2.99	10.25	5.47	1.35	10.05	3.42	3.31
Zr	264.1	207.8	305.7	688.2	308.9	198.2	259.0	795.0	198.9	186.2	936.0	221.6	236.3
Cu	93.7	46.5	41.8	28.6	60.3	30.1	25.1	4.2	62.2	13.1	4.0	25.9	23.9
Mo	0.1	0.2	0.4	0.1	0.9	0.3	0.3	0.2	0.6	0.1	3.0	0.3	0.4
Ni	51.6	35.8	42.7	22.6	47.2	16.5	9.0	0.5	14.9	8.5	1.0	14.1	80.3
Pb	23.0	8.8	2.2	4.8	6.2	14.8	3.8	5.5	2.1	8.5	15.0	17.3	8.9
Zn	141	97	90	38	109	68	67	202	37	52	205	59	79

Table 4.6 - U-Pb isotopic data results from sample PR-09

PR-09	206* (%)	Th/U	Ratios						Rho	Ages						Conc. %
			ratio 6/8	1 std (abs)	ratio 7/5	1 std (abs)	ratio 7/6	1 std (abs)		6/8 (Ma)	1 std (abs)	7/5 (Ma)	1 std (abs)	7/6 (Ma)	1 std (abs)	
043_Zir26	1.37	5284.387	0.2130	0.1204	-395.0324	-598.2545	-13.45249	-18.9000	0.37	1244.6	610.1	-	-	-	-	-
006_Zir3	1.79	11.174	0.2448	0.0742	1081.9993	661.4571	32.06013	17.0154	0.50	1411.4	373.5	7095.0	484.0	-	-	-
005_Zir2	-268586.75	10.690	13.8739	3.5054	971.8977	251.9175	0.50803	0.0293	0.97	17402.8	1364.2	6986.1	233.8	4264.7	82.4	409.1
042_Zir25	1.40	13.253	0.1582	0.0300	1.1719	0.2820	0.05373	0.0080	0.79	946.6	164.7	787.5	124.0	359.7	304.1	263.2
018_Zir10	0.77	90.186	0.2149	0.0461	1.9377	0.7107	0.06538	0.0195	0.58	1255.1	240.0	1094.2	220.0	786.5	525.2	159.6
044_Zir27	0.08	1.893	0.2399	0.0108	2.3974	0.1499	0.07246	0.0031	0.72	1386.3	56.1	1241.8	43.8	999.0	85.0	138.8
025_Zir15	0.05	1.511	0.1836	0.0036	1.8083	0.0427	0.07143	0.0009	0.84	1086.5	19.8	1048.4	15.3	969.8	24.8	112.0
033_Zir20	0.01	0.656	0.1545	0.0012	1.4527	0.0162	0.06817	0.0005	0.68	926.4	6.5	911.0	6.7	873.7	15.0	106.0
045_Zir28	0.08	0.350	0.1588	0.0063	1.5128	0.0620	0.06910	0.0006	0.97	949.9	35.2	935.6	24.7	901.7	17.4	105.3
020_Zir12	0.00	0.272	0.1656	0.0011	1.6169	0.0157	0.07081	0.0004	0.67	987.9	6.0	976.8	6.1	951.8	12.5	103.8
032_Zir19	0.04	0.157	0.1645	0.0012	1.6302	0.0172	0.07186	0.0005	0.70	981.8	6.8	981.9	6.6	982.0	13.2	100.0
012_Zir6	0.04	1.106	0.1562	0.0028	1.5518	0.0334	0.07203	0.0008	0.83	935.8	15.5	951.2	13.2	986.8	23.2	94.8
026_Zir16	0.05	5.911	0.1381	0.0014	1.3205	0.0217	0.06935	0.0009	0.61	833.9	7.9	854.7	9.5	909.1	25.4	91.7
030_Zir17	0.64	92.804	0.1420	0.0157	1.4107	0.2842	0.07205	0.0121	0.55	856.0	88.1	893.4	113.1	987.2	309.2	86.7
004_Zir1	3.01	2.870	0.1982	0.0028	2.4687	0.1078	0.09032	0.0037	0.32	1165.8	15.0	1262.9	31.1	1432.2	76.6	81.4
037_Zir22	1.40	0.282	0.1497	0.0017	1.6200	0.0271	0.07846	0.0009	0.69	899.5	9.7	978.0	10.5	1158.6	22.7	77.6
038_Zir23	0.36	12.173	0.1298	0.0097	1.3440	0.1560	0.07512	0.0067	0.64	786.5	55.1	864.9	65.4	1071.6	168.7	73.4
031_Zir18	1.11	2.606	0.1275	0.0039	1.6164	0.0533	0.09193	0.0011	0.92	773.7	22.1	976.6	20.5	1465.9	23.1	52.8
013_Zir7	2.81	0.605	0.1372	0.0028	1.9668	0.0547	0.10400	0.0020	0.72	828.5	15.6	1104.2	18.6	1696.6	34.3	48.8
036_Zir21	11.24	3.853	0.1744	0.0037	4.6022	0.2265	0.19137	0.0085	0.43	1036.3	20.3	1749.7	40.2	2754.0	70.9	37.6
024_Zir14	0.46	4.714	0.1904	0.0072	6.2102	0.3390	0.23648	0.0093	0.69	1123.8	38.6	2005.9	46.7	3096.4	61.5	36.3
023_Zir13	0.24	26.241	0.1606	0.0108	4.2362	0.3553	0.19126	0.0095	0.80	960.2	59.9	1681.1	66.7	2753.0	79.5	34.9
019_Zir11	0.41	11.128	0.1425	0.0268	3.3167	0.7231	0.16885	0.0186	0.86	858.5	149.4	1485.0	157.3	2546.3	173.9	33.7
017_Zir9	5.11	0.323	0.0820	0.0017	1.0920	0.0342	0.09661	0.0022	0.68	507.9	10.4	749.5	16.5	1559.7	41.9	32.6
011_Zir5	10.21	5.070	0.2230	0.0086	16.0788	1.0450	0.52292	0.0273	0.59	1297.7	45.1	2881.5	60.3	4307.2	74.6	30.1
014_Zir8	0.45	34.609	0.1610	0.0260	10.9665	1.8548	0.49405	0.0245	0.96	962.2	142.9	2520.3	146.3	4223.6	71.2	22.8
039_Zir24	1.67	13.628	0.0788	0.0323	2.5519	2.5834	0.23483	0.2173	0.41	489.0	190.4	1287.0	555.0	3085.3	1007.0	15.8
007_Zir4	1.09	34.537	0.2186	0.0574	1.3776	0.3920	0.04570	0.0050	0.92	1274.6	296.9	879.4	155.0	-18.3	245.1	-6957.7

Table 4.7 - U-Pb isotopic data results from sample IPC 184

IPC184	f(206)%	Th/U	Ratios						Rho	Ages						Conc (%)
			6/8 ratio	1s(%)	7/5 ratio	1s(%)	7/6 ratio	1s(%)		6/8 age	1 std (abs)	7/5 age	1 std (abs)	7/6 age	1std (abs)	
055-Z44	45.5534	0.716	0.11	3.88	0.81	11.13	0.05	10.13	0.36	698.0	30.3	605.0	49.5	270.6	217.1	258.0
008-Z06	0.0372	0.359	0.20	1.10	1.80	1.41	0.07	0.89	0.76	1163.0	11.7	1044.3	9.2	803.5	18.6	144.7
028-Z21	0.6262	0.924	0.19	1.06	1.71	1.17	0.07	0.50	0.90	1120.4	10.9	1013.1	7.5	787.9	10.6	142.2
037-Z28	0.4434	1.166	0.15	1.79	1.33	3.20	0.06	2.65	0.55	925.6	15.4	859.1	18.5	691.1	56.5	133.9
048-Z36	0.0300	0.259	0.14	1.34	1.20	2.00	0.06	1.48	0.66	859.6	10.8	802.5	11.1	647.2	31.8	132.8
058-Z44	0.0128	0.411	0.15	1.04	1.36	1.30	0.06	0.78	0.79	915.8	8.8	873.6	7.6	768.2	16.4	119.2
035-Z26	0.0522	0.151	0.15	1.17	1.33	1.37	0.07	0.71	0.85	888.0	9.7	858.8	7.9	784.3	14.9	113.2
036-Z27	0.0336	0.342	0.15	1.61	1.40	2.65	0.07	2.11	0.83	916.7	13.7	886.9	15.7	813.4	44.1	112.7
006-Z04	0.0037	0.489	0.14	1.87	1.23	2.13	0.06	1.02	0.96	837.0	14.6	815.0	11.9	755.3	21.5	110.8
034-Z25	0.0193	0.175	0.14	0.78	1.29	0.90	0.07	0.46	0.84	865.3	6.3	842.9	5.2	784.4	9.8	110.3
049-Z37	0.0133	0.242	0.12	1.08	1.04	1.40	0.06	0.90	0.76	742.8	7.6	726.2	7.3	675.1	19.2	110.0
016-Z12	0.0228	0.154	0.14	0.95	1.21	1.78	0.06	1.51	0.75	827.0	7.4	807.1	9.9	752.9	31.9	109.8
044-Z32	0.0168	0.109	0.14	1.19	1.20	1.38	0.06	0.70	0.85	820.6	9.2	801.5	7.7	748.8	14.8	109.6
039-Z30	0.1971	0.315	0.16	1.55	1.54	2.53	0.07	2.00	0.61	968.3	13.9	944.5	15.5	889.6	41.3	108.9
059-Z45	0.9587	0.220	0.14	1.33	1.30	2.82	0.07	2.49	0.46	855.2	10.7	845.3	16.2	819.5	51.9	104.4
038-Z29	0.0320	0.093	0.13	1.04	1.22	1.51	0.07	1.09	0.68	813.7	8.0	811.5	8.4	805.6	22.7	101.0
007-Z05	0.0185	0.438	0.15	0.84	1.37	1.04	0.07	0.61	0.79	875.7	6.9	877.2	6.1	880.8	12.5	99.4
003-Z01	0.0166	0.452	0.14	0.86	1.36	1.28	0.07	0.95	0.64	868.8	7.0	872.7	7.5	882.6	19.5	98.4
017-Z13	0.1808	0.355	0.17	1.11	1.80	2.11	0.08	1.79	0.51	1032.0	10.6	1046.9	13.7	1078.1	35.5	95.7
013-Z09	0.0150	0.510	0.25	1.83	3.19	2.09	0.09	1.00	0.87	1419.7	23.3	1454.5	16.0	1505.7	18.8	94.3
005-Z03	0.0076	0.364	0.11	0.95	0.99	1.22	0.06	0.76	0.76	690.0	6.2	700.0	6.1	732.3	16.0	94.2
010-Z08	0.0126	0.101	0.12	1.13	1.13	1.96	0.07	1.59	0.79	756.5	8.1	768.9	10.5	805.2	33.0	94.0
053-Z39	17.5793	0.720	0.21	6.70	2.38	10.82	0.08	7.14	0.68	1206.3	88.8	1236.8	74.6	1290.2	133.0	93.5
025-Z18	0.0962	0.589	0.13	1.54	1.18	2.19	0.07	1.56	0.70	763.2	11.1	789.5	12.0	864.6	32.0	88.3
033-Z24	0.0193	0.260	0.11	1.63	0.94	1.71	0.06	0.50	0.95	648.0	10.1	672.2	8.4	754.2	10.5	85.9
015-Z11	1.1169	0.760	0.09	3.07	0.79	3.82	0.06	2.23	0.81	555.8	16.5	593.1	17.0	738.4	46.6	75.3
009-Z07	0.0079	0.003	0.10	0.81	0.88	0.99	0.07	0.57	0.79	596.7	4.6	639.8	4.7	795.1	11.9	75.0
043-Z31	0.0449	0.313	0.11	2.15	1.12	2.82	0.07	1.83	0.76	686.9	14.0	763.0	15.0	992.8	36.8	69.2
029-Z22	0.3470	0.153	0.13	0.95	1.38	1.17	0.08	0.68	0.80	768.5	6.9	882.3	6.9	1179.5	13.3	65.2
024-Z17	0.5676	0.314	0.09	3.67	0.85	4.45	0.07	2.49	0.83	534.7	18.9	622.4	20.5	955.8	50.2	55.9
047-Z35	40.3042	0.946	0.05	3.02	0.46	6.69	0.06	5.78	0.46	341.0	11.2	385.2	21.2	659.8	419.2	51.7
046-Z34	0.1228	0.393	0.15	1.56	2.33	3.24	0.11	2.83	0.73	921.7	13.4	1222.2	22.7	1800.2	50.7	51.2
026-Z19	1.2319	0.763	0.11	1.43	1.43	3.40	0.09	3.08	0.67	689.9	9.4	901.1	20.1	1462.2	57.3	47.2
004-Z02	0.6854	0.663	0.05	1.11	0.48	1.26	0.07	0.59	0.88	325.3	3.5	397.8	4.1	843.8	12.1	38.6
018-Z14	1.2074	1.384	0.05	2.54	0.46	2.68	0.07	0.76	0.96	288.0	7.2	387.3	8.6	1033.4	15.2	27.9
057-Z43	1.3846	0.444	0.06	3.35	0.74	4.78	0.09	3.37	0.70	381.8	12.6	563.3	20.5	1385.7	63.4	27.6
054-Z39	29.7032	0.771	0.15	12.16	5.50	16.62	0.27	11.32	0.73	885.2	100.6	1900.9	142.8	3312.3	177.5	26.7
030-Z23	1.0944	0.868	0.03	5.25	0.27	6.66	0.06	4.03	0.93	191.6	10.0	242.9	14.3	773.7	82.6	24.8
019-Z15	0.0508	0.713	0.03	8.92	0.27	8.94	0.07	0.63	1.00	177.3	15.6	243.2	19.2	939.0	12.8	18.9
014-Z10	1.4791	0.705	0.03	6.89	0.33	7.12	0.10	1.35	0.98	159.4	11.0	289.0	17.8	1535.9	25.2	10.4
023-Z16	8.5927	0.887	0.01	16.83	0.17	18.54	0.11	2.09	0.99	69.6	12.7	159.5	27.0	1857.8	37.3	3.7
027-Z20	2.1178	1.211	-0.02	0.94	-0.17	1.06	0.07	0.46	0.89	111.4	-1.1	-188.2	-2.2	976.5	9.3	-11.4
045-Z33	0.0316	0.774	-0.04	3.36	-0.35	3.56	0.06	1.17	0.94	-287.6	-9.9	-439.4	-19.8	544.3	25.3	-52.8

Table 4.8 - U-Pb isotopic data results from sample PR-01a

PR-01a	206* (%)	Th/U	Ratios						Rho	Ages (1 std. abs)						Conc. %
			ratio 7/5	1 std (abs)	ratio 7/6	1 std (abs)	ratio 6/8	1 std (abs)		6/8 (Ma)	1 std (abs)	7/5 (Ma)	1 std (abs)	7/6 (Ma)	1 std (abs)	
024_Zir10	0.0569	0.536	1.3471	0.0261	0.06177	0.0007	0.1581	0.0025	0.81	946.5	13.8	866.3	11.2	666.3	22.8	142.0
033_Zir15	0.3946	0.017	0.8848	0.1137	0.05729	0.0060	0.1120	0.0084	0.59	684.3	48.7	643.6	59.5	502.8	214.2	136.1
043_Zir16RIM	0.0157	0.130	1.2327	0.0174	0.06546	0.0005	0.1366	0.0016	0.83	825.3	9.1	815.6	7.9	789.1	14.7	104.6
011_Zir3RIM	0.0364	0.038	0.9361	0.0138	0.06150	0.0005	0.1104	0.0013	0.78	675.0	7.3	670.8	7.2	656.8	18.3	102.8
014_Zir6	0.0294	0.664	1.6740	0.0241	0.07220	0.0006	0.1681	0.0019	0.78	1001.9	10.4	998.7	9.1	991.6	16.8	101.0
025_Zir17	0.0221	0.018	0.9449	0.0098	0.06193	0.0004	0.1106	0.0008	0.72	676.5	4.8	675.5	5.1	671.8	13.0	100.7
030_Zir24	0.0152	0.027	0.8975	0.0082	0.06128	0.0003	0.1062	0.0007	0.71	650.7	4.0	650.4	4.4	649.1	11.2	100.2
013_Zir4RIM	0.0244	0.267	1.4771	0.0198	0.07007	0.0005	0.1529	0.0016	0.78	917.1	8.9	921.0	8.1	930.3	15.4	98.6
026_Zir18	0.0154	0.368	1.2250	0.0136	0.06664	0.0004	0.1333	0.0012	0.79	806.7	6.6	812.0	6.2	826.5	11.9	97.6
018_Zir7RIM	0.0282	0.052	0.8492	0.0106	0.06091	0.0004	0.1011	0.0010	0.76	620.9	5.6	624.2	5.8	636.2	15.6	97.6
031_Zir25	0.0137	0.044	0.9077	0.0115	0.06193	0.0004	0.1063	0.0011	0.84	651.2	6.6	655.8	6.1	671.5	12.5	97.0
032_Zir26CORE	0.8198	0.736	6.1864	0.1297	0.12631	0.0018	0.3552	0.0054	0.73	1959.4	25.8	2002.5	18.2	2047.2	24.3	95.7
020_Zir8CORE	0.0193	0.355	7.3028	0.0822	0.13790	0.0009	0.3840	0.0032	0.74	2095.2	14.8	2149.2	10.0	2201.0	11.5	95.2
027_Zir23	0.0410	0.266	1.1987	0.0270	0.06744	0.0005	0.1289	0.0027	0.92	781.6	15.2	800.0	12.4	851.5	16.6	91.8
038_Zir22	0.2164	0.197	0.9031	0.0808	0.06274	0.0034	0.1044	0.0074	0.79	640.0	43.2	653.4	42.2	699.5	111.4	91.5
047_Zir11	0.2084	0.165	1.0458	0.0143	0.06633	0.0005	0.1143	0.0013	0.80	697.9	7.2	726.8	7.1	816.9	15.4	85.4
004_Zir0	0.1732	0.208	5.2649	0.0933	0.12848	0.0011	0.2972	0.0045	0.86	1677.3	22.5	1863.2	15.0	2077.3	14.4	80.7
021_Zir9	0.0467	0.180	4.7056	0.1441	0.12237	0.0015	0.2789	0.0078	0.91	1585.7	39.2	1768.2	25.3	1991.0	21.0	79.6
017_Zir7CORE	0.0858	0.025	0.9809	0.0109	0.06661	0.0004	0.1068	0.0009	0.74	654.1	5.1	694.1	5.6	825.7	13.4	79.2
012_Zir4CORE	0.8620	0.223	1.8063	0.0212	0.08202	0.0006	0.1597	0.0014	0.74	955.2	7.7	1047.8	7.6	1246.0	13.7	76.7
019_Zir8RIM	0.0193	0.114	1.1409	0.0130	0.07239	0.0005	0.1143	0.0010	0.75	697.7	5.6	772.9	6.1	996.9	13.4	70.0
007_Zir3CORE	0.2058	0.445	2.7077	0.0807	0.10497	0.0024	0.1871	0.0035	0.63	1105.5	19.0	1330.6	21.9	1713.8	41.5	64.5
036_Zir14RIM	0.1275	0.182	1.1541	0.0199	0.08310	0.0008	0.1007	0.0014	0.79	618.6	8.1	779.2	9.3	1271.7	19.0	48.6
039_Zir27	24.5254	0.393	9.4736	0.5136	0.38107	0.0123	0.1803	0.0078	0.80	1068.6	42.6	2385.0	48.6	3836.0	47.8	27.9
005_Zir1	23.0535	4.612	6.7303	0.5664	0.30968	0.0172	0.1576	0.0099	0.75	943.5	55.2	2076.6	71.8	3519.4	83.2	26.8
006_Zir2	29.0040	2.927	8.2522	0.8583	0.36877	0.0252	0.1623	0.0127	0.75	969.5	70.2	2259.1	90.1	3786.4	99.7	25.6
037_Zir13	15.4700	0.372	5.6484	0.3246	0.29219	0.0115	0.1402	0.0059	0.73	845.8	33.0	1923.5	48.4	3429.3	59.7	24.7
044_Zir28	26.4631	0.784	6.5013	0.3544	0.32743	0.0124	0.1440	0.0056	0.74	867.2	31.4	2046.1	46.8	3605.1	57.1	24.1
046_Zir30	33.5219	0.401	10.5294	1.7194	0.50768	0.0424	0.1504	0.0242	0.86	903.3	147.4	2482.5	141.1	4263.7	116.8	21.2
045_Zir29	40.4304	0.675	8.0282	1.1666	0.44744	0.0309	0.1304	0.0166	0.88	788.6	94.2	2234.2	123.4	4076.7	99.1	19.3

Table 4.9: U-Pb isotopic data results from sample PR-10

PR-10	Th/U	Ratios						Rho	Ages						Conc. %					
		ratio 6/8		1 σ (%)		ratio 7/5		1 σ (%)		ratio 7/6		1 σ (%)		6/8 (Ma)		2 σ (abs)		7/5 (Ma)		2 σ (abs)
013-ZR8	0.043	0.1346	0.67	1.245	0.81	0.06706	0.26	0.83	814	10	821	9	840	11	103.1					
010-ZR7	0.048	0.1362	1.09	1.262	1.21	0.06717	0.38	0.90	823	17	829	14	843	16	102.4					
024-ZR27	0.076	0.1364	0.79	1.223	1.11	0.06502	0.68	0.72	824	12	811	12	775	28	94.0					
019-ZR24	0.064	0.1360	0.80	1.229	1.15	0.06557	0.74	0.69	822	12	814	13	793	31	96.5					
018-ZR23	0.010	0.1368	0.72	1.244	1.03	0.06595	0.63	0.70	827	11	821	12	805	26	97.3					
014-ZR19	0.072	0.1348	0.86	1.210	1.36	0.06512	0.99	0.63	815	13	805	15	778	41	95.5					
010-ZR17	0.023	0.1343	0.77	1.217	1.40	0.06569	1.11	0.55	813	12	808	16	797	46	98.0					
003-ZR01	0.037	0.1371	0.93	1.254	1.15	0.06633	0.58	0.80	828	14	825	13	817	24	98.6					
007-ZR14	0.026	0.1298	0.82	1.184	1.19	0.06613	0.78	0.69	787	12	793	13	810	33	103.0					
006-ZR13	0.024	0.1309	0.61	1.199	1.01	0.06638	0.71	0.60	793	9	800	11	818	30	103.2					
005-ZR12	0.021	0.1256	0.80	1.128	1.09	0.06516	0.65	0.73	763	11	767	12	779	27	102.2					
016-ZR21	0.016	0.1321	0.63	1.200	0.89	0.06587	0.51	0.71	800	9	800	10	802	21	100.3					
020-ZR25	0.010	0.1192	1.01	1.056	1.47	0.06426	1.00	0.69	726	14	732	15	750	42	103.4					
006-ZR3	0.021	0.1217	0.54	1.099	0.71	0.06548	0.26	0.77	740	8	753	7	790	11	106.7					
004-ZR1	0.014	0.1199	0.81	1.076	0.98	0.06508	0.40	0.83	730	11	742	10	777	17	106.4					
009-ZR6	0.153	0.1197	0.50	1.097	0.73	0.06649	0.38	0.69	729	7	752	8	822	16	112.7					
015-91500	0.297	0.1800	0.71	1.851	1.00	0.07455	0.61	0.70	1067	14	1064	13	1056	24	99.0					
003-91500	0.295	0.1796	0.68	1.853	0.90	0.07484	0.46	0.75	1065	13	1065	12	1064	19	99.9					
025-ZR28	0.029	0.1323	0.88	1.068	4.77	0.05854	4.68	0.18	804	43	738	49	550	498	68.7					
007-ZR4	0.097	0.1297	1.30	1.148	2.58	0.06423	2.19	0.50	786	19	776	28	749	94	95.3					
023-ZR26	0.039	0.1382	1.28	1.243	3.03	0.06525	2.73	0.42	834	20	820	34	782	113	93.8					
017-ZR22	0.106	0.1368	0.61	1.235	1.25	0.06546	1.03	0.49	826	10	816	14	789	43	95.5					
015-ZR20	0.032	0.1373	0.73	1.124	5.60	0.05937	5.54	0.13	830	11	765	59	581	232	70.0					
013-ZR18	0.048	0.1333	0.92	1.095	3.45	0.05957	3.34	0.27	807	14	754	36	588	140	72.9					
009-ZR16	0.025	0.1358	0.89	1.137	3.18	0.06072	3.03	0.28	824	14	771	34	629	128	76.6					
008-ZR15	0.144	0.1349	0.65	1.202	1.76	0.06459	1.59	0.37	816	10	804	19	764	66	93.3					
004-ZR11	0.026	0.1338	0.82	1.164	2.77	0.06293	2.62	0.30	809	12	782	30	706	109	87.2					
026-ZR29	0.013	0.1350	0.68	1.130	2.55	0.06070	2.43	0.27	816	10	768	27	629	103	77.0					
014-ZR9	0.009	0.1235	0.92	1.070	2.00	0.06282	1.74	0.46	751	13	739	21	702	73	93.5					
008-ZR5	0.340	0.3543	4.36	5.842	5.11	0.11957	2.65	0.85	1955	146	1953	87	1950	93	99.7					
005-ZR2	0.038	0.1317	0.55	1.050	4.05	0.05785	3.99	0.14	797	8	729	42	524	170	65.7					

Tabela 4.10: U-Pb isotopic data results from supracrustal rock samples

PR-04	206* (%)	Th/U	Ratios								Rho	Ages						Conc (%)
			ratio 6/4	1 std (abs)	ratio 7/5	1 std (abs)	ratio 7/6	1 std (abs)	ratio 6/8	1 std (abs)		6/8 (Ma)	1 std (abs)	7/5 (Ma)	1 std (abs)	7/6 (Ma)	1 std (abs)	
098_Zr63	0.359	4.764	4318.1	642.9	-429.0908	-429.1396	-16.04164	-15.83377	0.1940	0.0313	0.16	1142.9	166.6	-	-	-	-	-
040_Zr25	0.204	0.268	7608.5	2120.9	0.8105	0.1274	0.04649	0.00655	0.1264	0.0088	0.44	767.5	50.2	602.7	69.1	23.1	307.3	3325.87
046_Zr29	-0226.745	0.204	34.1	1.9	408.3559	143.4315	0.68472	0.04039	4.3250	1.4975	0.99	10781.1	1597.5	6107.1	305.0	4699.0	82.3	220.44
070_Zr44	0.078	0.457	19726.8	4977.8	2.2169	0.0980	0.07428	0.00237	0.2164	0.0066	0.69	1263.0	34.7	1186.4	30.5	1049.1	63.1	120.39
020_Zr11_RIM	0.031	0.318	49278.5	16375.7	1.5617	0.0440	0.06713	0.00155	0.1687	0.0026	0.56	1005.0	14.5	955.2	17.3	841.9	47.4	119.37
039_Zr24	0.088	0.662	17173.8	2625.7	5.5497	0.3292	0.10783	0.00354	0.3732	0.0184	0.83	2044.7	85.7	1908.3	49.8	1763.1	58.9	115.97
050_Zr31	0.011	0.211	138177.9	25057.7	8.3815	0.3230	0.13351	0.00167	0.4553	0.0165	0.94	2418.6	72.7	2273.2	34.4	2144.7	21.7	112.77
012_Zr7	0.009	0.530	169568.9	32515.5	5.1355	0.1564	0.10579	0.00190	0.3520	0.0085	0.80	1944.3	40.6	1842.0	25.6	1728.2	32.7	112.51
096_Zr61	0.012	0.296	123984.5	19927.7	8.1445	0.1297	0.13212	0.00113	0.4471	0.0058	0.81	2382.2	25.7	2247.2	14.3	2126.3	14.9	112.03
005_Zr2	0.023	0.238	66401.3	14005.9	2.5834	0.0609	0.08045	0.00076	0.2329	0.0050	0.90	1349.7	25.9	1296.0	17.1	1207.9	18.5	111.73
065_Zr41	0.010	0.388	154088.3	21912.1	6.0659	0.2701	0.11463	0.00453	0.3838	0.0078	0.45	2093.9	36.1	1985.4	38.1	1874.1	69.5	111.73
059_Zr38_CORE	0.023	0.531	66263.5	15435.6	3.0829	0.0893	0.08602	0.00100	0.2599	0.0068	0.91	1489.3	34.8	1428.5	22.0	1338.7	22.3	111.25
097_Zr62	0.050	0.479	29891.9	4744.6	6.9402	0.3260	0.12267	0.00203	0.4103	0.0180	0.93	2216.3	81.6	2103.8	40.9	1995.4	29.1	111.07
057_Zr36	0.019	0.434	79356.4	10008.3	2.9980	0.0795	0.08541	0.00093	0.2545	0.0061	0.90	1461.9	31.2	1407.1	20.0	1325.0	21.0	110.33
099_Zr64	0.024	0.193	65555.2	9222.2	2.5410	0.0488	0.08080	0.00107	0.2281	0.0030	0.70	1324.4	16.0	1283.9	13.9	1216.6	25.9	108.86
063_Zr39	0.014	0.515	107473.6	13445.2	7.7021	0.1722	0.13119	0.00224	0.4258	0.0060	0.63	2286.6	26.9	2196.8	19.9	2113.9	29.6	108.17
089_Zr56	0.011	0.289	134778.2	26962.6	2.3279	0.0246	0.07935	0.00052	0.2128	0.0016	0.71	1243.5	8.4	1220.8	7.5	1180.8	12.8	105.31
076_Zr48	0.021	0.357	74470.1	13619.4	3.0225	0.0503	0.08744	0.00077	0.2507	0.0034	0.82	1442.0	17.6	1413.3	12.6	1370.2	16.9	105.24
024_Zr13	0.010	0.222	148880.3	36031.2	2.3193	0.0365	0.07940	0.00059	0.2118	0.0028	0.85	1238.6	15.1	1218.2	11.1	1182.2	14.5	104.77
056_Zr35	0.006	0.465	259358.8	33537.7	6.8703	0.1051	0.12642	0.00090	0.3941	0.0051	0.85	2141.9	23.7	2094.8	13.5	2048.8	12.6	104.54
019_Zr11_CORE	0.034	0.305	45714.0	7060.2	1.5927	0.0349	0.07035	0.00103	0.1642	0.0026	0.72	980.0	14.3	967.4	13.6	938.7	29.8	104.39
064_Zr40	0.015	0.669	103541.8	10123.5	5.3906	0.0770	0.11257	0.00103	0.3473	0.0036	0.72	1921.6	17.1	1883.4	12.2	1841.3	16.4	104.36
075_Zr47	0.019	0.657	78330.3	14939.1	7.0795	0.1947	0.12850	0.00111	0.3995	0.0103	0.94	2166.9	47.4	2121.5	24.2	2077.6	15.1	104.30
071_Zr45	0.008	0.317	190797.9	33397.6	1.7767	0.0315	0.07282	0.00045	0.1770	0.0029	0.91	1050.3	15.7	1037.0	11.4	1008.8	12.5	104.11
052_Zr33	0.030	0.635	50183.8	10536.1	5.5860	0.1188	0.11463	0.00138	0.3534	0.0061	0.81	1950.9	28.8	1913.9	18.2	1874.0	21.6	104.10
017_Zr9	0.061	0.493	25166.5	3357.3	4.9173	0.2038	0.10811	0.00322	0.3298	0.0094	0.69	1837.6	45.6	1805.2	34.4	1767.9	53.4	103.95
053_Zr34	0.023	0.464	61705.0	11226.2	20.0004	0.6734	0.22942	0.00316	0.6322	0.0193	0.91	3158.4	75.7	3091.4	32.1	3048.0	21.9	103.62
090_Zr57	0.015	0.741	102131.2	14233.2	7.1818	0.1223	0.13006	0.00117	0.4004	0.0056	0.82	2171.1	25.7	2134.3	15.1	2098.8	15.8	103.44
038_Zr23	0.044	0.733	34852.8	9791.9	4.5712	0.1325	0.10504	0.00213	0.3156	0.0064	0.70	1768.3	31.4	1744.0	23.9	1715.0	36.8	103.11
082_Zr52	0.027	0.248	57931.6	7513.4	2.8596	0.0549	0.08637	0.00118	0.2401	0.0031	0.67	1387.2	16.1	1371.3	14.3	1346.6	26.2	103.02
051_Zr32	0.015	0.732	104190.8	15438.1	6.5106	0.2173	0.12420	0.00359	0.3802	0.0062	0.49	2077.1	28.9	2047.3	29.0	2017.4	50.4	102.96
043_Zr26	0.152	1.217	10114.2	2471.2	2.9399	0.1593	0.08745	0.00341	0.2438	0.0091	0.69	1406.4	47.2	1392.2	40.3	1370.5	73.2	102.62
045_Zr28	0.019	0.204	83304.7	15362.2	2.7180	0.0376	0.08498	0.00059	0.2320	0.0026	0.82	1344.7	13.8	1333.4	10.2	1315.0	13.4	102.26
060_Zr38_RIM	0.109	0.680	14132.2	7960.4	2.7767	0.0558	0.08569	0.00128	0.2350	0.0030	0.64	1360.7	15.9	1349.3	14.9	1331.1	28.6	102.22
037_Zr22	0.209	0.522	7418.0	1717.2	1.6173	0.1181	0.07119	0.00401	0.1648	0.0076	0.64	983.1	42.2	976.9	44.8	962.9	110.9	102.10
077_Zr49	0.020	0.940	75393.2	16207.7	6.3829	0.1135	0.12398	0.00096	0.3734	0.0058	0.88	2045.2	27.2	2029.9	15.5	2014.3	13.6	101.53
084_Zr53_RIM	0.015	0.433	100933.1	16886.4	3.6014	0.0511	0.09545	0.00065	0.2736	0.0032	0.84	1559.3	16.4	1549.8	11.2	1536.9	12.8	101.46
088_Zr55	0.015	0.246	106003.1	17157.3	3.2111	0.0468	0.09106	0.00073	0.2557	0.0030	0.79	1467.9	15.2	1459.8	11.2	1448.0	15.2	101.38
058_Zr37	0.023	0.456	67546.6	16459.7	2.7518	0.0704	0.08572	0.00140	0.2328	0.0045	0.76	1349.2	23.5	1342.6	18.9	1331.8	31.2	101.31
025_Zr14	0.012	0.334	126678.0	19143.3	6.1720	0.1941	0.12221	0.00339	0.3662	0.0053	0.46	2011.7	24.8	2000.5	27.1	1988.8	48.5	101.15
047_Zr30	0.005	0.389	286877.6	160420.1	6.2471	0.1422	0.12335	0.00173	0.3673	0.0065	0.77	2016.6	30.3	2011.1	19.7	2005.2	24.7	100.57
032_Zr19	0.029	0.406	53834.2	14028.5	3.5005	0.0836	0.09475	0.00141	0.2679	0.0049	0.77	1530.3	24.9	1527.3	18.7	1523.1	27.7	100.47
092_Zr59	0.042	0.333	36474.4	4453.5	2.1996	0.0539	0.07927	0.00138	0.2012	0.0034	0.69	1181.9	18.2	1180.9	17.0	1178.9	33.9	100.26
026_Zr15	0.009	0.507	149691.7	31657.4	20.2498	0.7257	0.23705	0.00521	0.6195	0.0174	0.78	3107.9	68.8	3103.4	34.1	3100.3	34.6	100.25
006_Zr3	0.040	0.260	38785.2	7370.4	2.5103	0.0432	0.08319	0.00098	0.2188	0.0026	0.70	1275.7	13.9	1275.0	12.4	1273.7	22.8	100.15
081_Zr51	0.007	0.209	219086.0	32796.3	5.8054	0.0675	0.11994	0.00072	0.3510	0.0032	0.80	1939.5	15.5	1947.2	10.0	1955.3	10.6	99.19
078_Zr50	0.014	1.141	110985.1	21056.2	6.6253	0.1055	0.12813	0.00155	0.3750	0.0036	0.61	2052.8	17.0	2062.7	13.9	2072.5	21.2	99.05

Table 4.11 - U-Pb isotopic data results from supracrustal rock samples (continuation)

PR-04	206* (%)	Th/U	Ratios								Rho	Ages						Conc. (%)
			ratio 6/4	1 std (abs)	ratio 7/5	1 std (abs)	ratio 7/6	1 std (abs)	ratio 6/8	1 std (abs)		6/8 (Ma)	1 std (abs)	7/5 (Ma)	1 std (abs)	7/6 (Ma)	1 std (abs)	
069_Zr43	0.008	0.302	195076.1	33302.6	5.9850	0.0777	0.12272	0.00087	0.3537	0.0036	0.79	1952.2	17.2	1973.7	11.2	1996.1	12.6	97.80
033_Zr20	0.021	1.337	71555.6	13094.6	6.6268	0.0830	0.12930	0.00088	0.3717	0.0037	0.79	2037.3	17.2	2062.9	11.0	2088.5	11.9	97.55
004_Zr1	0.014	0.587	108433.9	18496.5	7.4019	0.1104	0.13705	0.00100	0.3917	0.0049	0.84	2130.6	22.6	2161.2	13.3	2190.3	12.6	97.28
011_Zr6	0.012	0.499	131278.1	18267.6	6.2015	0.0825	0.12568	0.00101	0.3578	0.0035	0.75	1971.9	16.8	2004.7	11.6	2038.4	14.2	96.74
085_Zr54	0.009	0.332	168680.7	33997.2	6.9767	0.0905	0.13360	0.00101	0.3787	0.0037	0.76	2070.2	17.5	2108.5	11.5	2145.9	13.1	96.48
014_Zr8_RIM	0.014	0.302	107402.4	19579.0	1.7785	0.0265	0.07480	0.00072	0.1724	0.0019	0.72	1025.5	10.2	1037.6	9.6	1063.1	19.2	96.47
021_Zr12_CORE	0.007	0.567	204325.5	32696.6	12.8585	0.2063	0.18881	0.00149	0.4939	0.0067	0.84	2587.5	28.7	2669.3	15.0	2731.8	12.9	94.72
034_Zr21	0.053	0.431	29171.5	6641.7	1.6604	0.0556	0.07366	0.00172	0.1635	0.0039	0.71	976.1	21.5	993.5	21.0	1032.2	46.5	94.56
044_Zr27	0.265	0.843	5774.6	1829.6	5.0845	0.1290	0.11565	0.00212	0.3188	0.0055	0.67	1784.0	26.6	1833.5	21.3	1890.1	32.7	94.39
031_Zr18	0.050	0.322	30896.8	4844.8	1.9612	0.0663	0.07863	0.00152	0.1809	0.0050	0.81	1071.8	27.1	1102.3	22.5	1162.8	37.8	92.18
095_Zr60	0.115	0.348	13526.2	7877.2	1.8481	0.0774	0.07725	0.00165	0.1735	0.0062	0.85	1031.3	34.0	1062.8	27.2	1127.7	42.1	91.45
027_Zr16	0.055	0.301	28242.9	5555.8	2.2050	0.0951	0.08236	0.00228	0.1942	0.0064	0.76	1143.9	34.4	1182.6	29.7	1254.0	53.2	91.22
028_Zr17	0.411	0.673	3644.3	550.4	11.1412	0.2288	0.18129	0.00228	0.4457	0.0070	0.77	2376.0	31.3	2535.0	19.0	2664.7	20.7	89.17
007_Zr4	0.056	0.350	27949.5	5132.8	1.6250	0.0403	0.07526	0.00127	0.1566	0.0028	0.72	937.8	15.5	979.9	15.5	1075.5	33.6	87.19
066_Zr42	0.263	0.975	5850.5	1853.7	4.1859	0.1397	0.11156	0.00260	0.2721	0.0064	0.71	1551.5	32.5	1671.3	27.0	1825.0	41.6	85.01
083_Zr53_CORE	0.169	0.622	9115.3	2938.4	3.0130	0.0426	0.09687	0.00077	0.2256	0.0025	0.78	1311.2	13.1	1410.9	10.7	1564.8	14.9	83.79
072_Zr45	0.236	0.476	6519.8	1493.9	4.6549	0.2397	0.12661	0.00329	0.2666	0.0118	0.86	1523.7	59.8	1759.2	42.1	2051.4	45.2	74.28
010_Zr5	0.126	0.648	12170.0	2727.4	7.8900	0.4065	0.17920	0.00862	0.3193	0.0058	0.35	1786.3	28.0	2218.5	45.4	2645.5	77.7	67.52
091_Zr58	0.022	0.388	69748.3	14566.1	2.7706	0.2161	0.10685	0.00178	0.1880	0.0143	0.98	1110.7	77.2	1347.6	56.6	1746.4	30.2	63.60
100_Zr65_RIM	4.067	0.475	379.5	28.4	6.5200	0.2228	0.20411	0.00366	0.2317	0.0067	0.84	1343.2	34.9	2048.6	29.6	2859.3	28.9	46.98
PR-11b	206* (%)	Th/U	Ratios								Rho	Ages						Conc. (%)
021_Zr11	0.344	0.686	4970.4	2792.3	0.7973	0.6816	0.02489	0.02122	0.2323	0.0147	0.07	1346.4	76.4	595.3	326.5	-	-	-
006_Zr3	0.054	0.533	28072.9	12571.7	5.7938	0.2654	0.11019	0.00267	0.3813	0.0147	0.84	2082.4	68.5	1945.5	38.9	1802.6	43.5	115.5
046_Zr25	0.091	0.230	17040.2	2747.4	1.5909	0.0743	0.06910	0.00237	0.1670	0.0053	0.68	995.4	29.0	966.7	28.7	901.8	69.0	110.4
004_Zr1	0.012	0.336	130312.2	31003.4	7.3727	0.2053	0.12825	0.00057	0.4169	0.0114	0.98	2246.4	51.5	2157.7	24.6	2074.2	7.8	108.3
039_Zr21_CORE	0.016	0.767	93991.4	16896.9	2.9855	0.0832	0.08662	0.00059	0.2500	0.0067	0.96	1438.3	34.4	1403.9	21.0	1352.0	13.1	106.4
042_Zr23	0.016	0.405	96921.9	24310.2	2.8686	0.0619	0.08540	0.00071	0.2436	0.0048	0.91	1405.3	24.7	1373.7	16.1	1324.7	15.9	106.1
027_Zr15	0.123	0.513	12375.6	3970.1	5.2054	0.2457	0.11067	0.00392	0.3411	0.0106	0.66	1891.9	50.6	1853.5	39.4	1810.5	63.0	104.5
035_Zr20_RIM	0.071	0.597	21585.7	5518.9	5.1371	0.1182	0.11124	0.00161	0.3349	0.0059	0.76	1862.1	28.2	1842.3	19.4	1819.8	26.1	102.3
010_Zr5	0.019	0.630	79583.5	21438.8	6.6938	0.0788	0.12666	0.00082	0.3833	0.0035	0.77	2091.5	16.2	2071.8	10.3	2052.2	11.4	101.9
040_Zr21_RIM	0.008	0.946	190816.1	51943.5	2.8055	0.0582	0.08615	0.00055	0.2362	0.0046	0.93	1366.7	23.8	1357.0	15.4	1341.6	12.4	101.9
028_Zr16	0.024	0.278	63605.3	11318.8	2.7053	0.0531	0.08571	0.00084	0.2289	0.0038	0.85	1328.8	19.9	1329.9	14.5	1331.6	18.8	99.8
017_Zr10	0.025	0.525	61582.2	12540.2	4.9490	0.1269	0.11088	0.00114	0.3237	0.0075	0.90	1807.7	36.4	1810.7	21.4	1813.9	18.6	99.7
032_Zr18	0.013	0.541	110889.1	23518.0	16.5588	0.2292	0.21146	0.00246	0.5679	0.0037	0.47	2899.2	15.2	2909.6	13.2	2916.8	18.7	99.4
033_Zr19	0.066	0.821	23440.6	4898.0	2.3900	0.0637	0.08021	0.00148	0.2114	0.0041	0.72	1236.1	21.6	1239.6	18.9	1245.6	35.0	99.2
022_Zr12	0.049	0.827	30909.9	11601.5	6.6329	0.2608	0.12824	0.00319	0.3751	0.0113	0.77	2053.3	52.9	2063.7	34.1	2074.0	43.2	99.0
029_Zr17	0.007	0.547	205887.5	35242.8	6.0371	0.0841	0.12270	0.00071	0.3568	0.0043	0.87	1967.1	20.5	1981.2	12.1	1995.8	10.3	98.6
045_Zr24	0.107	0.717	14317.4	6491.6	4.3755	0.1065	0.10571	0.00194	0.3002	0.0047	0.64	1692.2	23.1	1707.7	19.9	1726.6	33.3	98.0
015_Zr8	0.018	0.400	86152.9	13856.1	2.2277	0.0455	0.08041	0.00086	0.2009	0.0034	0.83	1180.3	18.3	1189.8	14.2	1206.9	21.0	97.8
024_Zr14	0.011	0.493	133016.4	75912.9	6.8939	0.1027	0.13276	0.00111	0.3766	0.0044	0.79	2060.3	20.7	2097.9	13.1	2134.8	14.6	96.5
041_Zr22	0.003	0.268	460699.5	89378.7	2.2173	0.0246	0.08096	0.00049	0.1986	0.0017	0.77	1167.9	9.1	1186.5	7.7	1220.5	11.8	95.7
034_Zr20_CORE	0.022	0.552	70454.6	12478.9	4.4843	0.0586	0.10855	0.00072	0.2996	0.0032	0.81	1689.3	15.8	1728.1	10.8	1775.2	12.0	95.2
012_Zr7	0.058	0.002	26860.1	5536.3	2.4214	0.0640	0.08420	0.00150	0.2085	0.0040	0.73	1221.0	21.3	1249.0	18.8	1297.3	34.2	94.1
047_Zr26	0.029	0.300	53062.4	8014.0	2.1653	0.0341	0.08091	0.00074	0.1941	0.0024	0.78	1143.5	12.8	1170.0	10.9	1219.2	17.9	93.8
016_Zr9	0.126	0.407	11875.9	5674.4	10.0134	0.2404	0.16719	0.00121	0.4343	0.0098	0.94	2325.2	43.9	2436.0	21.9	2529.7	12.1	91.9
048_Zr27	0.008	0.676	197902.9	36314.3	12.1511	0.1775	0.18666	0.00209	0.4721	0.0041	0.59	2492.7	17.9	2616.1	13.6	2713.0	18.3	91.9
005_Zr2CORE	0.029	0.174	53492.9	16455.9	2.8588	0.0340	0.09113	0.00048	0.2275	0.0023	0.84	1321.4	11.9	1371.1	8.9	1449.3	10.1	91.2
023_Zr13	0.008	1.215	199903.3	42388.6	5.3436	0.0620	0.12123	0.00081	0.3197	0.0028	0.75	1788.0	13.6	1875.9	9.9	1974.4	11.8	90.6
011_Zr6	1.068	0.280	1446.7	234.9	2.7796	0.0649	0.09344	0.00189	0.2157	0.0024	0.47	1259.3	12.6	1350.1	17.3	1496.8	37.8	84.1
009_Zr4	0.033	0.993	46635.7	8701.4	3.4916	0.0840	0.10418	0.00140	0.2431	0.0048	0.82	1402.6	24.7	1525.3	18.8	1699.8	24.5	82.5

Table 4.12 - U-Pb isotopic data results from supracrustal rock samples (continuation)

PR-12b	Th/U	206* (%)	Ratios								Rho	Ages						Conc. %
			ratio 6/4	1 std (%)	ratio 7/5	1 std (%)	ratio 7/6	1 std (%)	ratio 6/8	1 std (%)		6/8 (Ma)	1 std (abs)	7/5 (Ma)	1 std (abs)	7/6 (Ma)	1 std (abs)	
057_ZR40	0.90	3.83	441.88	42.14	5.48	7.18	0.23	3.42	0.18	6.08	0.87	1046.14	60.73	4897.58	59.88	3021.14	53.78	34.63
082_ZR60	0.38	0.42	4143.73	4.82	2.17	6.13	0.11	5.62	0.15	2.43	0.39	879.45	20.04	1170.67	41.70	1758.28	99.37	50.02
066_ZR46	0.35	0.58	2975.74	5.47	2.16	4.68	0.10	3.77	0.15	2.75	0.59	914.77	23.57	1169.45	31.96	1677.52	68.05	54.53
006_ZR03	0.30	0.44	3842.10	6.26	2.94	6.70	0.10	5.91	0.20	3.15	0.73	1193.11	34.33	1392.02	49.54	1711.53	104.93	69.71
089_ZR64	0.40	0.02	70389.97	6.14	6.91	4.93	0.15	3.84	0.33	3.09	0.83	1862.56	49.75	2100.21	42.78	2341.88	64.22	79.53
062_ZR45	0.40	0.02	70389.97	6.14	6.91	4.93	0.15	3.84	0.33	3.09	0.83	1862.56	49.75	2100.21	42.78	2341.88	64.22	79.53
062_ZR45	0.35	0.00	618925.78	5.43	10.46	4.05	0.18	2.99	0.41	2.73	0.70	2225.77	51.46	2476.66	37.55	2689.46	49.41	82.76
028_ZR20	0.40	0.13	12781.78	4.46	2.57	3.04	0.09	2.04	0.21	2.25	0.74	1233.36	25.27	1291.77	21.98	1390.20	38.63	88.72
037_ZR25_CORE	0.38	0.02	85566.28	2.64	6.96	1.46	0.14	0.54	0.36	1.36	0.93	2004.72	23.33	2106.10	12.87	2206.65	9.27	90.85
030_ZR22_RIM	0.40	1.24	1348.39	2.52	2.37	1.94	0.08	1.45	0.20	1.30	0.66	1194.64	14.15	1233.91	13.87	1303.18	28.09	91.67
059_ZR42	0.75	0.02	110251.98	1.70	2.17	1.45	0.08	1.13	0.19	0.91	0.60	1143.04	9.51	1170.00	10.05	1220.24	22.14	93.67
015_ZR10	0.15	0.00	894814.12	1.40	3.62	1.00	0.10	0.63	0.27	0.77	0.74	1518.00	10.39	1552.89	7.90	1600.69	11.79	94.83
031_ZR22_CORE	0.42	0.03	56650.62	3.53	2.28	2.87	0.08	2.24	0.20	1.79	0.81	1184.63	19.37	1207.17	20.05	1247.71	43.19	94.94
058_ZR41	0.37	0.00	532842.47	1.90	2.59	1.77	0.09	1.46	0.22	1.00	0.58	1272.12	11.54	1297.52	12.87	1339.77	27.92	94.95
067_ZR47	1.78	0.01	108784.37	2.92	4.89	2.73	0.11	2.29	0.31	1.49	0.54	1758.84	22.95	1801.36	22.77	1850.93	40.78	95.02
081_ZR59	0.49	0.02	111254.71	3.27	1.61	2.26	0.07	1.52	0.16	1.67	0.73	958.90	14.82	972.54	14.03	1003.47	30.64	95.56
080_ZR58	0.35	0.01	223111.79	1.61	2.21	1.28	0.08	0.94	0.20	0.87	0.65	1165.65	9.22	1184.19	8.89	1218.20	18.37	95.69
018_ZR13	0.37	0.01	161765.14	4.15	13.34	2.48	0.19	1.32	0.51	2.10	0.84	2638.33	45.27	2704.12	23.15	2753.67	21.52	95.81
077_ZR55	0.93	0.01	193294.82	2.71	5.89	2.01	0.12	1.45	0.35	1.39	0.68	1919.85	23.02	1959.97	17.28	2002.60	25.53	95.87
049_ZR34	0.48	0.02	69672.62	2.23	6.74	1.28	0.13	0.55	0.37	1.16	0.90	2034.92	20.19	2077.70	11.32	2120.38	9.61	95.97
011_ZR08	0.37	0.01	243041.85	1.57	3.41	1.17	0.10	0.81	0.26	0.85	0.70	1480.67	11.18	1506.12	9.15	1542.11	15.15	96.02
055_ZR38	0.39	0.03	46569.37	3.30	11.42	2.38	0.17	1.69	0.48	1.68	0.70	2508.11	34.79	2558.45	21.97	2598.59	27.83	96.52
010_ZR07	0.33	0.01	313100.55	1.77	2.67	4.41	0.09	4.31	0.22	0.94	0.38	1304.25	11.11	1320.13	32.08	1346.00	81.04	96.90
052_ZR37	0.66	0.09	16326.73	2.64	6.53	5.20	0.13	5.02	0.37	1.36	0.25	2018.34	23.46	2049.99	44.77	2081.97	85.76	96.94
016_ZR11	0.34	0.02	84438.08	1.86	2.30	1.55	0.08	1.20	0.20	0.98	0.61	1198.93	10.74	1212.23	10.93	1236.00	23.39	97.00
073_ZR53	0.47	0.02	86931.28	2.95	2.58	1.83	0.09	1.04	0.22	1.51	0.82	1280.23	17.47	1294.22	13.32	1317.52	20.08	97.17
056_ZR39	0.55	0.01	127646.70	2.75	2.31	1.67	0.08	0.90	0.21	1.41	0.84	1202.78	15.47	1215.36	11.80	1237.75	17.57	97.17
061_ZR44	0.70	0.04	47482.94	3.24	2.22	3.58	0.08	3.17	0.20	1.65	0.45	1178.95	17.76	1188.72	24.76	1206.53	61.28	97.71
087_ZR62	0.73	0.01	230780.60	2.03	2.34	1.57	0.08	1.15	0.21	1.06	0.66	1216.13	11.77	1224.77	11.09	1240.01	22.40	98.07
083_ZR61	0.29	0.02	95055.68	3.46	2.33	3.07	0.08	2.51	0.21	1.76	0.72	1215.22	19.43	1222.33	21.57	1234.91	48.53	98.41
059_ZR42	1.23	0.02	81705.30	2.07	6.44	2.16	0.13	1.87	0.37	1.08	0.48	2021.78	18.79	2038.03	18.85	2054.52	32.71	98.41
079_ZR57	0.87	0.01	203148.39	2.12	5.87	3.91	0.12	3.75	0.35	1.11	0.47	1942.06	18.55	1957.26	33.36	1973.38	65.32	98.41
009_ZR06	0.80	0.00	566663.97	1.82	5.29	1.07	0.11	0.46	0.33	0.96	0.89	1857.43	15.51	1867.97	9.09	1879.72	8.35	98.81
039_ZR27	0.60	0.02	60582.92	3.97	7.02	2.50	0.13	1.50	0.39	2.01	0.80	2101.81	35.92	2113.81	22.01	2125.51	25.95	98.88
048_ZR33	0.78	0.00	376639.76	1.89	6.05	1.13	0.12	0.54	0.36	0.99	0.87	1973.48	16.90	1983.02	9.87	1992.98	9.68	99.02
078_ZR56	0.27	0.01	131644.49	2.95	1.56	1.67	0.07	0.73	0.16	1.51	0.90	950.44	13.31	953.14	10.30	959.37	14.84	99.07
071_ZR51	0.38	0.03	56919.25	4.61	2.30	2.61	0.08	1.19	0.21	2.33	0.89	1209.09	25.60	1212.09	18.33	1217.44	23.22	99.31
008_ZR05	0.22	0.02	86112.08	3.32	7.10	1.78	0.13	0.57	0.39	1.69	0.95	2121.22	30.48	2124.05	15.76	2126.79	9.98	99.74
076_ZR54	1.26	0.08	20143.44	2.71	6.24	1.59	0.12	0.77	0.37	1.39	0.87	2009.83	24.00	2009.67	13.85	2009.50	13.67	100.02
069_ZR49	0.77	0.01	118401.48	2.24	1.91	2.08	0.08	1.73	0.18	1.16	0.54	1086.86	11.64	1084.10	13.87	1078.55	34.63	100.77
060_ZR43	0.53	0.01	191692.16	1.69	5.30	1.35	0.11	1.00	0.34	0.90	0.65	1877.09	14.69	1869.42	11.49	1860.91	18.03	100.87
046_ZR31	0.71	0.01	138938.26	2.47	7.34	1.91	0.13	1.42	0.40	1.27	0.66	2166.09	23.43	2153.75	17.05	2142.01	24.82	101.12
029_ZR21	0.42	0.02	82201.20	1.89	2.41	1.56	0.08	1.19	0.21	1.00	0.62	1252.87	11.37	1244.96	11.16	1231.30	23.42	101.75
041_ZR29	0.38	0.00	302818.59	2.03	7.41	1.18	0.13	0.52	0.40	1.06	0.89	2181.86	19.65	2162.44	10.56	2144.05	9.03	101.76
051_ZR36	1.13	0.01	104639.27	2.06	6.67	1.64	0.13	1.23	0.38	1.08	0.83	2090.48	19.24	2068.87	14.47	2047.41	21.82	102.10

Table 4.13 - U-Pb isotopic data results from supracrustal rock samples (continuation)

PR-12b	Th/U	206* (%)	Ratios								Rho	Ages						Conc. %
			ratio 6/4	1 std (%)	ratio 7/5	1 std (%)	ratio 7/6	1 std (%)	ratio 6/8	1 std (%)		6/8 (Ma)	1 std (abs)	7/5 (Ma)	1 std (abs)	7/6 (Ma)	1 std (abs)	
004_ZR01	0.28	0.00	747481.08	1.17	6.71	0.74	0.13	0.32	0.38	0.66	0.88	2098.68	11.91	2074.41	6.54	2050.40	5.73	102.35
040_ZR28	0.35	0.02	92199.98	2.05	1.67	1.33	0.07	0.80	0.17	1.07	0.79	1004.88	9.96	997.60	8.47	981.62	16.20	102.37
019_ZR14	0.44	0.01	137292.19	1.48	7.64	1.73	0.13	1.53	0.41	0.80	0.44	2216.71	15.08	2189.24	15.49	2163.60	26.63	102.45
036_ZR25_RIM	0.36	0.01	213632.07	2.95	7.57	1.96	0.13	1.24	0.41	1.51	0.77	2208.32	28.23	2180.80	17.54	2155.00	21.70	102.47
045_ZR30	0.87	0.01	256646.90	1.88	4.68	1.42	0.11	1.02	0.32	0.99	0.68	1786.15	15.50	1763.83	11.90	1737.50	18.67	102.80
072_ZR52	1.40	0.02	85833.29	2.70	2.22	2.38	0.08	1.94	0.20	1.39	0.76	1199.79	15.18	1188.13	16.68	1166.97	38.37	102.81
088_ZR63	1.56	0.00	450820.94	1.68	14.17	5.53	0.19	5.46	0.55	0.90	0.15	2805.78	20.43	2761.15	52.46	2728.68	89.87	102.83
070_ZR50	0.46	0.02	103968.29	2.67	2.33	2.13	0.08	1.63	0.21	1.37	0.63	1238.70	15.47	1221.62	15.17	1191.58	32.26	103.95
005_ZR02	0.37	0.02	80368.71	2.22	2.45	1.32	0.08	0.63	0.22	1.16	0.87	1276.82	13.39	1255.99	9.49	1220.47	12.39	104.62
050_ZR35	0.61	0.01	254229.25	5.05	2.28	2.74	0.08	1.01	0.21	2.55	0.93	1226.15	28.43	1204.71	19.31	1166.47	19.94	105.12
032_ZR23	0.26	0.01	226327.89	1.78	2.31	1.16	0.08	0.68	0.21	0.94	0.80	1236.11	10.59	1214.04	8.22	1175.03	13.42	105.20
026_ZR18	0.98	0.01	106054.43	1.69	6.54	1.33	0.12	0.98	0.39	0.90	0.66	2103.93	16.19	2051.35	11.70	1998.91	17.33	105.25
017_ZR12	0.82	0.01	118693.94	3.01	5.10	2.10	0.11	1.43	0.34	1.54	0.80	1881.51	25.08	1835.71	17.80	1784.16	26.01	105.46
061_ZR44	0.88	0.03	58066.49	2.69	2.30	1.91	0.08	1.32	0.21	1.38	0.71	1235.88	15.53	1212.75	13.54	1171.82	26.22	105.47
021_ZR16	0.51	0.01	215134.71	2.00	3.25	2.37	0.09	2.12	0.26	1.05	0.45	1501.25	14.05	1469.30	18.39	1423.43	40.57	105.47
014_ZR09	0.41	0.01	157193.72	2.08	8.19	1.22	0.14	0.55	0.43	1.08	0.89	2322.50	21.16	2252.63	11.00	2189.76	9.52	106.06
060_ZR43	0.27	0.03	50095.13	3.74	9.18	3.16	0.15	2.52	0.46	1.90	0.60	2431.55	38.39	2356.57	28.89	2292.31	43.39	106.07
027_ZR19	0.72	0.01	122682.32	2.66	12.56	1.70	0.17	1.01	0.53	1.37	0.86	2744.17	30.59	2647.00	16.01	2573.55	16.90	106.63
068_ZR48	0.75	0.01	111239.62	3.56	6.27	2.73	0.12	2.04	0.38	1.81	0.68	2083.26	32.18	2013.78	23.89	1943.27	36.55	107.20
025_ZR17	0.99	0.01	110816.37	1.82	5.92	2.52	0.11	2.33	0.37	0.96	0.36	2049.46	16.93	1963.59	21.88	1874.28	41.96	109.35
035_ZR24	2.26	0.07	19994.87	47.07	6.98	24.07	0.12	5.05	0.41	23.54	0.98	2211.43	440.63	2108.30	213.80	2009.13	89.68	110.07
047_ZR32	0.46	0.01	112744.56	2.99	1.98	2.68	0.07	2.20	0.20	1.53	0.80	1161.11	16.23	1109.80	18.06	1010.59	44.55	114.89
020_ZR15	0.46	0.02	83482.83	4.82	2.48	3.13	0.08	1.96	0.23	2.43	0.78	1345.38	29.53	1267.12	22.63	1136.65	39.07	118.36
038_ZR26	0.32	0.01	133415.98	7.12	2.60	7.29	0.08	6.36	0.24	3.58	0.74	1390.86	44.74	1299.41	53.47	1151.40	126.23	120.80
038_ZR26	0.32	0.01	133415.98	7.12	2.60	7.29	0.08	6.36	0.24	3.58	0.74	1390.86	44.74	1299.41	53.47	1151.40	126.23	120.80
007_ZR04	0.27	0.03	57406.94	4.94	4.68	3.08	0.06	3.02	0.19	0.61	0.17	1147.09	6.38	1002.29	19.44	697.77	63.08	164.99

5 CAPÍTULO 5 - DISCUSSÕES

5.1 Ambiente tectônico do magmatismo máfico

Características geoquímicas de litosfera oceânica primitiva são ferramentas úteis para a determinação de ambientes tectônicos e processos geológicos que envolvem geração de magmatismo máfico. A análise de elementos imóveis como indicadores é amplamente recomendada (como em Dilek & Furnes, 2011; Pearce, 2008, 2014) devido às possíveis mudanças ocorridas por metamorfismo e alteração durante a geração, extrusão e exposição durante sua história evolutiva.

O indicador Th-Nb, presente no diagrama Th/Yb-Nb/Yb (Fig. 4.23; Pearce, 2008, 2014) mostra certa contribuição crustal (enriquecimento por contaminação crustal, subducção e alteração por fluidos crustais ou reciclagem crustal). Apesar do enriquecimento de Th em relação ao Nb é maravilhosamente visível em diagramas multielementares normalizados ao MORB e no diagrama Th/Yb-Nb/Yb, onde a maioria das amostras apresenta razões baixas de Th/Nb que podem ser interpretadas, para os basaltos do tipo E-MORB, como uma alta taxa de fusão ocasionada por descompressão extensional e subsequente ascenção da astenosfera. Basaltos transicionais e algumas amostras do Grupo Araxá de tipo E-MORB mostram altas razões La/Nb e Th/Nb que, devido ao seu *trend* subvertical (enriquecimento de Th) no diagrama Th/Yb-Nb/Yb (Figura 4.23), podem ser interpretadas como resultado de interação magma-crosta ou indicar uma afinidade de arco vulcânico. O enriquecimento de Th em comparação ao Nb pode também ocorrer devido à mobilidade dos elementos durante a fusão e pela presença de fluidos aquosos de alta temperatura no metamorfismo em fácies anfibolito, e mais suscetível quando as rochas estão intercaladas com sequências vulcanossedimentares e sedimentos de *melânges* (Pearce, 2008), cenário semelhante e provável para a região de Pires do Rio-Catalão, onde as rochas, que atingiram fácies anfibolito alto, se apresentam acima do campo MORB-OIB (Figura 4.23).

No diagrama V-Ti (Figura 4.23), as amostras de anfibolitos são plotadas dentro do campo referente a basaltos do tipo MORB e BAB/FAB pertencentes às zonas de supra-subducção. Os processos de subducção geram eventos extensionais em ambientes de fore-arc, intra-arco ou antearco, devido à *hinge migration (rollback)* e a criação de uma nova frente de subducção. Os fluidos produzidos ocasionam uma alta taxa de fusão e subsequente enriquecimento da cunha mantélica, assim como a possível atenuação de litosfera continental.

5.1.1 Anfibolitos tipo E-MORB na Sequência Veríssimo e Grupo Araxá

Apesar dos anfibolitos do tipo E-MORB na Sequência Veríssimo e no Grupo Araxá apresentarem padrões similares de enriquecimento de LILE e LREE com padrão horizontalizado de MREE e HFSE, características distintivas entre as duas unidades são consideráveis. Os anfibolitos intrudidos na Sequência Veríssimo não apresentam enriquecimento de Th e Pb e anomalia de Nb-Ta proeminentes que são observadas nos anfibolitos pertencentes ao Grupo Araxá. Isto é uma evidência de que os anfibolitos da Sequência Veríssimo podem ser pertencentes a um ambiente não relacionado a subducção datado em aproximadamente 980 Ma.

Os anfibolitos presentes no sudeste da Faixa Brasília são por vezes relacionados à extensão continental/afinamento litosférico e o possível início de geração de crosta oceânica, comcomitantemente marcados por sedimentos pelágicos e hemipelágicos pertencentes à margem do Cráton São Francisco/Congo e, localmente, vinculados à melângue ofiolítica. O enriquecimento relativo de LILE e LREE pode ser associado a processos de interação magma-crosta, tal como a interação domanto litosférico subcontinental pouco depletado (Dilek & Furnes, 2011) e contaminação crustal. Tal influência crustal presente nas amostras é suportada por idades modelo mais velhas refletindo a influência de fluxo mantélico de fontes magmáticas mais ancestrais provindas do Cráton São

Francisco/Congo. O caráter E-MORB pode também ser explicado quando colunas de fusão mais frias e curtas fundem em uma taxa menor e geram, em sequência, fontes mais enriquecidas (Pearce, 2014). Esse modelo é suportado pelos diagramas Bowen (Fig. 4.24; Dilek & Furnes, 2011) e Vi-T (Fig. 4.23), onde as amostras do tipo MORB pertencem a campos caracterizados como margem continental passiva, pelos teores de TiO_2 , SiO_2 e MgO além da razão V/Ti. O indicador TiO_2/Yb para profundidade de fusão (Pearce, 2008, 2014) apresenta um *trend* diagonal entre composições magmáticas mais profundas do tipo OIB e fontes mais rasas do tipo MORB (interação pluma-cordilheira), em direção a composições de Manto Primitivo (Fig. 4.25). Tal característica pode ser indicativa de ressurgência mantélica durante afinamento crustal em ambientes tectônicos extensionais.

A anomalia negativa de Nb-Ta, similar às observadas em basaltos de arco vulcânico, associada ao enriquecimento de LILE e LREE presentes nos basaltos do tipo MORB do Grupo Araxá podem ser características de uma geração influenciada por fluidos e *melts* originários de um ambiente de subducção. Nesse ambiente, Nb e Ta atuam como elementos imóveis e geram a assinatura geoquímica caracterizada pela anomalia negativa, enquanto os elementos LILE e LREE são relativamente móveis durante o processo de subducção e, portanto, enriquecidos em zonas de suprasubducção quando comparados a basaltos tipo N-MORB. As anomalias positivas de Pb e Sr encontradas nessas amostras também são distintivas em zonas de suprasubducção (Dilek & Furnes, 2011).

A hipótese de uma bacia de backarc/forearc para a deposição do Grupo Araxá é sustentada pelos valores levemente positivos (+0,78 to +2,71) de $\varepsilon\text{Nd}_{(t)}$ e T_{DM} de 1,32-1,80 Ga que podem refletir uma fonte mista de MORBs juvenis enriquecidos com magmas referentes ao Cráton São Francisco. As idades U-Pb para os anfibolitos do tipo MORB (ex.: IPC184 em torno de 870 Ma) é compatível com o desenvolvimento de uma bacia marginal ativa, de forma análoga à algumas sequências pertencentes ao Arco Magmático de Goiás entre 890-830 Ma (Laux *et al.*, 2004, 2005), e por vezes também relacionados a lascas tectônicas do Grupo Araxá.

Apesar da provável contaminação crustal e/ou da influência do metamorfismo de alto grau, o diagrama ternário de Zr-Th-Nb (Wood, 1980) apresenta uma possível distinção entre os anfibolitos presentes no Grupo Araxá e na Sequência Veríssimo. Os anfibolitos do Grupo Araxá plotam preferencialmente no campo de basaltos de arco, enquanto os anfibolitos estudados da Sequência Veríssimo possuem variação dentro do campo E-MORB (Figura 22), corroborando ambas hipóteses de ambientes tectônicos para essas unidades.

5.1.2 Anfibolitos tipo OIB da Sequência Veríssimo e do Grupo Araxá

O magmatismo do tipo OIB pode ocorrer por processos extensivos localizados durante colapsos orogênicos, afinamento crustal, ressurgências mantélicas durante a quebra da placa subductada (formação de janelas astenosféricas), desidratação de fluidos hidrotermais no manto litosférico, fusão de crosta continental subductada ou convecção sub-litosférica (Kheirkhah *et al.*, 2014). As amostras analisadas de basaltos do tipo OIB possuem um enriquecimento relativo de LREE quando comparados a HREE, altas razões Nb/Yb e TiO_2/Yb , porém variáveis padrões de elementos traços exceto pela ausência de anomalia de Nb-Ta quando normalizado ao Manto Primitivo (Sun & McDonough, 1989). As análises de U-Pb em zircão do Grupo Araxá apresentam idades próximas às obtidas para o magmatismo E-MORB, de 819.7 ± 6.3 Ma para a amostra PR-10, e a idade do anfibolito PR-01a em cerca de 650 Ma. Tais idades mais jovens, quando comparadas às amostras de anfibolitos analisadas, foram obtidas em cristais de zonação magmática homogênea sobre núcleos mais antigos que, apesar de apresentarem razões Th/U baixas, são interpretadas como sobrecrescimento magmático (e.g. Lopes-Sánchez *et al.*, 2015) e, portanto, representam a idade de cristalização dos basaltos do tipo OIB. A ocorrência de magmatismo do tipo OIB é observada em diferentes níveis estratigráficos do Grupo Araxá (Valeriano & Simões, 1997), e ao longo das exposições do Complexo Anápolis-Itauçu onde o magmatismo máfico e anatexia foram parcialmente coevos (Piuçana *et al.*, 2003b;

Della Giustina *et al.*, 2011). Os dados apresentados de magmatismo do tipo OIB de idade próxima a 650 Ma são compatíveis aos estágios tardios do magmatismo colisional da Faixa Brasília, em ambiente continental.

Tal hipótese não exclui a possibilidade da ocorrência de outros diversos eventos magmáticos do tipo OIB no desenvolvimento da bacia, com idades de cristalização mais antigas, tal como aqui interpretado para as ocorrências de magmatismo OIB na Sequência Veríssimo. Ou seja, de forma sincrônica aos basaltos do tipo MORB em torno de 980 Ma, que apresentam idades T_{DM} em cerca de 1.3 Ga, enquanto os basaltos do tipo OIB relacionados a 650 Ma possuem idades T_{DM} mais jovens (1.0 Ga). Esta diferença nas idades modelo de Sm-Nd pode hipoteticamente refletir um intervalo de tempo de 300 Ma entre diferentes magmatismos do tipo OIB, no desenvolvimento de diferentes ambientes ao longo da evolução geológica regional.

5.2 Rochas supracrustais do Grupo Araxá e Sequência Veríssimo

Os registros sedimentares são usualmente estudados a fim de entender os processos magmáticos, sedimentares e tectônicos que envolvem a evolução e desenvolvimento de convergência de placas e crescimento de crosta continental (Drauft & Clift, 2012). Contudo, zonas colisionais entre arcos vulcânicos e continente pode ter interpretações complexas, sobretudo em orógenos acrecionários antigos, já que bacias marginais relacionadas podem ocorrer em diversas configurações tectônicas baseadas em paleogeografia, geometria da colisão, características estruturais, a própria evolução distinta do arco vulcânico, o aporte sedimentar, o potencial de preservação e tâos outros fatores geológicos.

O ambiente tectônico interpretado para o Grupo Araxá sempre foi amplamente discutido durante a evolução dos conhecimentos dentro da Faixa Brasília. Vários pesquisadores associam os metassedimentos a fácies sedimentares distais de margem passiva (como em Valeriano & Simões, 1997; Valeriano, 1999; Valeriano *et al.*, 2004, 2008) e as intrusões maficas relacionadas ao afinamento litosférico, sem a geração de crosta oceânica. Por outro lado, o Grupo Araxá é por vezes interpretado como sedimentos sobre crosta oceânica em um configuração de *back-arc* (como em Pimentel *et al.*, 1999; 2001; 2011; Seer *et al.*, 2001 Piuzana *et al.*, 2003), representando uma longa melângue ofiolítica orientada N-S (Strieder & Nilson, 1992).

Margens convergentes podem apresentar locais de extensão e/ou contração, assim como zonas sem stress, o que é por muitas vezes manifestado em regiões de *back-arc* e podem ocorrer durante múltiplos episódios na evolução da área. O registro sedimentar de *back-arc* é dominado por produtos vulcânicos e vulcanoclásticos do arco, com menor fluxo de argilas pelágicas e hemipelágicas, material biogênico e carbonatos ressedimentados. A ausência de grãos de zircão Neoproterozoicos nas porções mais ao sul de toda exposição do que é assumido como Grupo Araxá na Faixa Brasília pode ser explicado no modelo de *back-arc*, no qual o processo de extensão na bacia ocorre em porções mais próximas à trincheira (ante-arco), a subsidência do arco remanescente cria uma barreira à sedimentação de produtos vulcânicos para o ante-arco (Clift, 1995). O registro de bacias de *back-arc* é de difícil preservação em orógenos e, quando ocorre, é na forma de seções ofiolíticas crustais tal qual fragmentos obductados e deformados em sedimentos de prisma acrecionário. Entretanto, bacias de *back-arc* que contém uma grande quantidade de aporte siliciclástico devido à proximidade com fontes continentais tendem a serem preservadas no registro geológico, assim como o arco Macquarie a sudeste da Austrália, os terrenos de arco Alisitos na região de Baja Califórnia, dentre vários outros exemplos (Drauft & Clift, 2013 e referências citadas). As rochas metasedimentares analisadas do Grupo Araxá e da Sequência Veríssimo apresentam similaridades e diferenças de proveniência de potenciais fontes, do ponto de vista geoquímico e isotópico. Ambas unidades geológicas apresentam razões enriquecidas de LREE/HREE, com substanciais anomalias negativas de Eu quando normalizadas ao condrito

(Eu/Eu*=0.48-0.77), onde é interpretada a diferenciação intracrustal das fontes sedimentares, validada pelos altos valores de Th/Sc e La/Sc. Razões elevadas de Th/U e Zr/Sc podem ser indicativas de proeminente alteração e reciclagem sedimentar (McLennan, 1993), e são mais evidenciadas nas amostras pertencentes ao Grupo Araxá. Fontes relacionadas a crosta continental superior e/ou arco continental mais evoluído são interpretadas como prováveis fontes geoquímicas, como presentes no diagrama Th/Sc-Zr/Sc .

Ambas as sequências sedimentares apresentam duas fontes principais de proveniência, ao se analisar os dados isotópicos de U-Pb e Sm-Nd. Uma, caracterizada como imatura, de contribuição vulcanoclástica de 1,2-1,5 Ga, que é diretamente relacionada à dissecação de arco vulcânico intermediário a felsico. Rochas semelhantes são descritas por Klein (2008) a sudoeste da área de estudo, definidas como parte do Domínio Nova Aurora, e aqui interpretadas como uma provável área-fonte do aporte de sedimentos para a bacia. A segunda fonte é representada por um aporte siliciclástico continental, evidenciado por grãos detriticos de zircão com idades variando entre 1,7 a 1,9 Ga, provindos da margem passiva do Cráton São Francisco, a leste. O aporte e mistura de diferentes fontes é claramente visto nos dados de Sm-Nd, onde rochas supracrustais na área de Pires do Rio-Catalão são caracterizadas por valores negativos de $\epsilon_{Nd(t)}$ e idades modelo T_{DM} entre 1,75-2,26 Ga, ligeiramente acima do campo de rochas crustais Paleoproterozoicas do Cráton São Francisco, evidenciando a necessidade de uma contribuição da fonte vulcanoclástica mais jovem.

Apesar das semelhanças entre as sequências sedimentares, a Sequência Veríssimo é caracterizada por assinaturas geoquímicas mais amplas e variáveis. Isso pode ser explicado devido a um aporte sedimentar mais localizado e restrito, com menores efeitos de alteração, reciclagem sedimentar e maturidade quando comparado ao Grupo Araxá, onde é inferida uma proveniência mais abrangente e retrabalhada. A proveniência mais localizada e relacionada a uma área-fonte de arco vulcânico é corroborada por altas razões Ba/La além do aumento relativo de V e Sc.

As rochas metavulcânicas são também usadas para a individualização das bacias contidas no Grupo Araxá e na Sequência Veríssimo. As rochas metavulcânicas da Sequência Veríssimo apresentam um maior enriquecimentos de elementos menores, traço e terras raras, além de anomalias negativas de Cs, K, P e Ti. Junto com anomalias positivas de Nb-Ta, idades modelos de 1,16 Ga e valores de $\epsilon_{Nd(t)}$ de +3,78, o vulcanismo siliciclástico presente na Sequência Veríssimo pode ser relacionado a processos extensionais em ambiente continental, em um contexto de margem vulcânicas de rifte.

Amostras de rochas metavulcânicas do Grupo Araxá analisadas por Klein *et al.* (2008), possuem valores elevados de Sc, Rb, V, Ni e Cu, e ao lado de anomalias negativas de Nb-Ta levam a uma interpretação relacionada a arco vulcânico. Com idades modelo de 1.8 Ga, valores de $\epsilon_{Nd(t)}$ em -5.64 e idade U-Pb de 720 Ma, há a possibilidade da configuração de processos de reciclagem durante subducção para o vulcanismo inerente ao Grupo Araxá.

Apesar dos dados aqui apresentados, o mapeamento do Grupo Araxá representa uma vasta área geográfica, e para alguns dos autores citados ele não representa apenas uma unidade tectônica e é altamente recomendado a ser revisado, assim como diferentes dados geocronológicos entre porções a norte e a sul da unidade são apresentados (Piuzana *et al.*, 2003a e Valeriano *et al.*, 2004, respectivamente). Por fim, tal discussão é pertinente, desde que as relações entre as relações entre as rochas metaígneas e os metasedimentos do Grupo Araxá permanecem controversas devido a imbricações tectônicas (Pimentel *et al.*, 2016).

6 CAPÍTULO 6 - CONCLUSÕES

Os dados obtidos neste trabalho possibilitaram as seguintes conclusões:

Em torno de 0.98 Ga, a Sequência Veríssimo foi depositada em um ambiente tectônico extensional, onde o afinamento crustal e a ressurgência mantélica possibilitaram a geração e extrusão de basaltos do tipo MORB concomitantemente com basaltos do tipo OIB. A sedimentação da Sequência Veríssimo é caracterizada como uma sequência vulcanossedimentar, com a deposição de sedimentos derivados majoritariamente da margem oeste do Cráton São Francisco, com uma pequena contribuição de material vulcanoclástico do Domínio Nova Aurora, a oeste da área.

Estratificamente acima, o magmatismo máfico bimodal (E-MORB e OIB) do Grupo Araxá apresenta características relacionadas a subducção, como basaltos de antearco/back-arc datados em torno de 870-820 Ma. Os basaltos foram provavelmente gerados devido a processos extensionais em crosta continental, contudo sem mudanças significativas nas fontes da sedimentação.

Rochas gabróicas do tipo OIB intrudidas no Grupo Araxá em cerca de 650 Ma são coervas à exumação do núcleo metamórfico, representado pelo Complexo Anápolis-Itauçu, aqui são inferidas como parte do magmatismo máfico relacionado aos estágios finais de evento colisional e desenvolvimento do orógeno em um ambiente continental. Os processos geológicos associados com a geração de tal magmatismo (como por exemplo: delaminação de crosta inferior) requerem estudos detalhados e técnicas que estão além do foco deste trabalho.

Apesar dos dados geoquímicos e isotópicos de Sm-Nd e U-Pb auxiliarem na individualização dos basaltos do tipo MORB e OIB nos âmbitos temporais e genéticos, as discussões a respeito de fontes magmáticas, processos tectônicos e a devida individualização de lascas tectônicas superimpostas não são atenuadas. Uma maior quantidade de dados geoquímicos e isotópicos é altamente recomendada a fim de assegurar possíveis interpretações equivocadas e tendenciosas, e a aplicação de outras sistemáticas geológicas, geoquímicas e isotópicas para investigar outras diversas características determinantes e a correlação com estudos anteriores além de outras exposições de anfibolitos descritos regionalmente, já que a Faixa Brasília exibe uma complexa evolução de eventos geológicos superimpostos em um extenso intervalo de tempo.

7 REFERÊNCIAS BIBLIOGRÁFICAS

- Albarède, F., Telouk, S., Blichert-Toft, J., Boyet, M., Agranier, A., Nelson, B., 2004. Precise and accurate isotopic measurements using multiple-collector ICPMS. *Geochimica et Cosmochimica Acta*, 68, 2725–2744.
- Baldwin, J.A. & Brown, M. (2008). Age and duration of ultrahigh-temperature metamorphism in the Anápolis–Itauçu Complex, Southern Brasília Belt, central Brazil - constraints from U–Pb geochronology, mineral rare earth element chemistry and trace-element thermometry. *Journal of Metamorphic Geology*, 26, 213–233.
- Botelho, N.F.; Moura, M.A. Granite-ore deposit relationship in central Brazil. *Journal of South America Earth Science*, v.11, n.5, p.427-438, 1998.
- Brito Neves, B.B, Fuck, R.A., Pimentel, M.M (2014). The Brasiliano collage in South America: a review. *Brazilian Journal of Geology*, 44(3), 493-518.
- Brod, J.A., Leonardos, O.H., Meneses, P.R., Albuquerque, M.A.C., Almeida, R., Blanco, S.B., Cardoso, F.B.F., Romão, P.A., Tallarico, F.H.B., Thomsen, F.P.R. (1992). Geoquímica da Sequência Vulcano-Sedimentar de

Abadia dos Dourados e Complexo Chapada das Perdizes, Triângulo Mineiro – MG. *Rev. Esc. Minas de Ouro Preto*, 45(2), 164-166.

Buhn, B., Pimentel M.M., Matteini M., Dantas E.L., 2009. High spatial resolution analysis of Pb and U isotopes for geochronology by laser ablation multi-collector inductively coupled plasma mass spectrometry (LA-MC-ICPMS). *Annals of the Brazilian Academy of Sciences*, 81, 99–114.

Campos, J. E. G., Dardenne, M. A., Freitas-Silva, F. H., & Martins-Ferreira, M. A. C. (2013). Geologia do Grupo Paranoá na porção externa da Faixa Brasília. *Brazilian Journal of Geology*, 43(3), 461–476.

CPRM, (2001). Programa Levantamentos Geológicos Básicos do Brasil. Goiânia – Folha SE.22-X-B. Escala 1:250.000. Estado de Goiás. (Eds) José Domingos Alves Baêta Júnior – Brasília: CPRM, 2001. *Explanatory text*, p. 11-12.

D'el-Rey Silva, L. J. H., de Oliveira, . L., Pohren, C. B., Tanizaki, M. L. N., Carneiro, R. C., Fernandes, G. L. D. F., & Aragão, P. E. (2011). Coeval perpendicular shortenings in the Brasília belt: Collision of irregular plate margins leading to orocinal bending in the Neoproterozoic of central Brazil. *Journal of South American Earth Sciences*, 32(1), 1–13.

Dardenne M.A., Fuck R.A., D'el Rey Silva L.H., Pimentel, M.M.. (1994). Mapa Geológico - Projeto Rio Veríssimo. Brasília, *Undergraduate Final Essay*, Institute of Geosciences, University of Brasília.

Dardenne M.A., Fuck R.A., Meneses P.R., Pimentel, M.M.. (1991). Mapa Geológico - Projeto Sucuri. Brasília, Brasília, *Undergraduate Final Essay*, Institute of Geosciences, University of Brasília.

Dardenne, M.A., (2000). The Brasília Fold Belt. In: Cordani, U.G., Milani, E.J., Tomas Filho, A., Campos, D.A. (Eds.), Tectonic Evolution of South America. Proceedings of the XXXI International Geological Congress, Rio de Janeiro, pp. 231–263.

De Paolo, D.J. (1981). A neodymium and strontium isotopic study of the Mesozoic calc-alkaline granitic batholiths of the Sierra Nevada and Peninsular Range, California, *Journal of Geophysical Research*, 86, 10470-10488.

Della Giustina, M.E.S., Pimentel, M.M., Ferreira Filho, C.F., Hollanda, M.H.B.M. (2011). Dating coeval mafic magmatism in the Anápolis-Itauçu Complex, Central Brazil. *Lithos*, 124, 82-102.

Della Giustina, M.E.S.; Claudinei, G.O.; Pimentel, M.M.; Buhn, .B. (2009). Neoproterozoic magmatism and high-grade metamorphism in the Goiás Massif: New LA-MC-ICPMS U-Pb and Sm-Nd data and implications for collisional history of the Brasília Belt. *Precambrian Research* 172 (2009) 67–79.

Dias, H. P. A., Noce, C. M., Pedrosa-Soares, A. C., Seer, H. J., Dussin, I. A., Valeriano, C. M., & Kuchenbecker, M. (2011). O Grupo Ibiá (Faixa Brasília Meridional): evidências isotópicas Sm-Nd e U-Pb de bacia colisional tipo flysch. *Geonomos*, 19(2), 90–99.

Dilek, Y., & Furnes, H. (2011). Ophiolite genesis and global tectonics: Geochemical and tectonic fingerprinting of ancient oceanic lithosphere. *Bulletin of the Geological Society of America*, 123(3–4), 387–411.

Dilek, Y., & Furnes, H. (2014). Ophiolites and their origins. *Elements*, 10(2), 93–100.

Donato, M.M. (1991). Geochemical recognition of a captured back-arc basin metabasaltic complex, southwestern Oregon. *Journal of Geology*, 99, 711-728.

Draut, A. E., & Clift, P. D. (2013). Differential preservation in the geologic record of intraoceanic arc sedimentary and tectonic processes. *Earth-Science Reviews*, 116(1), 57–84.

Draut, A.E. & Clift, P.D. (2012). Basins in arc-continent collisions. In: Busby, E. and Azor, A. (Eds.) *Tectonics of Sedimentary Basins: Recent Advances*, First Edition, Blackwell Publishing Ltd. 347-368

Ferreira Filho, C.F., Kamo, S.L., Fuck, R.A., Krogh, T.E., Naldrett, A.J. (1994). Zircon and rutile U-Pb geochronology of the Niquelândia layered mafic and ultramafic intrusion, Brazil: constraints for the timing of magmatism and high grade metamorphism. *Precambrian Research*, 68, 241-255.

- Fuck, R.A., Jardim De Sá, E.F., Pimentel, M.M., Dardenne, M.A., Soares, A.C.P., (1994). As faixas de dobramentos marginais do Cráton do São Francisco; síntese dos conhecimentos. In: Dominguez, J.M.L., Misi, A. (Eds.), O Cráton do São Francisco. SBG-SGM-CNPq, Salvador, pp. 161–185.
- Gioia, S.M.C.L. & Pimentel, M.M. (2000). The Sm-Nd isotopic method in the Geochronology Laboratory of the University of Brasília. *Anais da Academia Brasília de Ciências*, 72(2), 219-245.
- Guimarães E.M., (1997). Estudos de proveniência e diagênese com ênfase na caracterização dos filossilicatos dos Grupos Paranoá e Bambuí, na região de Bezerra-Cabeceiras (GO). Doctorate thesis. Geosciences Institute, University of Brasília, 270p.
- Hickey-Vargas, R., Savov, I. P., Bizimis, M., Ishii, T., & Fujioka, K. (2013). Origin of Diverse Geochemical Signatures in Igneous Rocks from the West Philippine Basin: Implications for Tectonic Models. *Back-Arc Spreading Systems: Geological, Biological, Chemical, and Physical Interactions*, (June 2016), 287–303.
- Irvine, T. N. & Baragar, W. R. A., (1971). A guide to the chemical classification of the common volcanic rocks. *Canadian Journal Earth Sciences*. 8, 523-548.
- Jackson, S.E., Pearson, N.J., Griffina, W.L., Belousova, E.A., 2004. The application of laser ablation-inductively coupled plasma-mass spectrometry to in situ U-Pb zircon geochronology. *Chemical Geology*, 211, 47–69.
- Junges, S.L., Pimentel, M.M., Dantas, E.L., Laux, J.H. (2003). New ID-TIMS U-Pb ages in the western portion of the Mara Rosa Arc: two hundred million years of arc building. In: 4th South American Symposium on Isotope Geology, Salvador, 2003. Short Papers, Salvador, CBPM, IRD, v1:198-201.
- Kheirkhah, M., Neill, I., & Allen, M. B. (2015). Petrogenesis of OIB-like basaltic volcanic rocks in a continental collision zone: Late Cenozoic magmatism of Eastern Iran. *Journal of Asian Earth Sciences*, 106, 19–33.
- Klein, P.B.W., (2008). Geoquímica de Rocha Total, Geocronologia de U-Pb e Geologia Isotópica de Sm-Nd das Rochas Ortognáissicas e Unidades Litológicas Associadas da Região Ipameri – Catalão (Goiás). Doctorate thesis, Institute of Geosciences, University of Brasília.
- Košler, J., Fonneland, H., Sylvester, P., Tubrett, M., Pedersen, R.B., 2002. U-Pb dating of detrital zircons for sediment provenance studies, a comparison of laser ablation ICP-MS and SIMS techniques. *Chemical Geology*, 182, 605–618.
- Kröner, A., Wan, Y., Liu, X., & Liu, D. (2014). Dating of zircon from high-grade rocks: Which is the most reliable method? *Geoscience Frontiers*, 5(4), 515–523.
- Lacerda Filho, J.V.; Camargo, M.A.; Wildner, W. (1995). Granitoide Sintectônico de Maratá. In: SIMPÓSIO DE GEOLOGIA DO CENTRO-OESTE, 5, *Anais Goiânia: SBG-Núcleos Centro-Oeste e Brasília*, 1995.p.66-67.
- Laux, J. H. Pimentel M.M., Dantas E.L., Armstrong R., Armele A., Nilson A.A. (2004). Mafic magmatism associated with the Goiás magmatic arc in the Anicuns region, Goiás, Central Brazil: Sm-Nd isotops and new ID-TIMS and SHRIMP U-Pb data, *Journal of South American Earth Sciences*, 16, 599-614.
- Laux, J. H., Pimentel, M.M., Dantas, E. L., Armstrong, R., Junges, S.L. (2005) – Two Neoproterozoic crustal accretion events in the Brasília Belt, Central Brazil. *Journal of South American Earth Sciences*, 28, 183-198.
- Lopez-Sanchez, M. A., Aleinikoff, J. N., Marcos, A., Martínez, F. J., & Llana-Fúnez, S. (2016). An example of low-Th/U zircon overgrowths of magmatic origin in a late orogenic Variscan intrusion: the San Ciprián massif (NW Spain). *Journal of the Geological Society*, 173(2), 282–291.
- Matteini, M., Dantas, E.L., Pimentel, M.M., Alvarenga, C.J.S., Dardenne, M.A., (2012). U-Pb and Hf isotope study on detritial zircons from the Paranoá Group, Brasília Belt, Brazil: Constraints on depositional age at Mesoproterozoic – Neoproterozoic transition and tectonomagmatic events in the São Francisco Craton. *Precambrian Research*, 206-207, 168-181.

McLennan, S.M., Hemming, S., McDaniel, D.K., Hanson, G.N. (1993) Geochemical approaches to sedimentation, provenance, and tectonics. In: Johnsson, M.J., and Basu, A. (Eds.), Processes Controlling the Composition of Clastic Sediments: Boulder, Colorado. *Geological Society of America Special Paper*, 284.

McLennan, S.M., Taylor, S.R., McCulloch, M.T. and Maynard, J.B. (1990). Geochemical and Nd-Sr Isotopic Composition of Deep-Sea Turbidites - Crustal Evolution and Plate Tectonic Associations. *Geochimica et Cosmochimica Acta*, 54(7): 2015-2050.

Moraes, R.; Brown, M.; Fuck, R.A.; Camargo, M.A.; Lima, T.M. (2002). Characterization and P-T evolution of melt-bearing ultrahigh-temperature granulites: an example from the Anápolis–Itauçu Complex of the Brasília Fold Belt, Brazil. *Journal of Petrology*, 43, 1673–1705.

Navarro, G. R. B., Zanardo, A., & Da Conceição, F. T. (2013). O grupo araxá na região sul-sudoeste do estado de goiás. *Geologia USP - Série Científica, São Paulo*, 13(2), 5–28.

Pearce, J. A. (2008). Geochemical fingerprinting of oceanic basalts with applications to ophiolite classification and the search for Archean oceanic crust. *Lithos*, 100(1–4), 14–48.

Pearce, J. A. (2014). Immobile element fingerprinting of ophiolites. *Elements*, 10(2), 101–108.

Pimentel, M. M. (2016). The tectonic evolution of the Neoproterozoic Brasília Belt, central Brazil: a geochronological and isotopic approach. *Brazilian Journal of Geology*, 46(June), 67–82.

Pimentel, M. M., Dardenne, M. A., Fuck, R. A., Viana, M. G., Junges, S. L., Fischel, D. P., Dantas, E. L. (2001). Nd isotopes and the provenance of detrital sediments of the neoproterozoic Brasília belt, central Brazil. *Journal of South American Earth Sciences*, 14(6), 571–585.

Pimentel, M. M., Rodrigues, J. B., DellaGiustina, M. E. S., Junges, S., Matteini, M., & Armstrong, R. (2011). The tectonic evolution of the Neoproterozoic Brasília Belt, central Brazil, based on SHRIMP and LA-ICPMS U-Pb sedimentary provenance data: A review. *Journal of South American Earth Sciences*, 31(4), 345–357.

Pimentel, M. M.; Jost, H.; Fuck, R. A. (2004) O embasamento da Faixa Brasília e o arco Magmático de Goiás. In: Mantesso-Neto, V., Bartorelli, A., Carneiro, C. DAL RÉ; (Eds) Brito-Neves, B. B. Geologia do Continente Sul-Americano: evolução da obra de Fernando Flávio Marques de Almeida. São Paulo: Beca, 355-368.

Pimentel, M.M. & Fuck, R.A. (1992). Neoproterozoic crustal accretion in Central Brazil. *Geology*, 20:375-379.

Pimentel, M.M., Fuck, R.A. & Botelho, N.F., (1999). Granites and the geodynamic history of the neoproterozoic Brasília belt , Central Brazil :a review. *Lithos*, 46, pp.463–483.

Pimentel, M.M., Fuck, R.A. & Fischel, D.P., (1999). Estudo Isotópico Sm-Nd Regional da Porção Central Da Faixa Brasília, Goiás: Implicações para Idade e Origem dos Granulitos do Complexo Anápolis-Itauçu e Rochas Metassedimentares Do Grupo Araxá. . *Revista Brasileira de Geociências*, 29(2), pp.271–276.

Pimentel, M.M., Rodrigues, J.B., Della Giustina, M.E.S., Junges, S.L., Matteini, M., (2011). The tectonic evolution of the Neoproterozoic Brasília Belt, central Brazil, based on SHRIMP and LA-ICPMS U-Pb sedimentary provenance data: A review. *Journal of South American Earth Sciences*, 31(4), pp.345–357.

Pimentel, M.M.; Dardenne, R. A.; Viana, M. G.; Junges, S. L.; Fischel, D. P.; Seer, H. J.; Dantas, E. L. (2001). Nd isotopes and the provenance of detrital sediments of the Neoproterozoic Brasília Belt, central Brazil. *Journal of South American Earth Sciences*, 14, pp.571–585.

Piuzana D., Pimentel M.M., Fuck R.A., Armstrong R.A. (2003b). Neoproterozoic granulite facies metamorphism and coeval granitic magmatism in the Brasilia Belt, Central Brazil: regional implications of new SHRIMP U-Pb and Sm-Nd data. *Precambrian Research*, 125:245-273.

Piuzana, D., Pimentel, M. M., Fuck, R. A., & Armstrong, R. (2003a). SHRIMP U-Pb and Sm-Nd data for the Araxá Group and associated magmatic rocks: Constraints for the age of sedimentation and geodynamic context of the southern Brasília Belt, central Brazil. *Precambrian Research*, 125(1–2), 139–160.

- Reno B.L., Brown M., Kobayashi K., Nakamura E., Piccoli P.M., Trouw R.A.J.. 2009. Eclogite-high-pressure granulite metamorphism records early collision in West Gondwana: new data from the Southern Brasília Belt, Brazil. *Journal of the Geological Society*, 166(6), pp.1013–1032.
- Rodrigues, J.B., Pimentel, M.M., Dardenne, M.A., Armstrong, R.A. (2010). Age, provenance and tectonic setting of the Canastra and Ibiá Groups (Brasília Belt, Brazil): Implications for the age of a Neoproterozoic glacial event in central Brazil. *Journal of South American Earth Sciences*, 29(2), pp.512–521.
- Rodrigues, J.B., 2008. Proveniência de sedimentos dos grupos Canastra, Ibiá, Vazante e Bambuí – Um estudo de zircões detriticos e Idades Modelo Sm-Nd. Tese de Doutorado, Instituto de Geociências, Universidade de Brasília – UnB.
- Seer, H.J. (1999). Evolução tectônica dos Grupos Araxá, Ibiá e Canastra na sinforma de Araxá, Araxá, Minas Gerais. *Doctorate thesis*. Geosciences Institute, University of Brasília, 270p.
- Seer, H.J., Dardenne, M.A., Pimentel, M.M., Fonseca, M.A.F., Moraes, L.C. (2000). O Grupo Ibiá Na Sinforma de Araxá : Um Terreno Tectonoestratigráfico Ligado à Evolução de Arcos Magmáticos. *Revista Brasileira de Geociências*, 30(4), pp.737–744.
- Seer, H.J., Brod, J.A., Fuck, R.A., Pimentel, M.M., Boaventura, G.R., Dardenne, M.A. (2001). Grupo Araxá em sua Área Tipo : Um Fragmento de Crosta Oceânica Neoproterozóica na Faixa de Dobramentos Brasília. *Revista Brasileira de Geociências*, d(3), pp.385–396.
- Seer, H.J., Brod, J.A., Valeriano, C.M., Fuck, R.A. (2005). Leucogranitos Intrusivos no Grupo Araxá : Registro de um Evento Magmático durante Colisão Neoproterozóica na Porção Meridional da Faixa Brasília. *Revista Brasileira de Geociências*, 35(1), pp.33–42.
- Shervais, J. W. (2001). Birth, death, and resurrection: The life cycle of suprasubduction zone ophiolites. *Geochemistry, Geophysics, Geosystems*, 2(1), 45.
- Silva, C., Simões L.S., Damázio W.L., Ferreira S.N., Luvizotto G.L. 2012. O Grupo Canastra em sua área-tipo, região de Tapira, sudoeste do estado de Minas Gerais. *Geol. USP, Sér. cient.*, São Paulo, 12(2), pp.83–98.
- Stern, R. J. & Bloomer, S. H. (1992). Subduction zone infancy: Examples from the Eocene Izu-Bonin-Mariana and Jurassic California arcs. *Geological Society of America Bulletin*, 104, 1621-1636.
- Strieder A. J. & Nilson A. A., (1992). Mélange ofiolítica nos metassedimentos do Grupo Araxá de Abadiânia (GO) e implicações tectônicas regionais. *Revista Brasileira de Geociências*, 22: 204-215.
- Strieder, A. J. & Suita, M.T.F., (1999). Neoproterozoic geotectonic evolution of Tocantins Structural Province, Central Brazil. *Geodynamics*, 28, pp.267–289.
- Sun, S.S. and McDonough, W.F. (1989). Chemical and isotopic systematics of oceanic basalts; implications for mantle composition and processes. In: *Magmatism in the ocean basins*. Saunders, A.D. and Norry, M.J. (Editors), *Geological Society of London*, London. 42: 313-345.
- Taylor, S.R. and McLennan, S.M. (1985). *The Continental Crust; Its composition and evolution; an examination of the geochemical record preserved in sedimentary rocks*. Blackwell, Oxford. 312.
- Valeriano, C. M., Machado, N., Simonetti, A., Valladares, C. S., Seer, H. J., & Simões, L. S. A. (2004). U-Pb geochronology of the southern Brasília belt (SE-Brazil): Sedimentary provenance, Neoproterozoic orogeny and assembly of West Gondwana. *Precambrian Research*, 130(1–4), 27–55.
- Valeriano, C.M. & Simões, L.S.A. (1997). Geochemistry of Proterozoic mafic rocks from the Passos Nappe (Minas Gerais, Brazil): tectonic implications to the evolution of the southern Brasília Belt. *Revista Brasileira de Geociências*, 27(1), 99-110.
- Valeriano, C.M. (1992). Evolução tectônica da extremidade sul meridional da Faixa Brasília, região da represa de Furnas, Sudoeste de Minas Gerais. *Doctorate thesis*. Geosciences Institute, University of São Paulo. 258p

Wallin, E.T. & Metacalf, R.V. (1998). Supra-subduction zone ophiolite formed in an extensional forearc: Trinity Terrane, Klamath Mountains, California. *Journal of Geology*, 106, 591-608.

Wiedenbeck M., All , P., Corfu, F., Griffin, W.L., Meier, M., Oberli, F., Von Quadt, A., Roddick, J.C., Spiegel, W. 1995. Three natural zircon standards for U-Th-Pb, Lu-Hf, trace element and Ree analyses. *Geostandards Newsletter*, 19:1-23.

Wiedenbeck, M., Hanchar, J.M., Peck, W.H. Sylvester, P., Valley, J., Whitehouse, M., Kronz, A., Morishita, Y., Nasdala, L., Fiebig, J., Franchi, I., Girard, J.- P., Greenwood, R.C., Hinton, R., Kita, N., Mason, P.R.D., Norman, M., Ogasawara, M., Piccoli, P.M., Rhede, D., Satoh, H., Schulz-Dobrick, B., Sk R, ., Spicuzza, M.J., Terada, K., Tindle, A., Togashi, S., Vennemann, T., Xie, Q. E Zheng, Y.-F. 2004. Further characterisation of the 91500 zircon crystal. *Geostandards And Geoanalytical Research*, 28(1):9-39.

Wood, D.A. (1980). The application of a Th-Hf-Ta diagram to problems of tectonomagmatic classification and to establishing the nature of crustal contamination of basaltic lavas of the British Tertiary volcanic province. *Earth Planet. Sci. Lett.*, 50, 11